INFORMATION TO USERS

This material was produced from a microfilm copy of the original document. While the most advanced technological means to photograph and reproduce this document have been used, the quality is heavily dependent upon the quality of the original submitted.

The following explanation of techniques is provided to help you understand markings or patterns which may appear on this reproduction.

1. The sign or "target" for pages apparently lacking from the document photographed is "Missing Page(s)". If it was possible to obtain the missing page(s) or section, they are spliced into the film along with adjacent pages. This may have necessitated cutting thru an image and duplicating adjacent pages to insure you complete continuity.

2. When an image on the film is obliterated with a large round black mark, it is an indication that the photographer suspected that the copy may have moved during exposure and thus cause a blurred image. You will find a good image of the page in the adjacent frame.

3. When a map, drawing or chart, etc., was part of the material being photographed the photographer followed a definite method in "sectioning" the material. It is customary to begin photoing at the upper left hand corner of a large sheet and to continue photoing from left to right in equal sections with a small overlap. If necessary, sectioning is continued again – beginning below the first row and continuing on until complete.

4. The majority of users indicate that the textual content is of greatest value, however, a somewhat higher quality reproduction could be made from "photographs" if essential to the understanding of the dissertation. Silver prints of "photographs" may be ordered at additional charge by writing the Order Department, giving the catalog number, title, author and specific pages you wish reproduced.

5. PLEASE NOTE: Some pages may have indistinct print. Filmed as received.

University Microfilms International
300 North Zeeb Road
Ann Arbor, Michigan 48106 USA
St. John's Road, Tyler's Green
High Wycombe, Bucks, England HP10 8HR

78-4731

JENSEN, Mark Anton, 1951-
ELECTROCHEMICAL PROPERTIES OF THE NAD^+/ NADH REDOX COUPLE.

The University of Michigan,
Ph.D., 1977
Chemistry, analytical

University Microfilms International, Ann Arbor, Michigan 48106

ELECTROCHEMICAL PROPERTIES OF THE NAD^+/NADH REDOX COUPLE

by

Mark Anton Jensen

A dissertation submitted in partial fulfillment
of the requirements for the degree of
Doctor of Philosophy
(Chemistry)
in The University of Michigan
1977

Doctoral Committee

Professor Philip J. Elving, Chairman
Professor Herbert H. Cornish
Associate Professor Seyhan N. Ege
Professor Charles L. Rulfs
Associate Professor Richard D. Sacks

We shall not cease from exploration
And the end of all our exploring
Will be to arrive where we started
And know the place for the first time.
Through the unknown, remembered gate
When the last of earth left to discover
Is that which was the beginning;
At the source of the longest river
The voice of the hidden waterfall
And the children in the apple-tree
Not known, because not looked for
But heard, half-heard, in the stillness
Between two waves of the sea.
Quick now, here, now, always-
A condition of complete simplicity
(Costing not less than everything)
And all shall be well and
All manner of thing shall be well
When the tongues of flame are in-folded
Into the crowned knot of fire
And the fire and the rose are one.

from Little Gidding
by T.S. Eliot

ACKNOWLEDGEMENT

The author expresses his sincere appreciation to Professor P.J. Elving for his encouragement and guidance during the course of this work. Thanks are also due to Dr. T.E. Cummings for his help with the instrumentation and for the many helpful discussions throughout the last two years of this work.

The financial support of the Allied Chemical Corporation, the National Science Foundation, and the University of Michigan Chemistry Department, is gratefully acknowledged.

Lastly, the author thanks his parents for their moral support and for making the choice possible.

TABLE OF CONTENTS

Page

ACKNOWLEDGEMENTS. iii

LIST OF TABLES. viii

LIST OF FIGURES x

I. INTRODUCTION 1

A. Biochemical Properties 1

B. Electrochemical Behavior 4

C. Differences in Electrochemical and Biological Redox Behavior 6

D. Methodology. 7

II. EXPERIMENTAL 9

A. Chemicals. 9

B. Apparatus. 12

C. Instrumentation. 14

D. Technique. 15

1. Polarography 15

a. DC Polarography. 15

b. AC Polarography. 15

c. Pulse Polarography 24

2. Cyclic Voltammetry 26

3. Double Potential-Step Chronamperometry 27

4. Controlled Potential Electrolysis. 27

E. Design of a High-Speed Potentiostat. 28

1. Construction of Potentiostat 29

2. Timing Circuit and Sample-and-Hold 32

3. Testing of Rapid Response Potentiostat 33

a. DC Polarography 37
b. Cyclic Voltammetry. 37
c. Potential-Step Chronoamperometry. 42
d. AC Polarography 49
III. REDUCTION OF NAD^+ 57
A. Initial One-Electron Reduction. 57
1. Effect of Background Electrolyte. 57
a. DC and AC Polarography. 57
b. Cyclic Voltammetry. 64
2. Effect of Lewis Acids: Ca(II) 65
a. DC and AC Polarography. 65
b. Cyclic Voltammetry. 67
3. Effect of Lewis Acids: Zn(II) 70
a. DC and AC Polarography. 70
b. Mechanism 75
4. Dimerization of $NAD^{\cdot}$ 78
a. Double Potential-Step Chronoamperometry 78
b. Cyclic Voltammetry. 79
c. Activation Energy 85
5. Controlled Electrode-Potential Electrolysis 85
a. Determination of Dimeric Structure. 85
b. Decomposition of the Dimer. 87
c. Nature of the Yellow-Green Color. 91
B. Reduction of the Free Radical $NAD^{\cdot}$ 92
1. Effect of Brønsted Acids. 93
a. pH. 93

b. Ammonium Ion. 98

2. Effect of Lewis Acids: Ca(II) 102

a. DC and AC Polarography. 102

b. Titration of Ca(II) with NAD^+ 106

c. Effect of Ca(II) Adsorption on $k_{s,h}$ 108

3. Determinations of the Rate Constant for the Rearrangement 109

a. Effect of Available Proton Donor. 109

b. Effect of Background Electrolyte Concentration on k_2 and $k_{s,h}$. 115

4. Controlled Electrode-Potential Electrolysis 118

a. Determination of Reduction Products 120

b. Relationship of k_2 to 1,4-NADH:1,6-NADH Ratio 120

IV. OXIDATION OF 1,4-NADH 125

A. Pretreatment of Glassy Carbon Electrode 125

B. Effect of pH on the Oxidation of NADH 128

C. Effect of Lewis Acids: Ca(II) 135

D. Effect of Lewis Acids: Zn(II) 137

V. ADSORPTION OF ADENINE AND NAD^+. 139

A. Comparison of the Relative Adsorption of Adenine and NAD^+. 143

B. Adsorption Site of NAD^+ 146

VI. RELATION OF BIOLOGICAL AND ELECTROCHEMICAL REDOX PROCESSES 148

A. Summary of Electrochemical and Biological Redox Behavior. 148

B. NAD^+/NADH Redox Mechanism 149

1. Estimations of K_O and K_R. 159

C. Correlation of Electrochemical and Biological Redox Potentials. 163

VII. ANALYTICAL APPLICATION. 166

REFERENCES 168

LIST OF TABLES

Page

Table I. Composition of buffered background solutions. 11

Table II. Cyclic voltammetric behavior of 1.56 mM Fe(III) in 1 M $K_2C_2O_4$. 44

Table III. Ac polarographic faradaic response of 1.59 mM Fe(III) in 1 M $K_2C_2O_4$ 52

Table IV. Polarographic data for the one-electron reduction of NAD^+ showing the effect of replacing KCl with NH_4Cl. 59

Table V. DC polarographic data for the one-electron reduction of NAD^+ in the presence of $Ca(ClO_4)_2$. 66

Table VI. AC polarographic data for the one-electron reduction of NAD^+ in the presence of $Ca(ClO_4)_2$ 68

Table VII. Summary of determinations of the rate constant for the dimerization of $NAD^{\cdot}$ 84

Table VIII. Products of decomposition of $(NAD)_2$ in a nitrogen atmosphere 88

Table IX. Summary of polarographic behavior of the $NAD^{\cdot}/NADH$ redox couple as KCl is replaced with NH_4Cl 99

Table X. DC polarographic behavior of the $NAD^{\cdot}/NADH$ redox couple in the presence of Ca(II). 104

Table XI. AC polarographic behavior of the $NAD^{\cdot}/NADH$ redox couple in the presence of Ca(II) 105

Table XII. Formation constants of NAD^+:Ca(II) complex. 107

Table XIII. Summary of the variation with temperature and ionic strength of the rate constant for the rearrangement of $NADH\text{-}X^-$ 111

Table XIV. Effect of Tea^+ concentration of the heterogeneous charge transfer rate constants. 116

Table XV. Summary of data for the two-electron electrolysis of NAD^+. 119

Table XVI. Cyclic voltammetric data for the oxidation of 2.6 mM 1,4-NADH on a glassy carbon electrode. 129

LIST OF FIGURES

Page

Figure 1. Structure of NAD^+. 2

Figure 2. Summary of the electrochemical redox cycle of NAD^+/NADH. 5

Figure 3. Cross-sectional diagram of compact electrochemical cell with Luggin capillary 13

Figure 4. Potential and current phase relationships for the analysis of ac polarographic data. 17

Figure 5. AC polarographic potential and current relationships in the absence of a faradaic process 20

Figure 6. Timing sequences of the potential perterbation and current sampling for pulse polarography. 25

Figure 7. Potentiostat circuit diagram 30

Figure 8. Potentiostat timing circuit diagram. 34

Figure 9. Timing sequence for controlled drop-time and current sampling 36

Figure 10. Current-potential relationship for a dc polarogram of 1.59 m$\underline{M}$ Fe(III) in 1 $\underline{M}$ $K_2C_2O_4$. 38

Figure 11. Cyclic voltammograms of 1.56 m$\underline{M}$ Fe(III) in 1 $\underline{M}$ $K_2C_2O_4$. 40

Figure 12. Charging current-time behavior for 1 $\underline{M}$ $K_2C_2O_4$ on potential-step chronoamperometry. 47

Figure 13. Current-time behavior for 1.56 m$\underline{M}$ Fe(III) in 1 $\underline{M}$ $K_2C_2O_4$ obtained on potential-step chronoamperometry 48

Figure 14. Charging current-frequency behavior for ac polarograms of 1 $\underline{M}$ $K_2C_2O_4$ 54

Figure 15. Relationship of faradaic summit current with frequency for ac polarograms of 1.59 mM Fe(III) in $K_2C_2O_4$. 55

Figure 16. Logarithmic analysis of dc polarographic current-potential relationship for 0.88 mM NAD^+ in 0.4 M TeaCl and 0.1 M carbonate at pH 9.1. 62

Figure 17. Variation of the dc and ac polarographic behavior of mixtures of Zn(II) and NAD^+ in 0.10 M Teap and 0.01 M Tris at pH 7.2. 72

Figure 18. Variation of the dc and ac polarographic behavior of mixtures of Zn(II), adenosine diphosphoribose, and 1-methylnicotinamide in 0.10 M Teap and 0.01 M Tris at pH 7.2 76

Figure 19. Variation of the cyclic voltammetric peak-potential concentration function with scan rate for the initial one-electron reduction of NAD^+ in 0.4 M TeaCl and 0.1 M carbonate at pH 9.1. 82

Figure 20. Voltammetric peak-potential-pH relationship for the reduction of $\dot{NAD}$ in 0.1 M Teap and 0.01 M Tris 85

Figure 21. Variation of the differential pulse polarographic behavior of 0.42 mM NAD^+ in mixtures of NH_4Cl and KCl at pH 9.0. 101

Figure 22. Relationship of the first-order rate constant for the rearrangement of NADH-X^- with temperature. . . .112

Figure 23. Cyclic voltammograms of 2.6 mM NADH in 0.1 M Teap and 0.01 M Tris showing the effects of electrode pretreatment 127

Figure 24. Variation of cyclic voltammetric peak current with scan rate for the oxidation of 2.6 mM NADH on a glassy carbon electrode. 133

Figure 25. Currents obtained for 10 μM adenine and 10 μM NAD^+ in pH 4.8 McIlvaine buffer on modified pulse polarography. 141

Figure 26. Variation of normalized pulse polarographic current with initial polarization potential for 10 μM adenine and 10 μM NAD^+ in pH 4.8 McIlvaine buffer on modified pulse polarography 144

Figure 27. Composite representation of the voltammetric waves for the NAD^+/NADH redox system. 150

Figure 28. Schematic diagram of the resonance structures for $NA\dot{D}$ and the coupled reaction sequence 153

Figure 29. Schematic diagram of the redox participants in the $NA\dot{D}$/NADH redox couple and the equilibria of the coupled chemical reactions. 155

I. INTRODUCTION

A. Biochemical Properties

Nicotinamide-adenine dinucleotide (NAD^+; cf. Figure 1) is one of the most common respiratory coenzymes. Its principal function is that of a cofactor, which serves as a proton and electron acceptor in a broad range of enzymatically catalyzed biological redox reactions (cf. equation 1, where S represents the oxidized form of the substrate and SH_2 its reduced form).

$$NAD^+_{(ox)} + SH_2 \xrightleftharpoons{\text{enzyme}} 1,4\text{-}NADH_{(red)} + S + H^+ \qquad (1)$$

Some of the more familiar biological redox reactions, for which NAD^+ or NADH serve as a cofactor, are: (1) the glycolytic breakdown of glucose, where NAD^+ is cycled between its reduced and oxidized forms through the oxidation of 3-phosphoglyceraldehyde and the subsequent reduction of pyruvate which occurs later in the

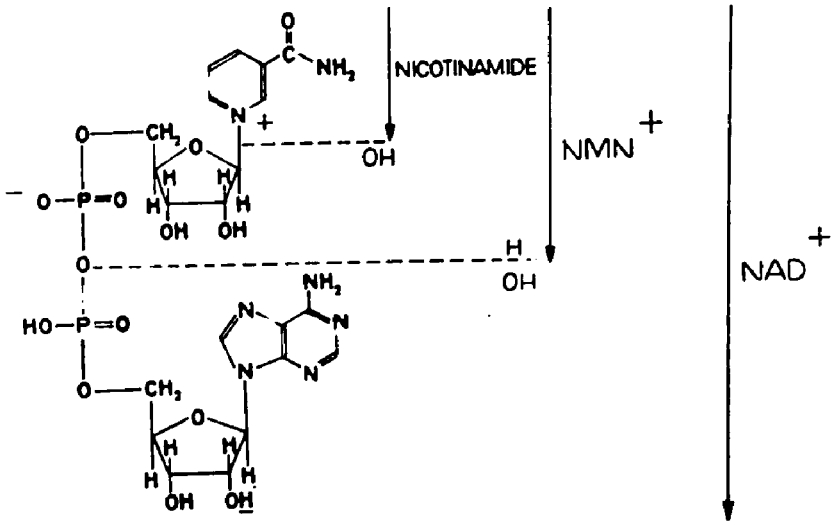


Figure 1. Structure of nicotinamide-adenine dinucleotide (NAD^+). Other names for this compound include diphosphopyridine nucleotide (DPN), coenzyme I, codehydrogenase and cozymase. Nicotinamide mononucleotide is designated by NMN^+.

process, (2) the Krebs tricarboxylic acid cycle (the process in which acetate is oxidized to CO_2 and water), where NAD^+ serves as oxidizing agent at three points in the reaction sequence, and (3) in the respiratory chain where NADH transfers two electrons to flavin-adenine dinucleotide, which then transfers one electron to ubiquinone (CoQ) thus initiating the cytochrome cycle (1).

One of the more frequently cited biological redox reactions, in which NAD^+ participates, is the oxidation of ethanol to acetaldehyde which is catalyzed by the enzyme alcohol dehydrogenase (ADH),

$$CH_3CH_2OH + NAD^+ \overset{ADH}{\rightleftharpoons} CH_3CHO + 1,4\text{-NADH} + H^+ \qquad (2)$$

This oxidation takes place with the net transfer of a hydride ion from the alpha carbon of ethanol to the 4 position of the nicotinamide moiety of NAD^+. The hydride transfer is stereospecific with respect to both NAD^+ and the substrate.

Thermal studies on the system of the equation 2 reaction and other analogous reactions such as those involving 2-propanol-acetone (2), and lactate-pyruvate (3), have lead to the calculation of an E_c^o = -0.56 V vs. sce (saturated calomel electrode) at pH 7 for the NAD^+/NADH redox couple,

$$NAD^+ + 2\ e^- + H^+ \rightleftharpoons 1,4\text{-NADH} \qquad (3)$$

Similar values for E_c^o have been obtained from potentiometric measurements on systems containing the NAD^+/NADH redox couple in the presence of an appropriate enzyme and a mediator (6). Due to the overall

electrochemical irreversibility of the NAD^+/NADH couple, there are at present no electrodes which will respond directly to the relative concentrations of NAD^+ and NADH. A mediating redox couple, which is both chemically reactive with NAD^+ and electrochemically responsive to the sensing electrode, must be present in order for the electrode to respond to the relative activities of NAD^+ and NADH.

B. Electrochemical Behavior

Over the past 12 years the electrochemical reduction of NAD^+ (4-9) and oxidation of NADH (10-13) has been extensively studied. The overall electrochemical redox behavior of the NAD^+/NADH redox couple is summarized in Figure 2. (The potentials given in the figure should not be taken as thermodynamic E^o but rather as polarographic $E_{1/2}$ values or slow-scan cyclic voltammetric peak potentials, E_p, where $E_{1/2}$ values were unobtainable.)

At a potential of -0.9 to -1.1 V depending on background electrolyte and concentration of NAD^+, NAD^+ undergoes a 1e reduction to form a free radical species, $\dot{NAD}$, which rapidly dimerizes. Nuclear magnetic resonance and ultraviolet (UV) absorption spectra of the dimeric product strongly suggest that the dimer is formed by a bond between the C(4) carbons of both monomers (14). The dimeric species may be oxidized back to the parent compound, NAD^+, at a potential of -0.3 V.

At pH 9, the 1e reduction of the free radical $\dot{NAD}$ to NADH is observed as a shoulder on the hydrogen discharge wave. At higher pH values, the negative shift of the background discharge allows the

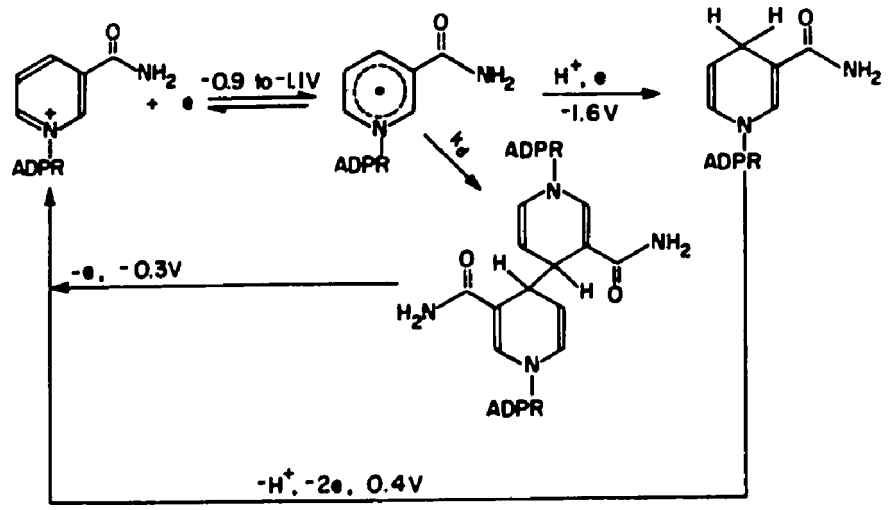


Figure 2. A summary of the electrochemical redox cycle of NAD^+/NADH. Approximately 50 to 70% of the free radical $NA\dot{D}$ is reduced to 1,4-NADH. ADPR represents adenosine diphosphoribose. All potentials given in this figure and throughout the text are versus an sce unless otherwise specified.

second wave to be more clearly resolved. The reduction of the free radical proceeds with the net addition of an electron and a proton to NAD· to form either 1,4-NADH or 1,6-NADH. Since in nonaqueous solvents NAD· was not reduced in the available potential range until a source of protons was added (9), the step which ultimately leads to the proton addition must occur simultaneously with or prior to the charge transfer.

Electrochemically, NADH is oxidized back to NAD^+ at E_p = +0.4 V. This oxidation proceeds with the loss of two electrons and a proton and appears to be quite irreversible.

C. Differences in Electrochemical and Biological Redox Behavior

There are some very striking differences between the biological and electrochemical redox properties of NAD^+. Under biological conditions, the NAD^+/NADH redox couple appears to be macroscopically reversible in the presence of an appropriate enzyme and substrate. Electrochemically, both the reduction of NAD^+ to NADH and the oxidation of NADH appear to be irreversible. The overpotentials in either case are about one volt, if the biological E_c^o at pH 7 is taken to be the true thermodynamic E^o for the redox couple.

Second, electrochemically NAD^+ undergoes a one-electron reduction to form a free radical species. To this point in time, no evidence for the existence of the free radical in the biological redox mechanism has been found. This should not be taken to imply that a free radical intermediate does not exist in the biological redox. It does imply, however, that the life span of such a free radical

would have to be quite short.

Third, the biological reduction of NAD^+ is stereospecific in respect to both the nicotinamide moiety of NAD^+ and the substrate with the product of the reduction being entirely 1,4-NADH. Electrochemically, NAD^+ is reduced to 1,4-NADH plus some other dihydro species. (Postulation of the additional dihydro species is based on the observation of a net transfer of two electrons per mole NAD^+ reduced and on a material balance of the products.) Ultraviolet spectroscopic evidence points strongly to the fact that the other dihydropyridine nucleotide is 1,6-NADH (cf. subsequent discussion in Section IIIB.).

D. Methodology

In order to obtain a more explicit picture of the electrochemical redox scheme for NAD^+/NADH and, as a result, possibly some clarification of the differences between the electrochemical and biological redox couples, each reaction involving the redox participants and intermediates shown in Figure 2 was examined in detail. The types of reactions which were studied include: (1) protonation and complexation equilibria, (2) free radical dimerization, (3) charge-transfer processes, and (4) subsequent rearrangements. The kinetics and equilibria of these reactions were examined to determine the effects of the following solution conditions: (1) composition and concentration (ionic strength) of background electrolyte, (2) presence of Lewis and Brønsted acids. The effect of variation in temperature on the rates of free radical dimerization and rearrangements following charge-transfer was studied in order that activation energies and frequency

factors for these reactions could be determined.

The electroanalytical methods, which were applied to the study of the NAD^+/NADH redox couple, included a variety of polarographic techniques, e.g., direct current, alternating current, pulse and differential pulse polarography. Other voltammetric techniques which were used include linear scan chronoamperometry (single-sweep cyclic voltammetry), multi-sweep cyclic voltammetry and double potential-step chronoamperometry. A discussion of these techniques may be found in Section II.

II. EXPERIMENTAL

A. Chemicals

The nicotinamide nucleotides and related compounds were obtained from the following sources: oxidized nicotinamide-adenine dinucleotide (NAD^+), reduced nicotinamide-adenine dinucleotide disodium salt (1,4-NADH), adenosine diphosphoribose sodium salt (ADPR), nicotinamide mononucleotide (NMN^+), and yeast alcohol dehydrogenase from P-L Biochemicals; 1-methylnicotinamide chloride from Signa; and adenine from Calbiochem.

Background electrolyte and buffer solutions were prepared from reagent grade chemicals which were obtained from the following sources: tetraethylammonium chloride (TeaCl), and tetraethylammonium hydroxide (TeaOH) from Aldrich; tetraethylammonium perchlorate (Teap), zinc perchlorate, and perchloric acid from G. Frederick Smith; potassium bicarbonate, and potassium phosphate (K_2HPO_4) from Mallinckrodt; 2-amino-2-hydroxymethyl-1,3-propanediol (Tris) from Sigma; other chemicals were obtained from J. T. Baker. The buffers

and background electrolytes which were used during the course of study are summarized in Table I.

Purity of the reduced and oxidized forms of NAD^+ was determined from enzymatic assays (15). These assays were monitored spectrophotometrically using either a Beckman Model DU spectrophotometer or a Cary Model 14 spectrophotometer, with standard silica rectangular cells with a transparency range of 220-2500 nm and a path length of 10 mm. The procedure for determining the purity of NAD^+ was the following: NAD^+ was stored under vacuum over a desiccant ($CaSO_4$) prior to the assay. A 0.5 mM NAD^+ solution, which was 0.1 M in Tris (pH 9.8), was prepared. A second solution was prepared which was 0.5 M in ethanol (U.S. Industrial Chemicals Co., U.S.P. grade) and 0.1 M in Tris. One ml of a 0.1% solution of yeast alcohol dehydrogenase (ADH) was added to 1.00 ml of the NAD^+ solution, which was then diluted to 10.0 ml with the alcoholic Tris solution. A second 1.00 ml sample of the NAD^+ solution was also diluted to 10.0 ml with the alcoholic Tris solution. The absorbance of these two solutions at 340 nm was then compared. The solution, which contained no ADH, gave an absorbance peak at 260 nm which is due to both the unreduced nicotinamide and the adenine moieties (ε = 17,800)(16). No other absorbance peak is found in the ultraviolet region above 230 nm. In the solution containing ADH, the enzymatically active NAD^+ is reduced to NADH. NADH gives two ultraviolet absorbance peaks; one peak at 260 nm (ε = 14.400) is due to the adenine moiety; the other peak at 340 nm (ε = 6,200) is due to the 1,4-dihydronicotinamide moiety (17). Since only the enzymatically active NAD^+ will be reduced to 1,4-NADH, the percentage of enzymatically active NAD^+

Table I. Composition of Buffered Background Solutions

Buffer No.	pH Range	Composition	μ,[a] M
1	4.8	Na_2HPO_4 + citric acid + KCl	0.5
2	7.2-9.6	Tris + $(C_2H_5)_4$ $NClO_4$[b]	0.10-0.11
3	9.05	NH_3 + NH_4Cl[c]	0.4
4	9.1	K_2CO_3 + $KHCO_3$ + KCl[d]	0.5
5	9.1	K_2CO_3 + $KHCO_3$ + $(C_2H_5)_4$ NCl[e]	0.5
6	9.3	Tris + $(C_2H_5)_4$ NCl[f]	0.5

[a] Ionic strength.

[b] $(C_2H_5)_4$ $NClO_4$ concentration: 0.10 M.

[c] NH_4Cl concentration: 0.4 M.

[d] KCl concentration: 0.4 M.

[e] $(C_2H_5)_4$ NCl concentration: 0.4 M.

[f] $(C_2H_5)_4$ NCl concentration: 0.5 M.

in the sample can be calculated from the difference in absorptivity of the two samples at 340 nm.

The assay procedure for NADH is similar to that of NAD^+ with the following changes. In place of 0.1 M Tris, a 0.1 M phosphate buffer (pH 7.5) is used and ethanol is replaced by acetaldehyde (Matheson, Coleman & Bell). The percent of 1,4-NADH in the sample is determined from the difference in absorptivity of the two samples at 340 nm.

A similar assay procedure was used to analyze electrolysis products of NAD^+ with some minor modifications which will be discussed in detail later.

B. Apparatus

Polarographic and other voltammetric studies were conducted in a water jacketed one-compartment cell with a Luggin capillary (Figure 3). Oxygen was removed from solution by bubbling water-pumped nitrogen through the solution for 30 minutes. The nitrogen stream was first passed through two washing towers, which contained a reduced vanadium chloride/hydrochloric acid solution, to remove any residual oxygen in the N_2. The nitrogen was next bubbled through a saturated $Ca(OH)_2$ solution to remove any HCl which might be entrained in the gas stream. Finally, the N_2 was passed through a thermostated distilled water solution to saturate the N_2 with water vapor and to bring its temperature to that of the solution.

Samples, which were to be used for electrochemical studies, were weighed to an accuracy of 0.05 mg using an Ainsworth Type DLB

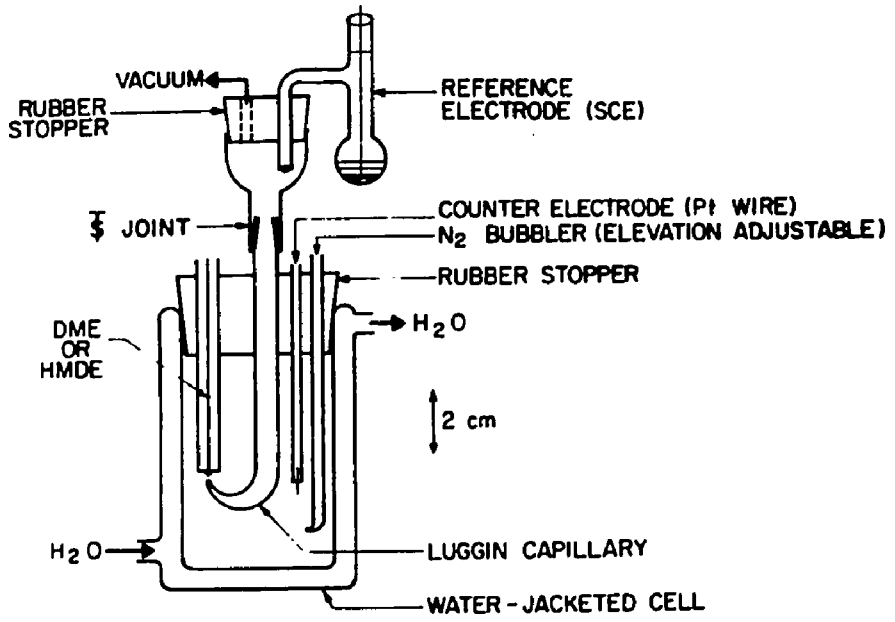


Figure 3. Cross-sectional diagram of compact electrochemical cell with Luggin capillary. DME and HMDE represent dropping-mercury electrode and hanging-mercury drop electrode, respectively.

analytical balance. Materials for the background electrolyte and buffers were weighed to an accuracy of 0.01 gm using an Ohaus Centogram single-pan balance.

C. Instrumentation

The electroanalytical studies made of NAD^+ and NADH may be divided into two types. First, there were those for which the response time of the potentiostat was not of critical importance, e.g., dc polarography, ac polarography (at 40 and 100 Hz), normal and differential pulse polarography, and controlled electrode-potential electrolysis. These particular studies were carried out using a PAR Model 174 polarographic unit; for the ac polarography, a PAR Model 121 lock-in amplifier/phase detector was interfaced with the Model 174. Second, there were studies which required a potentiostat with a rapid response time, e.g., fast-scan cyclic voltammetry, double potential-step chronoamperometry, and pulse polarography. These studies were carried out using a potentiostat, which was constructed for the research investigation and which was designed to have a minimal response time. The requirements and testing of this potentiostat will be subsequently discussed. Ordinarily, pulse polarographic studies were made using the Model 174. However, studies of the adsorption behavior of adenine and NAD^+ required current sampling capabilities, which could not be obtained from the Model 174 and, hence, had to be carried out using the high-speed potentiostat.

Polarographic and coulometric data were recorded using a Houston Instrument Series 2000 Omnigraphic X-Y recorder, which has an accuracy of 0.2% of full scale on the X and Y axes and an accuracy of 1% for the time base.

High-speed potentiometric data acquisition and observation of transient signals was accomplished using a Tektronix 5103N power supply/amplifier as the basic oscilloscope system with the Tektronix C-12 camera system. Observations of voltage amplitude versus time (Y-t) were made using a 5A18N dual-trace amplifier and a 5B10N time base/amplifier as plug-in modules. When the 5103N was used as an X-Y recorder, the 5B10N was replaced by a 5A15N amplifier. Accuracy for the 5A18N and 5A15N amplifier modules is within 2%. Both modules have an input resistance of 10^6 ohms and an input capacity of 47 pf. The 5B10 has an accuracy of within 3% when the sensitivity is set in the range of 1 μs/div to 1 s/div.

D. Techniques

1. Polarography

a. DC Polarography. DC polarography is a fundamental and widely used analytical technique and as such will not be discussed here. There are numerous reviews and books which examine both the theory and the application of this technique (18,19).

b. AC Polarography. In an ac polarographic experiment, the impedance of an electrochemical system is determined under polarographic conditions by means of an alternating potential. The impedance to the fundamental harmonic alternating current may be measured by an impedance

bridge or one may directly measure the alternating current which occurs as a result of the alternating potential.

The alternating current arises from two sources: (1) the charging current which is required to charge the double layer at the solution-electrode interface, and (2) the faradaic processes which would include charge transfer to an electroactive species.

The current, which charges the double layer, is essentially capacitive in nature and is 90° out of phase with the applied alternating potential. It is consequently often referred to as the quadrature current. The current, which flows due to the faradaic process at the electrode surface, has a phase angle which is dependent on such factors as (1) the frequency of the applied potential, (2) the kinetics of the charge transfer, and (3) any intervening chemical steps which affect the concentration of either the oxidized or the reduced species. The phase angle for such a faradaic current generally falls in the range of 0° to 45° behind the applied potential. A phase angle of 45° is observed for an uncomplicated reversible electron transfer process. The phase relationship between the ac working electrode potential and the alternating faradaic current is illustrated in Figure 4A.

It is possible to distinguish between the faradaic and quadrature currents by means of phase-selective detection. The phase-sensitive detection is accomplished by means of a full-wave synchronous rectifier which inverts the polarity of the voltage signal from the current follower relative to the polarity of the applied potential. The dc component of the output signal is then measured. A signal which is 90° out of phase with the applied input will produce an

Figure 4. (A) Phase relation between the applied working electrode potential, ΔE, and the ac faradaic current, $I(\omega t)$.

(B) Vector representation of potential and current phase relationships for the analysis of ac polarographic data. Symbols are defined in the text.

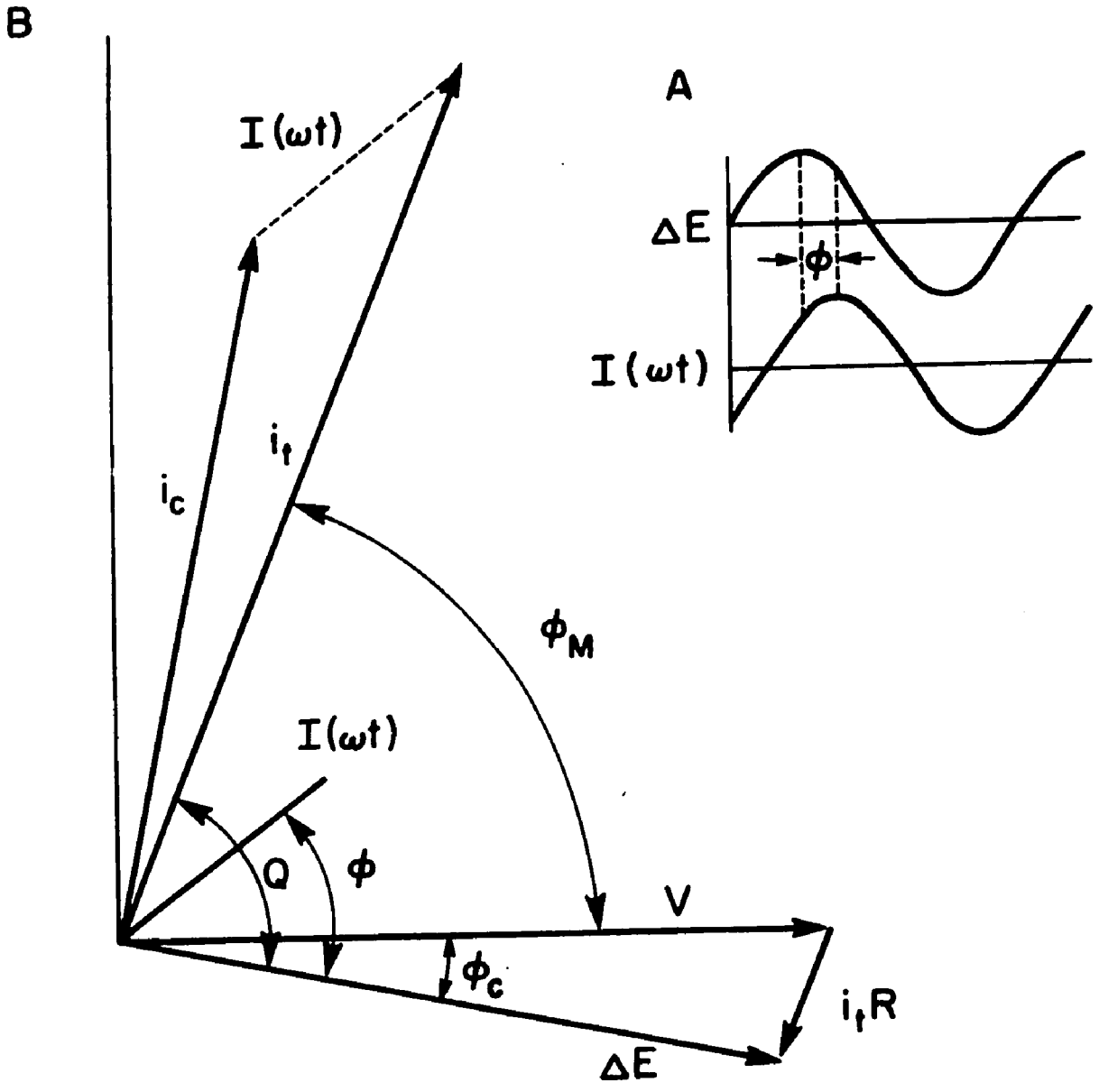


Figure 4.

output which has no dc component.

By using phase-selective detection with an applied input voltage which is in phase with the alternating voltage applied to the reference electrode, the capacitive current component is cancelled out, providing there is no ohmic resistance which would cause a phase difference between the working electrode and reference electrode voltages. In addition to causing such a phase shift, an ohmic resistance between the reference and working electrodes will also bring about an attenuation of the potential at the working electrode when a current is flowing; the effect of an uncompensated resistance on the working electrode potential and on the phase angle difference between the applied and working electrode voltages is illustrated in Figure 5.

Through the use of Luggin capillary (Figure 3) it is possible to minimize the ohmic resistance in an electrochemical cell. However, it may still be necessary to correct ac polarographic data for phase angle shifts and attenuation of the working electrode potential. The procedure for correcting the ac polarographic data is described in a review article by Smith (20).

Because of the phase relationships between the potential and current components, the procedure involves treating the potentials and currents as vectorial quantities, as illustrated in Figure 4B. Each of the components is represented as a vectorial quantitity where the angle between the vector representing the component and the vector representing the alternating voltage, V, is equivalent to the phase angle between the applied potential and the component.

Figure 5. Effect of uncompensated resistance, R, on the working electrode potential, ΔE, and the phase angle difference, θ, between the applied potential, V, and the working electrode potential in the absence of a faradaic process (vector representation).

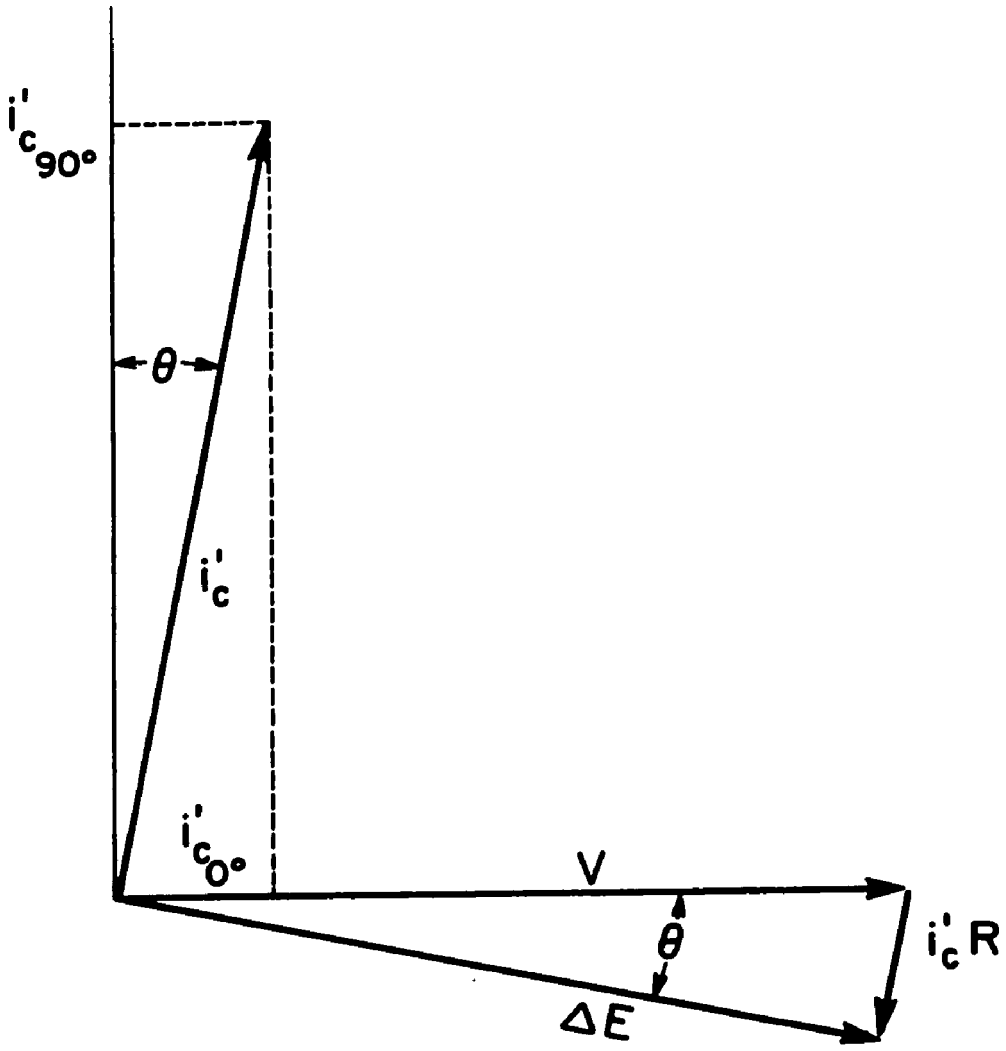


Figure 5.

When an alternating voltage is applied to the working electrode, the resulting current i_t is the vectorial sum of the charging current i_c and the current due to the faradaic process $I(\omega t)$. The potential drop due to the ohmic resistance R is equal to the product of the ohmic resistance times the total current, i_t, and is represented by a vector which is opposite in sign to the total current. This potential loss due to the resistance R is shown in Figure 4B as $i_t R$. The potential at the working electrode, ΔE, is the vector sum of the applied potential V and the potential drop $i_t R$.

The ohmic resistance is determined by measuring the charging current in the absence of any faradaic process at phase angles of 0° and 90° relative to the applied potential. Since the charging current is 90° out of phase with the potential at the working electrode, one will observe a charging current at a phase angle of 0° which is a function of the magnitude of the total current and the ohmic resistance (cf. Figure 5). The total current is given by the vector expression,

$$\vec{i}'_c = \vec{i}'_{c_{90°}} + \vec{i}'_{c_{0°}} \tag{4}$$

where $i'_{c_{0°}}$ is the magnitude of the charging current at 0° relative to the applied potential and $i'_{c_{90°}}$ is the magnitude of the charging current at 90° relative to the applied potential. The phase relationship between the applied potential and the potential at the working electrode can be calculated from the relation,

$$i'_{c_{0°}} / i'_c = \sin \theta \tag{5}$$

where θ is the phase angle between the applied potential and the working electrode potential. The ohmic resistance may be calculated from

$$\sin \theta = i_t R/V \tag{6}$$

Since R is independent of potential, this resistance may then be used in calculations of working electrode potential and phase angle shifts in the presence of a faradaic process regardless of the dc potential at the working electrode.

In the presence of a faradaic process, i_t and θ_m are determined experimentally. The phase angle between the applied and working electrode potentials is calculated from

$$\sin \theta_c = \frac{i_t R \sin \theta_m}{[V^2 + (i_t R)^2 - 2V i_t R \cos \theta_m]^{\frac{1}{2}}} \tag{7}$$

and the working electrode potential is given by

$$\Delta E = [V^2 + (i_t R)^2 - 2V i_t R \cos \theta_m]^{\frac{1}{2}} \tag{8}$$

where $Q = \phi_m + \phi_c$.

Since i_c and $I(\omega t)$ show a linear relationship with ΔE for $\Delta E <$ 10 mV, the calculation of ΔE makes it possible to normalize the values of i_c and $I(\omega t)$ for variations in ΔE at various dc potentials in the ac polarogram.

c. Pulse Polarography. In pulse polarography, the potential at a dropping mercury electrode is maintained at a base potential until just before the drop is dislodged. This potential will be referred to as the initial polarization potential, E_{ip}, (In the literature, this potential is also referred to as the prepolarization potential.) At a set time, prior to the dislodging of the drop, the potential is stepped to a new level, E_{fp}. The current, which results from the potential step, is sampled after sufficient time has been allowed for the decay of the charging current. The time required for this decay is dependent on the magnitude of the pulse and on the response time of the particular potentiostat being used. (The PAR Model 174 allows 40 ms for the decay of the capacitive current while less than 3 ms was a sufficient time for the decay, using the in-house built potentiostat.) Succeeding pulses are incrementally increased, where the actual increase in the pulse amplitude is dependent on the scan rate, e.g., for a scan rate of 2 mV/s and a 5-s drop-time the increase in amplitude would be 10 mV with each drop (Figure 6A).

A variation of this technique, which has been applied for studies of adenine adsorption (21,22), was also used to study the potential-dependent adsorption of NAD^+. In the modified approach, the initial polarization potential, E_{ip}, was varied but the final potential in each cycle remained constant (Figure 6B). Such a type of potential perturbation is not directly obtainable from either the PAR 174 or the in-house potentiostat. However, application of the pulse was achieved as follows: The frequency of a Wavetek Model 114 signal generator was set to give a pulse of 13.7 ms, when triggered by the signal which also triggers the gate to the potentiostat sample-

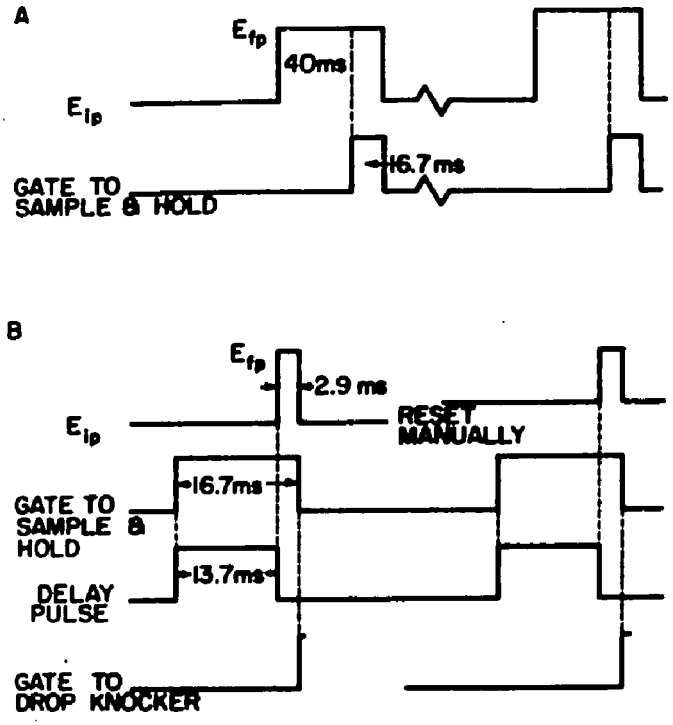


Figure 6. Pulse polarographic patterns. (A) Potential pulse and sample-and-hold gating sequence for normal pulse polarography. (B) Modified potential pulse pattern for studies of adenine and NAD^+.

and-hold amplifier (the sample-and-hold amplifier stays active for 16.7 ms). The falling edge of the pulse from the Model 114 triggered a Wavetek Model 112 signal generator whose frequency was adjusted to give a 3-ms pulse, which was applied to the working electrode. Current sampling by the sample-and-hold was ceased 0.05 to 0.01 ms prior to the end of the 3 ms pulse. Since the acquisition time for the sample-and-hold amplifier is 25 μs, the time interval from the application of the pulse to the measurement of the current was 2.93 ±0.05 ms.

The current data had to be taken point by point because each time the initial polarization potential was changed, it was necessary to reset the pulse amplitude from the Wavetek 112 to insure that the potential was still being pulsed to the same level.

2. Cyclic Voltammetry

Cyclic voltammetry involves a linear change in potential at a stationary constant-area electrode. At a given potential, the sweep is reversed and continued back to the starting potential. Both the rate and range of the potential sweep may be varied either for a full cycle or for each half-cycle. Reversibility, rate of charge transfer, and transfer coefficients may be determined from the relationships of peak currents and peak current potentials to the rate and range of the potential sweep. In cases where first-order or pseudo first-order chemical reactions involving redox participants, i.e., chemical reactions coupled to the electron transfer reaction, are on a time scale comparable with the scan rate, the rate constants for these reactions can be determined. It is also possible to determine

second-order rate constants for reactions between electroactive species, i.e., dimerization rates.

Voltammetric studies were carried out using the following types of working electrodes: (1) hanging mercury drop electrode, (2) slow flowing dropping mercury electrode, and (3) glassy carbon disk electrode (area of 0.20 cm^2).

3. Double Potential-Step Chronoamperometry

In addition to cyclic voltammetry, double potential-step chronoamperometry may also be used to observe the kinetics of chemical reactions which are coupled to a charge transfer. In this technique, the potential at a stationary electrode is set to an initial level; it is then stepped to a new level for a period of time τ. The potential is then stepped back to the original potential. The relative ratios of cathodic and anodic currents at given time periods in the pulse may then be related to the rates at which electroactive species undergo chemical reactions.

4. Controlled Potential Electrolysis

Controlled electrode potential electrolyses of NAD^+ were carried out at a Hg pool electrode (area of ca. 3.7 cm^2) in a water-jacketed three-compartment cell, where agar salt bridges were inserted on the reference and counter electrode sides of the medium porosity glass frits, which separated the working electrode chamber (Hg pool) from the reference electrode (sce) chamber and the counter electrode (platinum gauze in saturated KCl solution) chamber.

The products of the electrolyses were evaluated polarographically and by enzymatic assay. The procedure for the evaluation of the 1-

and 2-electron reduction products will be discussed in those appropriate sections.

E. Design of a High-Speed Potentiostat

At the present time, most of the emphasis in commercially available electroanalytical instrumentation has come in the area of producing instruments with a multifunctional capability. This multifunctional character is achieved, however, at the expense of rapid perturbation and rapid sensing capability.

In order to study adequately an electrochemical redox system, which involves rapid homogeneous and heterogeneous kinetics, such as the NAD^+/NADH redox couple, it was necessary to use a potentiostat which was specifically designed for fast perturbation techniques (23). In order to be suitable for studying rapid kinetics, a potentiostat should show the following characteristics: (1) rapid response time, (2) high current capacity, and (3) long term stability. In order to achieve these response characteristics, the following criteria had to be met: (1) use of high quality passive and active components; (2) concise physical placement of the components; (3) minimal capacitance between components, which requires a minimal use of switches in those areas where high frequency signals will be transmitted; and (4) current capacity of 50 mA for potential-step chronoamperometry to insure rapid charging of the electrical double layer - if only cyclic voltammetry and ac polarography are being considered, a current capacity of 1 mA should be sufficient.

1. Construction of Potentiostat

The potentiostat used for studying the NAD^+/NADH redox couple was of the standard three-electrode, three-operational amplifier design (24); the schematic circuit is shown in Figure 7. The three-operational amplifiers have the following open loop characteristics: (1) a slewing rate of 500 V/μs; (2) a settling time to 0.1% of 75 ns; (3) a maximum current output of 50 mA; (4) a common mode input impedance of 10^{12} ohms; (5) a full output frequency response of 5 M Hz. The stable closed loop characteristics are, of course, somewhat poorer.

In order to insure a minimal number of switches, the built-in perturbation techniques were restricted to a linear ramp generator for dc polarography and slow-scan single-sweep voltammetry. The sinusoidal, triangular and square wave perturbations were obtained from external function generators and could be introduced at the front panel of the potentiostat.

The potentiostat was so constructed that the cell connections, external inputs, capacitive shunt, iR compensation, and the cell function switch were located a minimal distance from the operational amplifiers; the latter were arranged in a tight linear fashion and mounted near the front panel. In this manner, the lengths of all connecting wires are minimized.

To obtain an optimum response time from the potentiostat, a small tunable capacitor was connected across the output of the controller to the non-inverting input of the voltage follower. This capacitive shunt makes it possible to remove the stabilization

Figure 7. Potentiostat circuit diagram. Part number symbols: P, potentiometer; S, switch; OA, operational amplifier; BNC, BNC receptacle; BJ, banana jack (B for black; R for red). Operational amplifiers 1 to 3 are Teledyne Philbrick Model 1025; operational amplifier 4 is Teledyne Philbrick 1026. The power supply is a Teledyne Philbrick Model 2419, 0.5 A, dual power supply. Fixed resistors are 1% precision. Fixed capacitors are 10% precision. The variable capacitor, C1, is a 4-30 pF ceramic capacitor. Potentiometers are wirewound. Switch 5 is multipole; hyphenated number refers to pole number. All switches and potentiometers are shown in counterclockwise or down position.

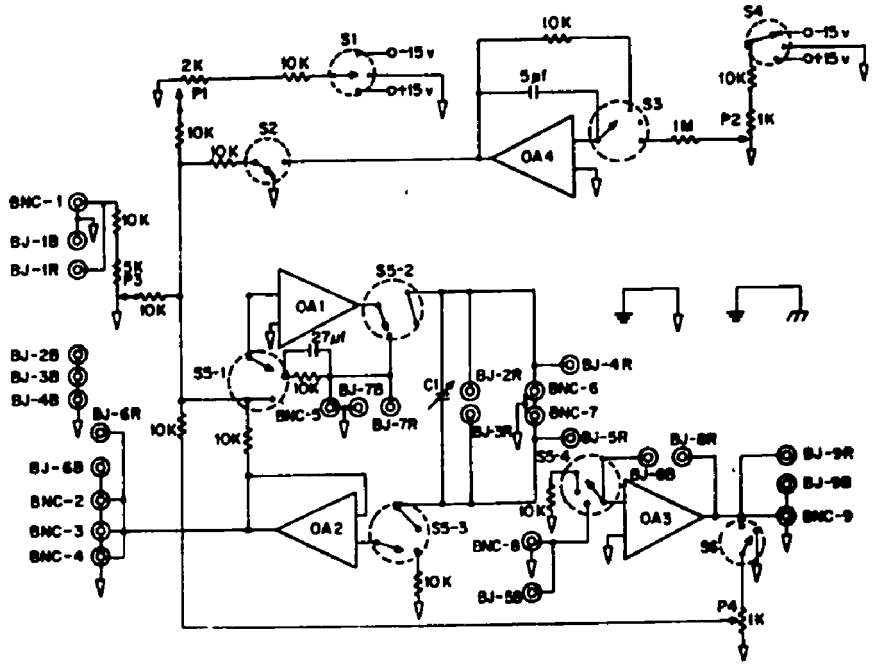

S1
0-15 v
0+15 v
2K
P1
10K
S2
10K
10K
5pf
S3
OA4
1M
S4
0-15 v
0+15 v
10K
P2 1K
BNC-1
BJ-1B
BJ-1R
10K
5K
P3
10K
OA1
S5-2
27M
S5-1
10K
BJ-7B
BNC-5
BJ-7R
C1
BJ-2R
BNC-6
BNC-7
BJ-3R
BJ-4R
BJ-5R
BJ-8R
BJ-8B
S5-4
BJ-2B
BJ-3B
BJ-4B
BJ-6R
BJ-6B
BNC-2
BNC-3
BNC-4
10K
10K
OA2
S5-3
10K
BNC-8
BJ-5B
OA3
BJ-9R
BJ-9B
BNC-9
P4
1K

Figure 7.

capacitor at the controller. The amount of capacitance in the shunt, required to stabilize the potentiostat, is strongly dependent on solution conditions. For this reason, a variable ceramic capacitor (4-30 pf) was used as the capacitive shunt. An external input in parallel with the capacitive shunt was mounted on the front panel in order to permit the addition of more capacitance on the shunt.

The following three operational amplifier configurations are available, using the cell function switch: (1) A balance mode, in which each operational amplifier is isolated with either a positive or negative input grounded through a resistor. This mode allows all the amplifiers to be balanced such that a 0.0-volt input produces a 0.0-V output, without any interaction from the other operational amplifiers. (2) A standby mode, whereby the output of the controller is connected to the counter electrode and the non-inverting input of the voltage follower is connected to the reference electrode, while the current amplifier inverting input is grounded through a 10 kohm resistor. In this mode, the capacitive shunt may be tuned to stabilize the potentiostat without involving the working electrode. (3) A cell mode, in which the potentiostat is in an operational three-electrode configuration.

2. Timing Circuit and Sample-and-Hold

For a number of electroanalytical techniques such as ac polarography and pulse polarography, it is necessary to use a dme (dropping mercury electrode) at a controlled drop-time with appropriate sample-and-hold acquisition of the current prior to the dislodging of the drop. The timing circuitry for the drop-knocker is relatively

elementary; however, the synchronization of the sample-and-hold timing with that of the drop-knocker is somewhat more complex. The schematic circuit for the drop-knocker and sample-and-hold circuitry is shown in Figure 8; and the timing sequence is shown in Figure 9. The timing circuit consists of three Signetics NE 555 timers wired as a series of monostable multivibrators. Drop time could be preset to 1 s, 2 s, 3 s, or 5 s by use of switch S7. The drop-knocker is fired when the silicon controlled rectifier is gated open by monostable III going to its high state. This allows a 20-μf capacitor to discharge through the drop-knocker solenoid. The time constant for the charging of the capacitor is controlled by potentiometer P5. Since the force of the drop-knocker strike is dependent on the current flow through solenoid, which is dependent on the charge on the capacitor, the striking force of the drop knocker is controlled by P5.

Because a large current pulse is required to recharge the capacitor after each strike, a second power supply is used to charge the 20-μf capacitor. Since the current pulse possibly could load the power supply, thus causing momentary changes in its output voltage, it was imperative that the operational amplifiers and multivibrators should be on a separate power supply.

3. Testing of Rapid Response Potentiostat

The primary objective in testing the potentiostat was to ascertain the maximum useful perturbation rates, which could be obtained for such techniques as cyclic voltammetry, potential-step chronoamperometry and ac polarography, prior to the onset of instrumental artifacts. These limits were determined by examining an electrochemical system, which had been well characterized and reported to be

Figure 8. Potentiostat timing circuit diagram. Part number symbols: MS, monostable multivibrator; SH, sample-and-hold operational amplifier; S, switch; P, potentiometer. Monostables are Signetics NE 555 timers. Sample-and-hold operational amplifier is Hybrid Systems SH725LH. Silicon controlled rectifier is General Electric C11B (2N1774). Power supply for drop-knocker is a Philbrick/Nexus Model 2203, 0.1 A, dual power supply. Resistors are 1% precision. Capacitors are 5% precision. Potentiometers are wirewound. All items except the drop-knocker are powered by the Model 2419 power supply of Figure 7. X preceding connection to SH marks the location for connection of an optional front panel BNC jack permitting access to the 5-V trigger signal from MS II.

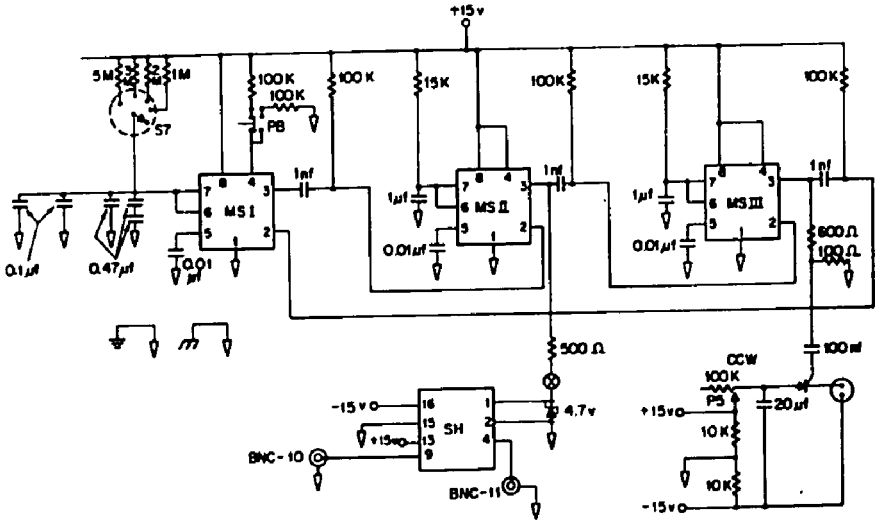

+15v
5M
1M
100K
100K
100K
15K
100K
15K
100K
S7
PB
MS I
MS II
MS III
1mf
1mf
1mf
1μf
1μf
0.1μf
0.47μf
0.001μf
0.01μf
0.01μf
600Ω
100Ω
500Ω
100mf
CCW
100K
P3
20μf
+15v
10K
10K
-15v
-15v
+15v
SH
4.7v
BNC-10
BNC-11

Figure 8.

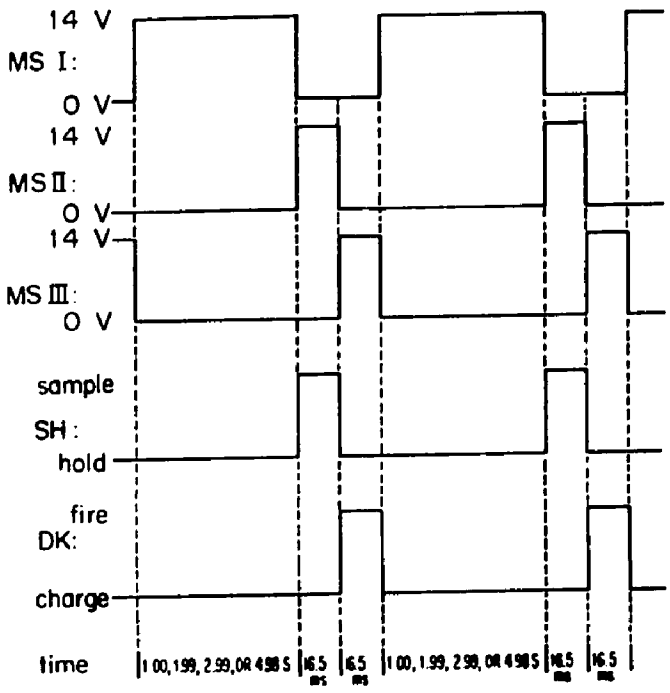


Figure 9. Timing sequences for controlled drop-time and current sample-and-hold obtainable from the Figure 8 circuit. DK, drop-knocker; other symbols are as in Figure 8.

reversible on mercury, i.e., the Fe(III)/Fe(II) couple in aqueous oxalate medium (25-28). The electrochemical response of this system was compared to the theoretically calculated response of a diffusion-controlled reversible system for each of the perturbation techniques listed. A reversible electrochemical system was chosen to minimize the problems of differentiation between instrumental and chemical kinetic effects.

A resistive and capacitive dummy cell could not be used to test the response limits of the potentiostat since the impedance characteristics of an electrochemical cell are rather more complex.

a. DC Polarography. A dc polarogram of 1.59 mM Fe(III) in 1 M $K_2C_2O_4$ was run to provide confirmatory evidence of the reversibility of the Fe(III)/Fe(II) couple in 1 M oxalate, and to provide a diffusion current constant, I_d, and an $E_{\frac{1}{2}}$, which could be compared with earlier published results. Analysis of the dc polarographic gave an $E_{\frac{1}{2}}$ of -0.236 V and a plot of E vs. log $[i/(i_d - i)]$ which was linear with a slope of 55.0 mV/decade, where i_d is the maximum diffusion-limited current and i is the measured current (Figure 10). The linearity of the plot in Figure 10 confirms that the system behaves reversibly on a dc polarographic time scale, i.e., the heterogeneous charge transfer rate constant, $k_{s,h}$, exceeds 0.02 cm/s. The polarographic I_d of 1.36 for the average current is in agreement with previously published values (29,30).

b. Cyclic Voltammetry. Cyclic voltammetric studies of 1.57 mM Fe(III) in 1 M $K_2C_2O_4$ were carried out at a dme with a controlled drop-time (5 sec.). The perturbation signal was synchronized to the

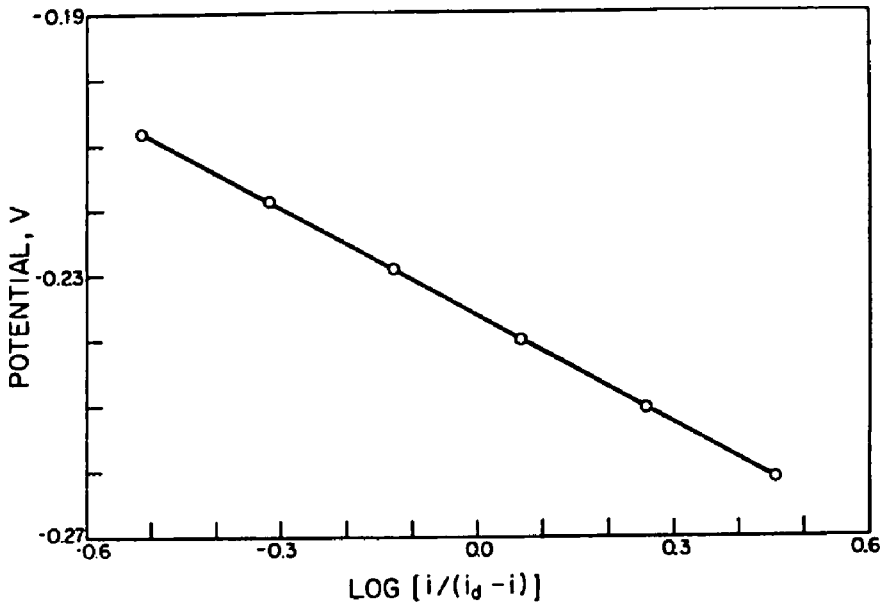


Figure 10. Current-potential relationship for dc polarogram of 1.59 m$\underline{M}$ Fe(III) in 1 $\underline{M}$ $K_2C_2O_4$ solution. Linear least-squares data fit gives a slope of 55 mV/decade with $E_{1/2}$ = -0.236 V.

drop-life to insure that uniform electrode areas were obtained. Since a controlled drop-time was used, monostable II (Figure 8) provided the trigger signal for the triangular wave. The signal from monostable II occurs 16.7 ms prior to the firing of the drop-knocker so a second triggerable function generator was inserted in the triggering circuit to provide a delay line which would trigger the perturbation 3.0 ms before the end of the drop life.

In an uncomplicated reversible one-electron transfer, a separation between cathodic and anodic peaks of 58 mV at 25°C. is predicted providing that the switching potential is 200 mV negative of the $E_{\frac{1}{2}}$ for the reduction (31). The examination of peak separation should be a sensitive test of the response of the potentiostat since any lag in the response times of the operational amplifiers will result in a larger peak separation.

Since iR compensation was being used, the observed peak potentials as they appear at the output of the voltage follower must be corrected to obtain the potential at the working electrode. Cyclic voltammograms of 1.57 m$\underline{M}$ Fe(III) in 1 $\underline{M}$ $K_2C_2O_4$ at a scan rate of 302 V/s with no iR compensation (1) and with 59 ohms of iR compensation (2) are shown in Figure 11 A. The maximum iR compensation, which could be applied while still maintaining a stable potentiostat response, was 59 ohms; this was determined by observing the effect of 57, 59 and 60 ohms of compensation at 2016 V/s (Figure 11 B-D). When iR compensation is used, the potential at the output of the voltage follower is given by

$$V_a + iR_c = -V_{vf} \qquad (9)$$

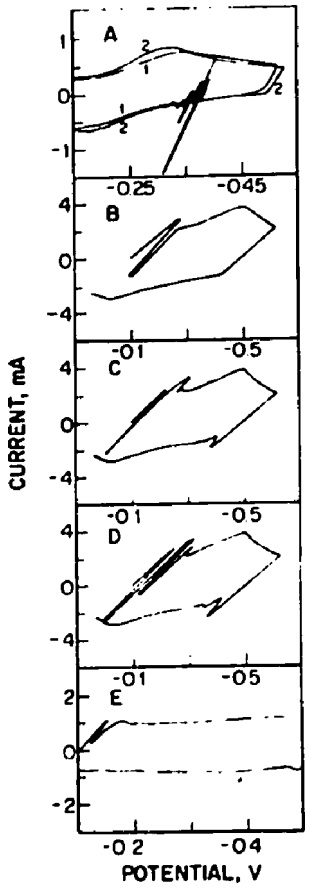


Figure 11. Cyclic voltammograms of 1.56 mM Fe(III) in 1 M $K_2C_2O_4$. (A) scan rate, 302 V/s; curve 1, no iR compensation; curve 2, 59 ohms iR compensation. (B) scan rate, 2016 V/s; 57 ohms iR compensation. (C) 2016 V/s; 59 ohms iR compensation. (D) 2016 V/s; 60 ohms iR compensation. (E) 1 M $K_2C_2O_4$ solution; 1008 V/s; 59 ohms iR compensation.

where V_{vf} is the potential at the voltage follower output, V_a is the applied potential, and iR_c is the product of the current times the compensated resistance. The effective potential at the working electrode, V_{we}, is given by

$$V_{we} = -V_{vf} - iR_c \tag{10}$$

By combining equations 9 and 10 it follows that the potential at the working electrode is equal to the applied potential.

In the scan at 302 V/s with iR compensation (2), it appears that the switching potential, E_λ, lies somewhat negative of the switching potential obtained when no iR compensation (1) was applied. The skewness of trace in the area of E_λ is also brought about by the application of iR compensation. In voltammogram 2 , E_λ for the negative going sweep is -0.528 V whereas the initial potential for the anodic sweep is -0.499 V, with the zero current crossover at -0.506 V. Since, at the point of zero current the potentials at the working electrode and at the voltage follower are equal but of opposite sign (iR_c = 0.0 V), the zero current potential should represent a working electrode E_λ of -0.506 V. Because the cathodic current at E_λ for the negative going sweep is 0.41 mA, 59 ohms of compensation should shift the potential at the voltage follower 24 mV positive of E_λ at the working electrode. Hence, the working electrode E_λ calculated from the cathodic current and the E_λ of the negative going sweep would be -0.528 + 0.024 or -0.504 V. The agreement in observed and calculated working electrode E_λ is well within experimental uncertainties.

Since a Luggin capillary was employed with its tip only one drop diameter from the dme, the resistence of 59 ohms could hardly

represent the resistance between the Luggin capillary tip and the working electrode. When the tip of the dme capillary was placed in a Hg pool it was found that the resistance between the Hg reservoir and the Hg pool was ca. 36 ohms. The bulk of the resistance is probably to be found in the capillary itself.

The scan rates for the cyclic voltammetric studies ranged from 302 to 4032 V/s. The results are summarized in Table II. At 4032 V/s, the value of ΔE_p, corrected for iR_c, has a 95% confidence range which includes the ΔE_p for a reversible charge transfer, 58 mV.

In view of the reasonably constant ΔE_p values obtained with 59 ohms of compensation, it appears that the potentiostat is performing well at scan rates up to 4032 V/s.

The major areas of uncertainty, that one encounters in determining peak separations at rapid scan rates. are, first, the flatness of the peaks and, second, the sensitivity of the peak separation to the amount of iR compensation which is applied, e.g., Table II shows the affect of 57, 59 and 60 ohms on ΔE_p at a scan rate of 2016 V/s. Because of these two factors, the use of peak separations to determine large heterogeneous rate constants does not yield precise results and should, therefore, only be used to set upper and lower limits on the more rapid rate constants.

c. Potential-Step Chronoamperometry. The triggering procedure used for the potential-step technique is identical to that employed for cyclic voltammetry except that the perturbation signal is a square wave rather than a triangular wave.

In a potential-step experiment, the critical factor in the response time of the potentiostat is how rapidly the electrode-solution

Table II. Cyclic Voltammetric Behavior of 1.56 mM Fe(III) in 1 M $K_2C_2O_4$ Solution

Scan Rate	R_c	Measured Potentials		i_{pc} [b]	i_{pa} [b]	$i_t R_c$ [c]	Corrected [a] Potentials		
		E_{pc}	ΔE_p				E_{pc}	ΔE_p [d]	
V/s	Ohm	V	V	mA	mA	V	V	V	
302	0	-0.350	0.188	0.74	0.59	0	-0.350	0.188	(0.003)
302	59	-0.322	0.144	0.82	0.63	0.085	-0.274	0.059 [e]	(0.006)
605	59	-0.356	0.201	1.42	1.07	0.146	-0.273	0.055 [e]	(0.006)
1008	57	-0.402	0.292	2.12	1.58	0.210	-0.283	0.082	(0.012)
1008	59	-0.409	0.291	2.13	1.69	0.224	-0.283	0.067 [e]	(0.018)
2016	57	-0.509	0.485	3.71	2.98	0.379	-0.299	0.106	(0.014)
2016	59	-0.496	0.457	3.73	2.93	0.391	-0.277	0.066 [e]	(0.014)
2016	60	-0.499	0.458	3.73	2.96	0.399	-0.276	0.059	(0.014)
4032	57	-0.662	0.784	6.53	5.51	0.683	-0.291	0.101	(0.022)
4032	59	-0.680	0.820	6.67	5.73	0.728	-0.289	0.074 [e]	(0.022)

[a] Corrected for iR compensation effect.

[b] Total peak current including charging current at peak potential.

[c] $i_t = i_{pc} + i_{pa}$.

[d] Values in parentheses are 95% confidence intervals. The uncertainties for the true peak separation are based on maximum errors of 3% in scope accuracy on each axis, maximum mechanical measurement errors of 0.01" of each peak height, and the maximum uncertainty in the location of the actual E_p for each peak. Each uncertainty was assumed to represent three population standard deviations, from which the standard deviation of ΔE_p was calculated.

[e] Values for optimum iR compensation.

double layer can be charged following the application of the potential pulse. Rapid charging of the double layer insures that the charging current, i_c, will decay to a negligible level in the shortest time possible. A rapid decay of the charging current is desirable because in those studies, where the faradaic current must be measured at time intervals shortly following application of the pulse, the charging current represents a noise signal of unknown magnitude.

A number of factors affecting the response time of the potentiostat were discussed earlier in this section. In the case of a potential step experiment, two additional factors must be considered: (1) the electrode area and (2) the resistance between the counter and reference electrodes, R_s, which defines the R_sC time constant controlling the potentiostat's rise time (C is the capacitance of the solution-electrode double layer and is proportional to electrode area). The current required to charge the double layer is directly proportional to C and hence to the electrode area. Because the current follower has a finite current capacity, the electrode area should be kept as small as possible. This has the effect of decreasing the current required to charge the double layer and decreasing the R_sC time constant for the rise-time of the potentiostat. By placing the counter electrode as close as is chemically and physically feasible to the Luggin capillary, the resistance R_s and hence the time constant R_sC can be further reduced.

The current follower feedback resistance, R_f, is also important in determining the time required to charge the solution-electrode double layer. If an R_f of 1 kohm is used, the 12 V voltage limit for

the operational amplifier will then allow for a maximum of 12 mA to charge the double layer. However, if an R_f of 200 ohms is used, the 50-mA current capacity of the current follower may be completely utilized before voltage limiting occurs.

Potential-step experiments on the 1 M $K_2C_2O_4$ background electrolyte with an iR compensation of 49 ohms, gave a plot of log i_c vs. time for t > 15 μs, which was linear within experimental uncertainty (Figure 12). Since the charging current should decay exponentially with time, the negative deviation from a linear response before 15 μs had elapsed may be due to some residual effects from the ringing of the voltage and current followers which was observed for the first 2 μs following application of the pulse. (Reduction of iR compensation only prolonged the ringing and the time required to charge the double layer.) The charging current decayed to a level. which was less than the peak to peak noise level of 56 μA, within 70 μs.

In a diffusion-controlled process, the faradaic current is expected to decay as a function of $t^{-\frac{1}{2}}$. In a plot of i vs. $t^{-\frac{1}{2}}$ for 1.57 mM Fe(III) in 1 M $K_2C_2O_4$ such behavior was observed within the 68% uncertainty bars for t > 100 μs (Figure 13). The attempt to extend the linear range of this plot into a shorter time range by subtracting the charging current for the 1 M $K_2C_2O_4$ solution from the total current observed in the presence of Fe(III) was not successful.

For the potential-step technique, it appears that the shortest time period following the application of the pulse, for which reliable faradaic current can be measured, is 100 μs. On this time scale, heterogeneous rate constants as large as 0.1 to 0.2 cm/s can be

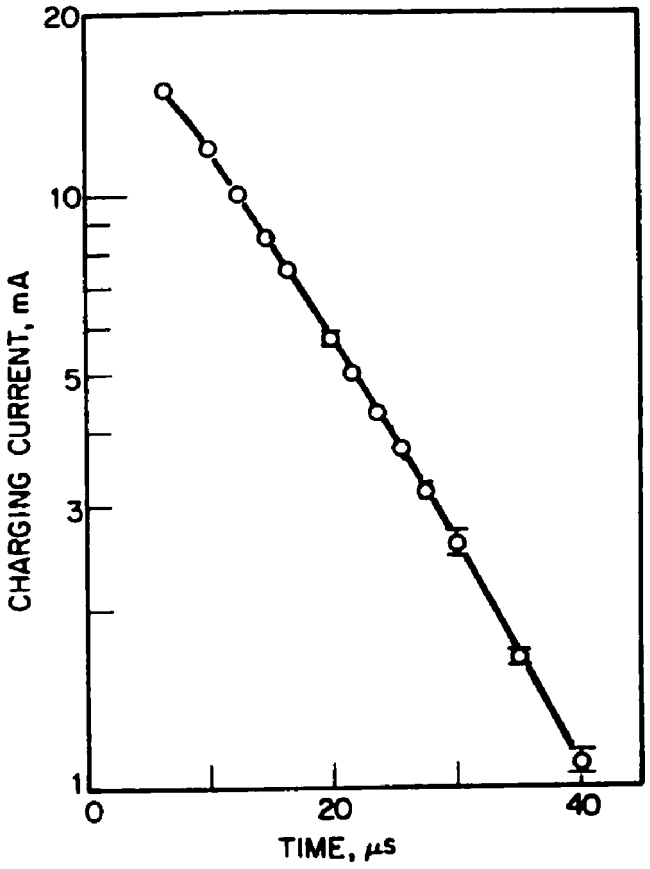


Figure 12. Charging current-time behavior (log i_c vs. t) for 1 M $K_2C_2O_4$ solution on potential-step chronoamperometry. Potential-step is from -0.16 to -0.56 V; 49 ohms of iR compensation was used.

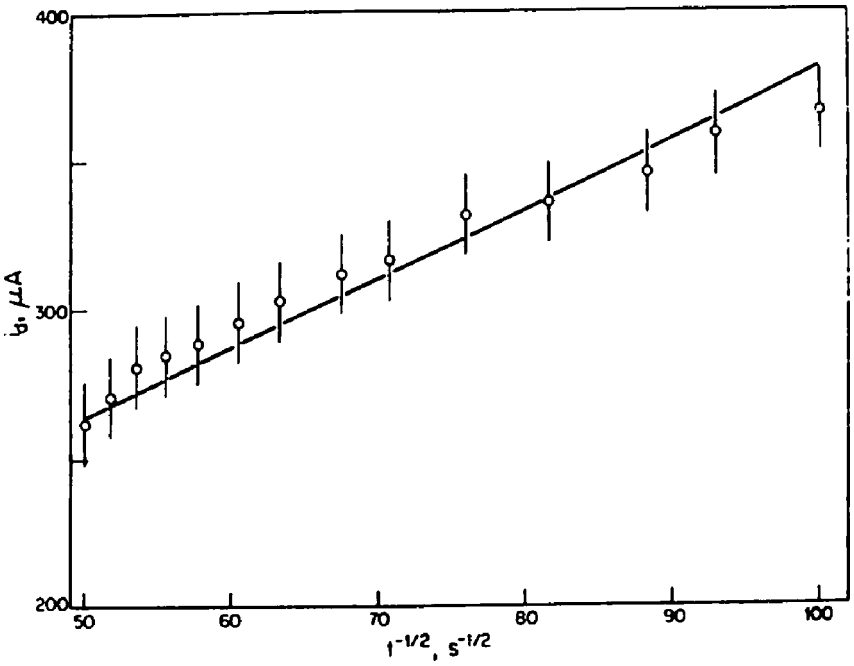


Figure 13. Current vs. time relationship for 1.56 mM Fe(III) in 1 M $K_2C_2O_4$ obtained on potential-step chronoamperometry, which demonstrates diffusion-control. Potential-step is from -0.16 to -0.56 V; uncertainty bars show a 68% confidence interval based on a peak noise level equal to 3 standard deviations.

determined by potential-step (32); first-order rate constants on the order of 10^4 to 10^5 s^{-1} associated with an ECE (charge transfer followed by a chemical reaction which produces an electroactive species) mechanism (33), first-order rate constants on the order of 10^4 s^{-1} associated with an EC (charge transfer followed by a chemical reaction) mechanism (34), and, at a concentration of 0.3 mM, dimerization rates of the order of 10^7 M^{-1} s^{-1} (35) can be evaluated by double potential-step.

d. AC Polarography. AC polarographic studies of 1.59 mM Fe(III) in 1 M $K_2C_2O_4$ solution and 1 M $K_2C_2O_4$ solution with no Fe(III) present were made over a frequency range from 600 to 15,000 Hz. The perturbation signal was a 5-mV peak ac modulation voltage.

The gain for the lock-in amplifier (PAR Model 121 lock-in amplifier/phase detector) was adjusted, at each frequency used, to give a 5-mV output when the applied ac voltage was fed into the signal input of the lock-in amplifier. Since the ac current is proportional to the ac voltage, this serves as an internal correction for any error in setting the amplitude of the ac modulation voltage. The fact that the apparent current response is normalized for variations in the applied ac potential means that such parameters as $I(\omega t)/\Delta E$ and ϕ, where $I(\omega t)$ is the ac faradaic current, ΔE is the applied potential at the working electrode and ϕ is the phase angle of the faradaic current, will be correct. The applied ac potential, as it appears at the voltage follower output when the potentiostat is in the standby mode, is defined as the 0° reference signal. The ac data were analyzed using the procedure outlined by Smith (20) which was discussed previously.

The onset of phase shifts brought about by the response time limitations of the operational amplifiers, is one of the important factors which determine the upper limit of the frequency range at which meaningful ac polarographic data can be obtained. Since the parameters being examined could be obtained only if valid phase relationships were retained, it was necessary to insure that the operational amplifiers in the potentiostat did not change the phase of the applied ac voltage. Phase angle shifts in the controller-voltage follower loop were examined by comparing the phase angle of the ac voltage at the voltage follower output with the ac voltage generated by the lock-in amplifier. The lock-in reference signal output, which is defined as having 0° phase, is connected to the potentiostat external input and the quadrature component (90° out of phase with the reference signal) of the voltage follower output is monitored by the lock-in. If no phase shift has occurred through the controller and voltage follower, the voltage follower output should have no quadrature component. Under the conditions of a current load in the cell mode and of no current load in the standby mode, no phase shift in the applied ac voltage was observed in the controller-voltage follower loop in the frequency range from 600 to 15,000 Hz.

By monitoring the ac capacitive current, i_c', at a fixed E_{dc} for the 1 $\underline{M}$ $K_2C_2O_4$ solution, it was possible to determine whether there was a phase shift occurring in the current follower. A plot of $i_c'/\Delta E$ should be linear with frequency, f. Since the calculations of ΔE are based on a properly measured phase angle for the capacitive current,

a phase shift in the current follower would result in a non-linear relationship for $i_c'/\Delta E$ vs. f and in variations in the calculated uncompensated resistance. When the ac charging current for 1 M $K_2C_2O_4$ was measured at E_{dc} = -0.245 V and was normalized for variations in ΔE due to the uncompensated resistance, the resulting plot of $i_c'/\Delta E$ vs. f was linear over the range to 600 to 15,000 Hz (Figure 14). Calculations of the uncompensated resistance ranged from 88 ohms at 600 Hz to 78 ohms at 15,000 Hz. In view of the linearity of the $i_c'/\Delta E$ vs. f plot, this slight variation in the calculated uncompensated resistance is not considered significant.

The ac faradaic response of 1.59 mM Fe(III) in 1 M $K_2C_2O_4$ was studied over the same frequency range. The summit currents, $I_s(\omega t)$, normalized for changes in ΔE, are plotted vs. $\omega^{1/2}$ ($\omega = 2\pi f$) in Figure 15. The linearity of the plot indicates that, at frequencies up to 15,000 Hz, the Fe(III)/Fe(II) redox couple is behaving reversibly. At the summit potential, E_s, the phase angles, ϕ_s, observed for the reduction of Fe(III) (Table III) are slightly greater than the 45° phase angle predicted for a reversible diffusion-controlled process. However, at the larger values of ω, 45° does lie within the experimental uncertainty of the phase-angle determinations. All phase angles at the polarographic $E_{1/2}$ have experimental uncertainties which include 45°.

Since a plot of the normalized faradaic summit current vs. $\omega^{1/2}$ defines a linear relationship with a zero intercept, it is unlikely that the deviation of ϕ_s from 45° represents either experimental or instrumental error, inasmuch as the evaluation of $I_s(\omega t)$ and ϕ_s are dependent on the same parameters and the evaluation of ϕ_s is dependent

Table III. AC Polarographic Faradaic Response of 1.59 m$\underline{M}$ Fe(III) in 1 $\underline{M}$ $K_2C_2O_4$[a]

f	ω	$\phi_{\frac{1}{2}}$[b]	$-E_s$	$\Delta E_{w,s}$[c]	$I_s(\omega t)$	$I_s(\omega t)/\Delta E_{w,s}$	ϕ_s[d]
kHz	10^{-4} s^{-1}	degr.	V	mV	μA	μA/mV	degr.
0.60	0.377	45	0.245	4.24 (0.04)	8.8 (0.13)	2.1 (0.04)	47 (1.3)
1.50	0.942	47	0.245	3.74 (0.03)	12.2 (0.20)	3.3 (0.06)	48 (1.7)
3.00	1.89	47	0.245	3.14 (0.03)	14.5 (0.34)	4.6 (0.12)	47 (2.8)
4.50	2.83	49	0.250	2.72 (0.03)	15.2 (0.52)	5.6 (0.20)	51 (4.0)
6.00	3.77	50	0.245	2.40 (0.03)	14.9 (0.68)	6.2 (0.29)	50 (5.5)
9.0	5.66	50	0.250	1.93 (0.03)	14.6 (1.03)	7.7 (0.54)	53 (9.0)
15.0	9.42	53	0.250	1.33 (0.02)	14.6 (2.19)	10.3 (1.66)	51 (22.1)

[a] Values in parentheses are 95% confidence interval; uncertainties shown in parentheses are based on maximum errors equal to three population standard deviations and assume maximum errors of (a) ±0.01" mechanical measuring error plus 1% of signal for each phase selective signal, (b) ±0.2° for the measured phase angle, and (c) ±1% of full scale in setting the lock-in gain for the voltage follower output. Subscript s indicates value at ac summit potential. Phase angles, ϕ, are in degrees relative to working electrode ac voltage.

[b] Phase angle at dc polarographic $E_{1/2}$.

[c] $\Delta E_{w,s}$ is the working electrode ac modulation potential at the ac summit potential, E_s. The rms value would be 0.707 $\Delta E_{w,s}$.

[d] Phase angle at the ac polarographic summit potential.

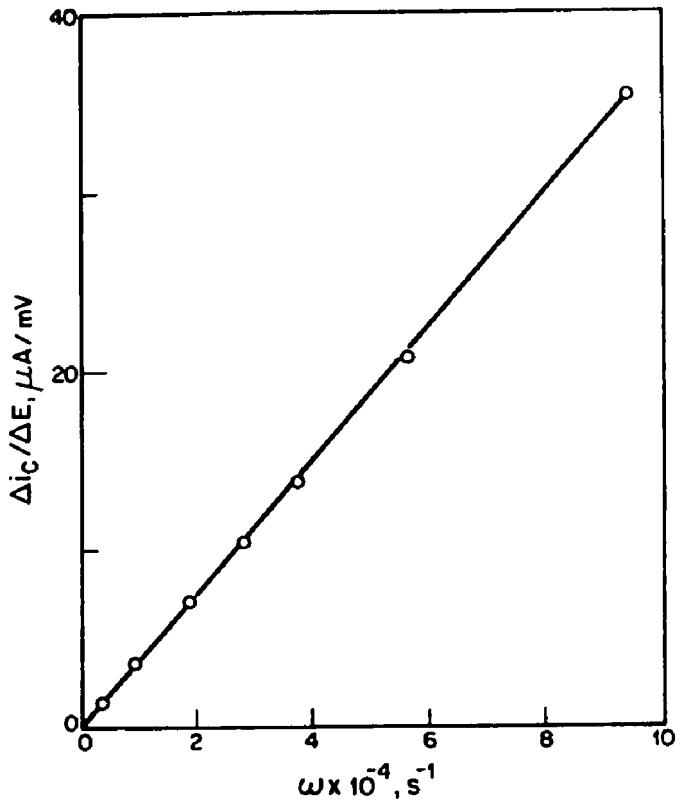


Figure 14. Relationship of the normalized charging current with frequency for ac polarograms of 1 M $K_2C_2O_4$ solution over a frequency range of 600 to 15,000 Hz. Controlled drop-time = 2.0 s; ac modulation voltage = 5 mV peak; E_{dc} = -0.245 V.

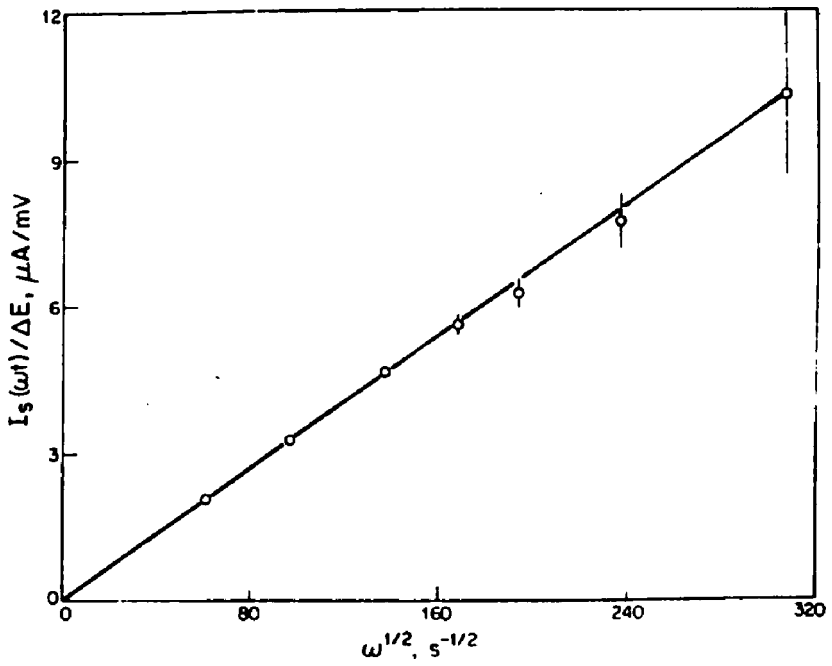


Figure 15. Relationship of faradaic summit current, $I_s(\omega t)$, with $\omega^{\frac{1}{2}}$ ($\omega = 2\pi f$) for ac polarograms of 1.59 m$\underline{M}$ Fe(III) in 1 $\underline{M}$ $K_2C_2O_4$. Controlled drop-time = 2.0 s; ac modulation voltage = 5 mV peak.

on $I_s(\omega t)$. The precise reason for the slight variation in phase angles at the summit potential from the predicted values is not clear.

The nearly reversible behavior of the Fe(III)/Fe(II) redox couple at frequencies up to 15,000 Hz demonstrates that the potentiostat is performing well up to this frequency. Frequencies greater than 15,000 Hz were not examined because, at higher frequencies, the magnitude of the charging current was sufficiently large that, even with phase-selective current detection, the uncertainty in the determination of $I_s(\omega t)$ was untenably large.

III. REDUCTION OF NAD^+

A. Initial One-Electron Reduction

The initial step in the reduction of NAD^+ is a one-electron transfer to the nicotinamide moiety, which produces an uncharged free radical. The free radical rapidly dimerizes, forming a bond at the C(4) carbons of the nicotinamide moieties (14).

$$NAD^+ + e \rightleftharpoons NAD\cdot \xrightarrow{k_d} 0.5(NAD)_2 \qquad (11)$$

1. Effect of Background Electrolyte

a. DC and AC Polarography. In the presence of a background electrolyte, whose cation has a low surface activity, e.g., KCl or NH_4Cl, NAD^+ is adsorbed at the solution-electrode interphase of a dme in the potential range where reduction takes place. The dimer, which is subsequently formed, is also adsorbed (4). If the cation of the electrolyte is only weakly adsorbed, the adsorption of NAD^+ and the dimer will be a dominant force in shaping the electrochemical response of the $NAD^+/NAD\cdot$ redox couple. Hence, the characteristics of the couple

are relatively constant regardless of whether KCl or NH_4Cl was used as a background electrolyte. A summary of the dc and ac polarographic data showing the effect of replacing KCl with NH_4Cl is given in Table IV.

The dc polarograms of 0.42 mM NAD^+ were essentially unaltered when KCl was replaced with NH_4Cl at a constant ionic strength. In the dc polarograms, $E_{1/2}$ = -0.897 ± 0.003 V and the slope of the polarographic wave ($E_{1/4}$ - $E_{3/4}$) = 63 ± 2 mV for all of the mixtures which were run.

As the NH_4^+ concentration was increased, the ac polarographic data showed a small positive shift in the summit potential, E_s, for the reduction of NAD^+ and a slight decrease in the in-phase current (Table IV). Since ac polarography is inherently more sensitive to changes in adsorption phenomena, these slight changes probably reflect modest changes in the adsorption equilibria involving NAD^+ and the background electrolyte cation as K^+ is replaced with NH_4^+.

Although semiquantitative observations on the ease of reducibility, $E_{1/2}$, can be made, little kinetic data, i.e., rates of charge transfer and of homogeneous reactions involving redox participants, can be determined from the electrochemical response of the $NAD^+/N\dot{A}D$ redox couple when the adsorption of both the reducible species and the final product dominates the observed electrochemical response of the redox couple. For this reason, the $NAD^+/N\dot{A}D$ redox couple was also studied in the presence of the tetraethylammonium ion (Tea^+), which is more strongly adsorbed than NAD^+ or $(NAD)_2$ in the potential region where NAD^+ is reduced to the free radical.

Table IV. Polarographic Data for the One-electron Reduction of NAD^+. Effect of Replacing KCl with NH_4Cl at Constant pH and Ionic Strength[a]

DC Polarography

KCl/NH_4Cl	$-E_{1/2}$	$E_{1/4} - E_{3/4}$	I_d[b]
M/M	V	mV	
0.40/0.00	0.900	62	1.22
0.36/0.04	0.897	62	1.19
0.32/0.08	0.897	64	1.18
0.24/0.16	0.899	63	1.26
0.08/0.32	0.896	62	1.14
0.00/0.40	0.894	65	1.20

AC Polarography[c]

KCl/NH_4Cl	$-E_s$[d]	$E_{+s/2} - E_s$	$E_s - E_{-s/2}$	i_s[g]
M/M	V	mV	mV	nA
0.40/0.00	0.984	72	70	136
0.36/0.04	0.980	80	75	130
0.32/0.08	0.980	82	72	124
0.24/0.16	0.972	67	73	124
0.08/0.32	0.970	64	70	121

[a] All solutions are 0.42 mM in NAD^+ at pH 9.1 with μ = 0.4 M.

[b] Polarographic diffusion current constant: $I_d = i_d/Cm^{2/3}t^{1/6}$, where i_d is the average diffusion current, m is the mercury flow rate, and t is the drop time.

[c] Measurements at 40 Hz with a 5-mV peak ac modulation voltage.

[d] AC polarographic in-phase summit potential.

[e] Potential on the positive side of the ac polarographic peak where the in-phase current is one-half of i_s.

[f] Potential on the negative side of the ac polarographic peak where the in-phase current is one-half of i_s.

[g] In-phase summit current.

The effect of replacing K^+ with Tea^+ has been previously studied (4) and will not be discussed in great detail. The most notable change observed, when Tea^+ was substituted for K^+ at the 0.4 M level, was a decrease in the ease of reducing NAD^+ as evidenced by a shift in $E_{1/2}$ for the reduction to a potential 130 mV more negative. The increased ease of reducing NAD^+ in the presence of a weakly adsorbed cation such as K^+ or NH_4^+ can be explained in terms of the relative strengths of adsorption of the starting material NAD^+ and the end products $NA\dot{D}$ and $(NAD)_2$.

When a species is adsorbed, the free energy of the species decreases. In an electrochemical reduction, adsorption of the starting material will have the effect of making the reduction more difficult, since the potential required for the reduction of the adsorbed species must be increased to overcome the stabilization of the energy of adsorption. Correspondingly, stabilization of the end product by adsorption, will enhance the ease of reducing the starting material since the adsorption decreases the free energy of the product (36). Since adsorption of both NAD^+ and its reduction products has the effect of increasing the ease of reducing NAD^+, the stabilization of the reduction products, i.e., $NA\dot{D}$ and $(NAD)_2$ through adsorption at the solution-electrode interphase, must be greater than the stabilization of the starting material NAD^+.

In the presence of 0.4 M TeaCl and 0.1 M carbonate at pH 9.1, the reduction of NAD^+ to $NA\dot{D}$ showed a dc polarographic wave with an $E_{1/2}$ of -1.035 V. A plot of E vs. log $[i/(i_d - i)]$ (Figure 16), where i_d is the diffusion limited current and i is the current at potential

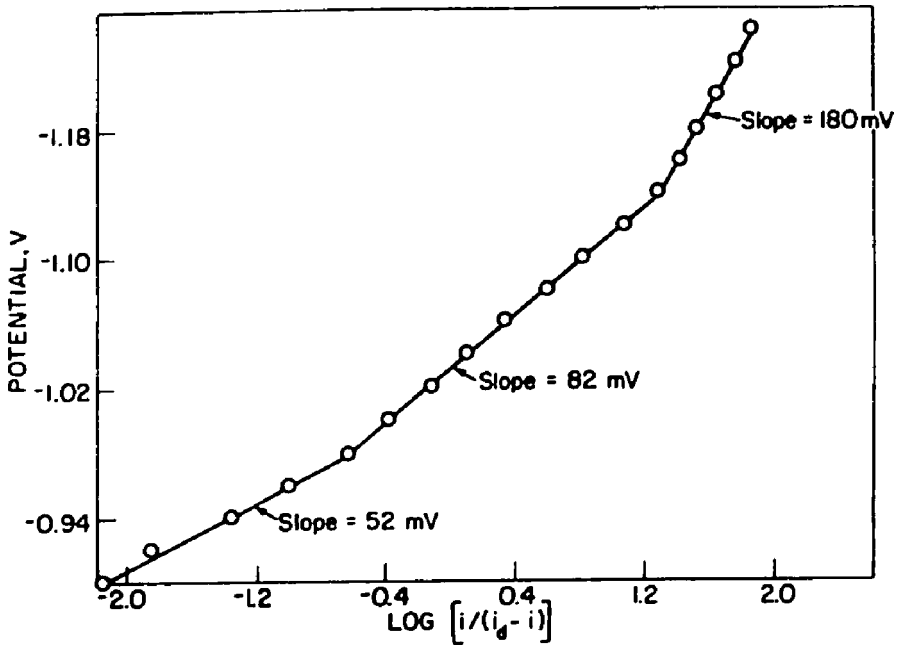


Figure 16. Logarithmic analysis of dc polarographic current-potential relationship for 0.88 mM NAD^+ in 0.4 M TeaCl and 0.1 M carbonate at pH 9.1. i_d is the maximum diffusion-limited current; i is the maximum current at potential E.

E, was non-linear with a slope of 52 mV at the foot of the polarographic wave and a slope of 180 mV near the plateau of the wave.

The theoretical current-potential relationship for a reversible one-electron transfer followed by an irreversible dimerization at 25°C. is given by equation 12 (37).

$$E = E_c^\circ - 0.059 \log \frac{i^{2/3}}{i_d - i} - 0.0197 \log \frac{1.5\ F\ m}{\lambda_f^2\ C_o} \qquad (12)$$

where $m = D_o/\delta$, $\lambda_f^2 = (\delta^2 k_d)/D_o$, C_o is the concentration of the oxidized species, D_o is the diffusion coefficient of the oxidized species, k_d is the dimerization rate constant, δ is the thickness of the diffusion layer, and F is Faraday's constant.

From equation 12, it is apparent that, under conditions where $i \ll i_d$, i.e., at the foot of the dc polarographic wave, a plot of E vs $\log [i/(i_d - i)]$ approaches a limiting value of 39 mV. Under conditions where $(i_d - i) \ll i$, i.e., near the plateau of the dc polarographic wave, a plot of E vs. $\log [i/(i_d - i)]$ approaches a limiting slope of 59 mV.

Thus, the plot of E vs $\log [i/(i_d - i)]$ for the NAD^+ reduction has substantially larger slopes than those predicted by equation 12 both at the foot and near the plateau of the polarographic wave. These larger slopes indicate that the NAD^+ reduction wave is more drawn out than the wave which would be predicted from equation 12.

The drawn-out character of the NAD^+ polarographic wave could be caused by some type of physical interaction between NAD^+ and the product of the reduction, $(NAD)_2$, e.g., the formation of a charge transfer complex. The ability of NAD^+ to form charge transfer

complexes with species containing a reduced nicotinamide moiety has been well established (38,39). Since the nicotinamide moiety of NAD^+ has a net positive charge, while the dimer nicotinamide moieties are uncharged, a physical interaction of the type mentioned would serve to increase the electron density in the nicotinamide moiety of NAD^+ and, hence, make NAD^+ more difficult to reduce. The effects of the physical interaction would be expected to be most prominent in that potential region of the dc polarographic wave where the concentration of $(NAD)_2$ is the greatest, i.e., near the plateau of the polarographic wave. A comparison of experimental and theoretical slopes shows that at the foot of the wave the experimental slope is 40% greater than the theoretical slope while near the plateau of the wave the experimental slope is 300% greater than the theoretical slope. Since the type of chemical interaction which is responsible for the non-theoretical behavior of the first NAD^+ reduction wave in the presence of Tea^+, is most dominant in that potential region of the wave where the concentration of reduction products is greatest an interaction between NAD^+ and its reduction products is indicated.

b. Cyclic Voltammetry. Slow-scan cyclic voltammograms of NAD^+ at a hmde also show a slope, $E_{p/2} - E_p$, which is greater than the predicted slope of 39 mV for a reversible charge transfer followed by a rapid dimerization (40). At a scan rate of 30 mV/s, a 0.50 mM NAD^+ solution, which was 0.4 M in TeaCl and 0.1 M in carbonate at pH 9.1 at 25°C., gave a slope of 65 mV. When the scan rate was increased to 240 mV/s, the slope decreased to 57 mV. At 1°C, a solution 0.60 mM in NAD^+ gave a slope of 66 mV at 30 mV/s and a slope of 60 mV at 240 mV/s.

The chemical interaction of starting material and reduction product discussed in the previous section would be expected to produce the deviation from predicted current-potential behavior which was observed in the slow-scan cyclic voltammograms. As the potential is scanned into the potential region where NAD^+ is reduced to $\dot{NAD}$, which subsequently dimerizes, the $(NAD)_2$ which is formed can react with the NAD^+ making the remaining NAD^+ more difficult to reduce. The increased difficulty in reducing NAD^+ would tend to draw out the voltammetric peak, resulting in a value of $E_{p/2} - E_p$ which is greater than the theoretically predicted value.

The fact that the peak becomes more steep as the scan rate is increased from 30 to 240 mV/s indicates that the chemical interaction between NAD^+ and its reduction products is sufficiently slow that the reaction is beginning to be outrun at a scan rate of 240 mV/s.

2. Effect of Lewis Acids: Ca(II)

a. DC and AC Polarography. Dc and ac polarographic behavior of mixtures of 0.42 mM NAD^+ and Ca(II) were studied at pH 7.2 and pH 9.3 in 0.1 M tetraethylammonium perchlorate (Teap) and 0.01 M Tris buffer (the pH was adjusted by addition of $HClO_4$). Additions of $Ca(ClO_4)_2$ were made to give a concentration range from 0.25 mM to 100 mM. The addition of Ca(II) had little effect on the dc polarographic wave until sufficient Ca(II) was added to raise significantly the ionic strength of the solution. At that point, the slope of the dc wave became more steep, $E_{\frac{1}{2}}$ shifted 15 mV positive and the diffusion current constant, I_d, decreased 10-15% (Table V).

Table V. DC Polarographic Data for the One-electron Reduction of NAD^+ in the Presence of $Ca(ClO_4)_2$.[a]

Ca(II)	$E_{1/2}$	$E_{1/4} - E_{3/4}$	I_d[b]
mM	V	mV	
	pH 7.2		
0	-1.077	64	1.17
0.50	-1.073	58	1.14
5.0	-1.073	56	1.18
50	-1.058	61	1.05
	pH 9.3		
0	-1.074	63	1.17
0.50	-1.073	58	1.04
10.0	-1.070	62	1.10
50	-1.063	57	1.05
100	-1.056	53	0.99

[a] All solutions are 0.42 mM NAD^+ in 0.10 M Teap and 0.01 M Tris.

[b] Polarographic diffusion current constant = $i_d/Cm^{2/3}t^{1/6}$.

Essentially the same behavior was observed for the ac polarographic response of NAD^+ when Ca(II) was added (Table VI). At low Ca(II) concentrations, changes in the ac peak were slight. At the 50 and 100 mM Ca(II) levels, the ac summit potential, E_s, was shifted 10-25 mV more positive, the half-peak width decreased, and the peak became broader on the negative side of the summit potential (in the absence of Ca(II), the peak was broader on the positive side of E_s).

Since adding Ca(II) at the 50 or 100 mM level has the effect of producing an ac polarographic response for the reduction of NAD^+, which more closely approximates the response predicted for a reversible charge transfer followed by an irreversible dimerization (41), it appears that the addition of Ca(II) must do at least one of the following: (1) increase the rate of charge transfer and/or (2) decrease an intermolecular interaction between NAD^+ and its reduction products. These two alternatives can not be distinguished solely on the basis of changes in the ac and dc polarographic behavior.

b. Cyclic Voltammetry. Rapid-scan cyclic voltammetric studies (v > 100 V/s) of NAD^+ in the presence and absence of Ca(II) suggest that large Ca(II) concentrations have the affect of increasing the rate of charge transfer. The heterogeneous charge transfer rate constant, $k_{s,h}$, has units of cm/s. The product of the charge transfer rate times the concentration (M/cm^3) of electroactive species in the solution-electrode interphase is equivalent to the moles of electroactive species which undergo charge transfer per unit of electrode area per second.

Table VI. AC Polarographic Data for the One-electron Reduction of NAD^+ in the Presence of $Ca(ClO_4)_2$[a]

Ca(II) mM	$-E_s$ V	$E^b_{+s/2} - E_s$ mV	$E_s - E^c_{-s/2}$ mV	ϕ_s[d]	$I(\omega t)$[e] nA
		pH 9.6; 40 Hz			
0	1.128	60	57	16°	160
0.50	1.125	56	58	13°	170
50	1.108	52	56	12°	170
100	1.103	51	55	12°	170
		pH 9.6; 100 Hz			
0	1.133	64	57	18°	180
0.50	1.133	62	57	17°	200
50	1.116	55	59	16°	200
100	1.105	53	55	14°	180
		pH 7.2; 40 Hz			
0	1.122	65	55	15°	180
0.50	1.122	61	58	14°	200
5.0	1.119	59	54	15°	180
50	1.112	55	52	14°	170
		pH 7.2; 100 Hz			
0	1.129	68	60	17°	210
0.50	1.130	65	59	17°	220
5.0	1.130	59	59	18°	210
50	1.117	56	57	14°	190

Table VI. Continued - AC Polarographic Data for the One-electron Reduction of NAD^+ in the Presence of $Ca(ClO_4)_2$[a]

Ca(II) mM	$-E_s$ V	$-E^b_{+s/2} - E_s$ mV	$E_s - E^c_{-s/2}$ mV	ϕ_s[d]	$I(\omega t)$[e] nA
		pH 7.2; 400 Hz			
0.0	1.134	72	61	27°	290
0.50	1.135	67	60	25°	310
5.00	1.128	67	64	27°	300

[a] All solutions are 0.42 mM NAD^+ in 0.10 M Teap and 0.10 M Tris.

[b] Defined in Table IV.

[c] Defined in Table IV.

[d] Phase angle at the ac polarographic peak potential.

[e] Total faradaic current.

In 0.1 M Teap and 50 mM Ca(II) with a 0.01 M Tris buffer adjusted to pH 9.3, 0.30 mM NAD^+ shows a charge transfer with a cathodic E_p of -1.18 ± 0.005 V, a slope of 60 ± 5 mV for $E_{p/2} - E_p$ of the cathodic peak and a separation of 60 mV between the cathodic and anodic peaks for a scan rate of 200 V/s. The slope and peak separation indicate that, at 200 V/s for the solution conditions specified, the rate of charge transfer is sufficiently rapid to appear reversible, i.e., $k_{s,h}$ exceeds 1 cm/s, and any homogeneous reactions involving redox participants are being outrun (31). In the absence of Ca(II), the potential separation between cathodic and anodic peaks is 116 mV; this peak separation corresponds to a charge transfer rate of 0.2 cm/s (42).

Since the dimerization and any interaction involving NAD^+ are being outrun at a scan rate of 200 V/s, the changes in voltammetric behavior brought about by the addition of Ca(II) must be due to an increase in the rate of charge transfer. This does not prove, however, that Ca(II) would not also affect an intermolecular interaction between NAD^+ and the dimer.

3. Effect of Lewis Acids: Zn(II)

a. DC and AC Polarography. The addition of 0.42 mM NAD^+ (final concentration) to 1 mM Zn(II) at pH 7.2 brought about quite striking changes in the electrochemical behavior of the Zn(II)/Zn redox couple. In the absence of NAD^+, Zn(II) in 0.10 M Teap and 0.01 M Tris buffer at pH 7.2 showed a kinetically controlled wave with a slope of 92 mV and $E_{½}$ = -1.41 V. The ac polarographic peak corresponding to this wave had a summit potential of -1.510 V and a half-peak width of 214 mV.

When 0.42 mM NAD^+ was added to the Zn(II) solution, the foot of the dc Zn(II) wave shifted positive and overlapped the NAD^+ reduction wave, whose $E_{1/2}$ = -1.07 V. The shift of the Zn(II) wave was time-dependent with an overall shift in $E_{1/2}$ of 260 mV in four hours. When NAD^+ was first added to Zn(II), three waves appeared. The first came in the region where one would expect to see the wave corresponding to the reduction of NAD^+. Before this wave reached a plateau, a second wave of roughly equal height began. This wave also did not reach a plateau but was overlapped by a third layer wave which apparently was due to the reduction of Zn(II). With time, the third wave shifted positive, beginning to merge with the first two waves. The second wave began to develop into a sharp polarographic maximum about two-thirds of the way up the third wave. A second sharp maximum appeared at the top of the third wave. As the third wave continued to shift positive, the first maximum disappeared leaving behind an inflection in the slope of the third wave in the potential region where this maximum had previously been observed. The second maximum remained at the top of the third wave and became quite broad. A series of dc polarographic curves for the NAD^+-Zn(II) mixture appear in Figure 17. When Zn(II) was then precipitated by adding Na_2HPO_4, the NAD^+ wave reappeared and was the same within experimental error as the NAD^+ wave in the absence of Zn(II); the only difference was a 6% decrease in the diffusion current constant which may have been due to some hydrolytic decomposition of the NAD^+.

The ac polarographic response of the NAD^+-Zn(II) mixture was compatible with the dc polarographic behavior. When NAD^+ was added

Figure 17. (A) Variation of the dc polarographic behavior of mixtures of Zn(II) and NAD^+ in 0.10 M Teap and 0.01 M Tris at pH 7.2. Solution composition and nature: 1, 1 mM Zn(II); 2, solution 1 plus 0.42 mM NAD^+, 80 minutes after addition of NAD^+; 3, solution 2, 100 minutes after addition of NAD^+; 4, solution 2, 245 minutes after addition of NAD^+; 5, solution 4 after Zn(II) was precipitated with Na_2HPO_4.

(B) Variation of the ac polarographic behavior (in-phase current) of mixtures of Zn(II) and NAD^+ in 0.10 M Teap and 0.01 M Tris at pH 7.2. Solution composition and nature: 1, 1 mM Zn(II); 2, solution 1 plus 0.42 mM NAD^+, 85 minutes after addition of NAD^+; 3, solution 2, 145 minutes after addition of NAD^+; 4, solution 2, 235 minutes after addition of NAD^+; 5, solution 4 after Zn(II) was precipitated with Na_2HPO_4. Controlled drop-time = 2.0 s; ac modulation voltage = 5 mV peak; frequency 100 Hz.

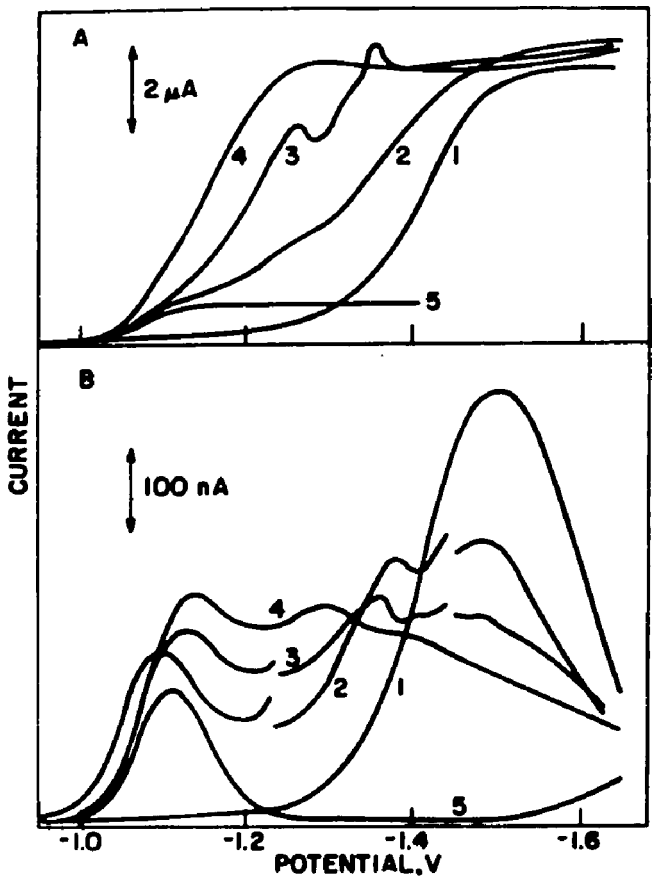


Figure 17.

to Zn(II), three peaks were formed. The first peak, corresponding to reduction of NAD^+ to $\dot{NAD}$, increased in amplitude and shifted negative with time. The Zn(II) peak split into two peaks, both of which shifted positive and decreased in amplitude. A series of ac polarographic curves for the mixture is given in Figure 17.

In order to determine whether NAD^+ was responsible for the shift in the Zn(II) wave, dc and ac polarograms were run for a solution of 1 m$\underline{M}$ Zn(II) in 0.10 $\underline{M}$ Teap and 0.01 $\underline{M}$ Tris buffer at pH 7.2 over a three hour period. No shift in $E_{\frac{1}{2}}$ or E_S was observed. Sufficient adenosine diphosphoribose (ADPR) was added to the Zn(II) solution to give a concentration of 0.5 m$\underline{M}$ ADPR. (ADPR is similar to NAD^+ except that it does not contain the nicotinamide moiety.) After 2½ hours, a dc polarogram showed that $E_{\frac{1}{2}}$ for Zn(II) had shifted only 5 mV negative. After over three hours, the total shift was 10 mV. Comparable shifts in the summit potential, E_S, were observed for the ac polarograms.

At this point, sufficient 1-methylnicotinamide was added to give a concentration of 0.5 m$\underline{M}$. The dc polarogram run 45 minutes later showed that the Zn(II) wave had shifted 210 mV positive. Because of this shift the wave for 1-methylnicotinamide could not be resolved. The composite wave had an $E_{\frac{1}{2}}$ of -1.193 V and a slope of 135 mV. AC polarograms of the mixture revealed that the Zn(II) peak had split into two peaks with summit potentials of -1.250 and -1.490 V. An E_S for 1-methylnicotinamide could not be resolved because it was overlapped by the more positive of the two Zn(II) peaks. During an additional 40 minute period, there was no change in the ac polarogram. The series of dc and ac polarograms for the experiments described are

given in Figure 18.

The behavior of the Zn(II)/Zn redox couple in the presence of ADPR and 1-methylnicotinamide suggests that the nicotinamide moiety is in some fashion responsible for the behavior of the Zn(II) wave.

b. Mechanism. The fact that the shifts in $E_{\frac{1}{2}}$ take place quite slowly in the presence of NAD^+ and occur in less than 45 minutes in the presence of 1-methylnicotinamide suggests two possibilities:

(1) Zn(II) complexes slowly with NAD^+ and more rapidly with 1-methylnicotinamide. The resulting complexed Zn(II) is either more easily reduced or is reduced in a manner akin to the following mechanism:

$$Zn(II)\text{-}NAD^+ + e^- \rightleftharpoons Zn(II)\text{-}NAD^{\cdot} \rightleftharpoons NAD^+ - - -Zn(I) \xrightarrow[\text{rapid}]{e^-} Zn^0 \qquad (13)$$

$$NAD^+ \xrightarrow{e^-} NAD^{\cdot}$$

(2) The reduction of Zn(II) is catalyzed by some decomposition product of NAD^+, which contains the nicotinamide moiety:

$$Nic^+\text{-}X + e^- \rightleftharpoons Nic^{\cdot}\text{-}X \xrightarrow{Zn(II)} Nic^+\text{-}X + Zn(I) \xrightarrow[\text{rapid}]{e^-} Zn^0 \qquad (14)$$

$$Nic^+\text{-}X \xrightarrow{e^-} Nic^{\cdot}\text{-}X$$

In the case of 1-methylnicotinamide, X = methyl group.

Since the ratio of Zn(II):NAD^+ was 5:2, it seems unlikely that a slow complexation with NAD^+, which could at most complex only 40% of the Zn(II), could bring about a shift of the entire dc polarographic Zn(II) wave. Therefore, it appears that the behavior of the Zn(II)/Zn redox couple is the product of a catalytic reduction (equation 14) via

Figure 18. (A) Variation of the dc polarographic behavior of mixtures of Zn(II), ADPR, and 1-methylnicotinamide in 0.10 M Teap and 0.01 M Tris at pH 7.2. Solution compositions and nature: 1, 1 mM Zn(II) at 5 and 180 minutes after the addition of Zn(II); 2, solution 1 plus 0.5 mM ADPR, 150 and 195 minutes after the addition of ADPR; 3, solution 2 plus 0.5 mM 1-methylnicotinamide, 45 and 120 minutes after the addition of 1-methylnicotinamide.

(B) Variation of the ac polarographic behavior (in-phase current) of mixtures of Zn(II), ADPR and 1-methylnicotinamide in 0.10 M Teap and 0.01 M Tris at pH 7.2. Solution composition and nature: 1, 1 mM Zn(II) at 10 and 170 minutes after the addition of Zn(II); 2, solution 1 plus 0.5 mM ADPR 160 and 200 minutes after the addition of ADPR; 3, solution 2 plus 0.5 mM 1-methylnicotinamide 60 and 100 minutes after the addition of 1-methylnicotinamide. Controlled drop-time = 2.0 s; ac modulation voltage = 5 mV peak; frequency = 100 Hz.

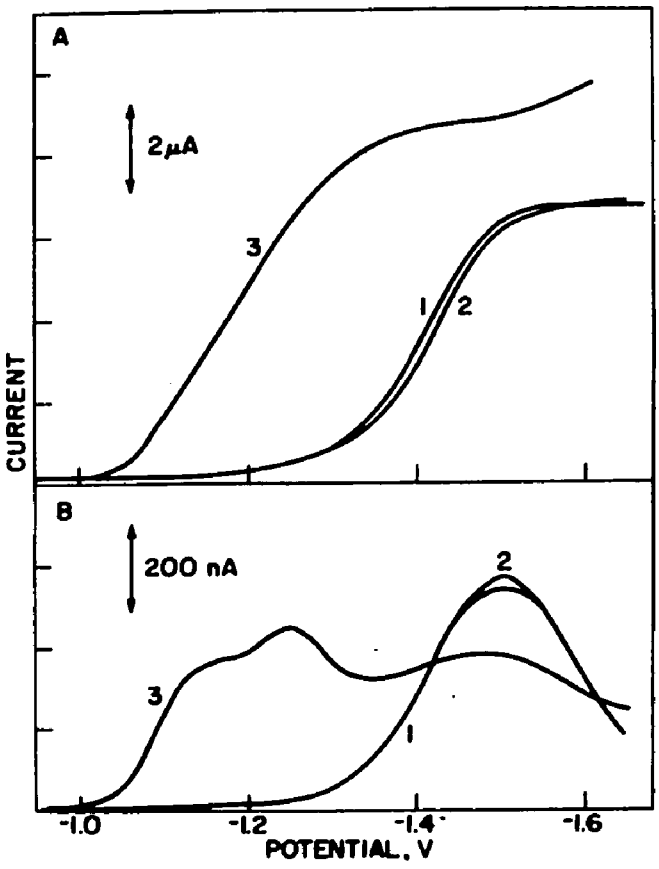


Figure 18.

one of the decomposition products of NAD^+. Since the changes in the Zn(II) redox couple were not brought about by intact NAD^+, this particular phenomenon was not examined further.

4. Dimerization of $NA\dot{D}$

The dimerization of $NA\dot{D}$ forming $(NAD)_2$ exerts a profound effect on the electrochemical response which is observed for the reduction of NAD^+ to $NA\dot{D}$. In order to get a clearer picture of this first reductive step, it was necessary to determine the rate constant, k_d, for the $NA\dot{D}$ dimerization. The three techniques, which were used to measure the dimerization rate, were double potential-step chronoamperometry, slow-scan cyclic voltammetry, and fast-scan cyclic voltammetry.

a. Double Potential-Step Chronoamperometry. The double potential-step method, using a pulse duration, τ, of 60 to 120 μsec and NAD^+ concentrations of 0.1 to 0.2 mM in 0.4 M TeaCl and 0.1 M carbonate buffer at pH 9.1 did not give overly reproducible determinations for the rate constant of the dimerization (35). For six determinations, an average k_d of 4×10^7 $M^{-1}s^{-1}$ with a standard deviation of 2.7×10^7 $M^{-1}s^{-1}$ was calculated. The primary difficulty with the double potential-step method was that the charging current following each of the potential steps was several times greater than the faradaic current, which resulted in an extremely poor signal:noise ratio. The rapid nature of the dimerization prohibited the use of larger concentrations of NAD^+ or longer τ values, either of which would have increased the ratio of the cathodic faradaic current to charging current, but would have decreased the anodic faradaic current.

b. Cyclic Voltammetry. Rate constants for the dimerization of an electrochemically generated free radical may be determined by fast-scan cyclic voltammetry providing scan rates can be obtained which are sufficiently rapid to be on a time scale which is competitive with the dimerization under conditions where the charge transfer is reversible. The determination of k_d is based on the behavior of the ratio of the cathodic to anodic peak currents as a function of scan rate, switching potential and concentration of reacting species (43).

In 0.4 M TeaCl and 0.1 M carbonate at pH 9.1, the reduction of NAD^+ to $NA\dot{D}$ shows a voltammetric response at scan rates of 200 to 500 V/s which is indicative of a reversible charge transfer within an experimental uncertainty of 5 mV in each peak potential. The minimum charge transfer rate constant, which would result in a separation of cathodic and anodic peaks that was contained within the uncertainty of the experimental peak separation at 500 V/s, is 1 cm/s at 25°C.

Using scan rates in the range of 250 to 500 V/s for NAD^+ concentrations of 0.30 and 0.50 mM, a k_d of $(2 \pm 0.3) \times 10^7$ $M^{-1}s^{-1}$ was determined at 25°C. (mean and standard deviation for six measurements).

Assuming that both NAD^+ and $NA\dot{D}$ have comparable diffusion coefficients, the formal redox potential for the $NAD^+/NA\dot{D}$ redox couple can be calculated from the voltammetric peak potential, E_p. The relationship of E_p to the reversible polarographic half-wave potential, $E_{1/2}$, for a reversible charge transfer is given by equation 15 (31).

$$E_p = E_{1/2} - \frac{28.5}{n} \text{ mV} \qquad (15)$$

where n is the number of electrons transfered in equivalents per mole.

Since the diffusion coefficients for the oxidized and reduced species are assumed to be equal, $E_{1/2}$ is equivalent to the formal redox potential. The formal redox potential for the $NAD^+/NAD\cdot$ redox couple in 0.4 M TeaCl and 0.1 M carbonate at pH 9.1, calculated from voltammetric peak potentials, was -1.155 V at 25°C. and -1.149 V at 1°C.

To determine the dimerization rate via slow-scan cyclic voltammetry, the peak potential, E_p, is observed as a function of scan rate, $\underline{v}$, at scan rates where the following condition is met;

$$\underline{v} < 3\ k_d\ C_o/n \quad mV/s \tag{16}$$

where C_o is the bulk concentration of the electroactive species.

Under these conditions, the peak potential, E_p, and peak current, i_p, are described by equations 17 and 18, respectively (40):

$$E_p = E^o - \left(\frac{RT}{3nF}\right) \ln \left[\frac{4.78\pi 3D_o}{2\ D_r}\right] - \left(\frac{RT}{3nF}\right) \ln \left(\frac{a}{k_d C_o}\right) \tag{17}$$

$$i_p = 0.526\ n\ F\ A\ D_o^{1/2}\ C_o\ a^{1/2} \tag{18}$$

where $a = nF\underline{v}/RT$, where R and T have the usual Nernst equation definitions, and D_r and D_o are the diffusion coefficients for the reduced and oxidized species, respectively. The rate constant for the dimerization was determined from a plot of $[E_p - (2.303\ RT/3nF)\log C_o]$ *vs.* $\log \underline{v}$. A linear least-squares fit of the data defined a line with a y-axis intercept which is described by the following equation, obtained by setting $\log \underline{v}$ equal to zero:

$$E_p - \left(\frac{2.303RT}{3nF}\right) \log C_o = E^o - \left(\frac{2.303RT}{3nF}\right) \log \left[\frac{4.78\pi 3D_o nF}{2D_r RT}\right] + \left(\frac{2.303RT}{3nF}\right) \log\ k_d \tag{19}$$

Determinations of k_d, based on the shift in E_p as a function of scan rate, were made at the same temperatures and concentrations of NAD^+, which were used in the fast-scan voltammetric determinations. At 25°C., using the previously determined E^0, $k_d = (3 \pm 1.7) \times 10^7$ $\underline{M}^{-1}s^{-1}$, while at 1°C. $k_d = (1.5 \pm 0.9) \times 10^7$ $\underline{M}^{-1}s^{-1}$. The uncertainties in k_d are based on the maximum and minimum values for the y-axis intercept, given in equation 19, assuming an uncertainty of ±3 mV in the determination of E_p. The linear least squares fit of the plot of $[E_p - (2.303RT/3nF) \log C_o]$ $\underline{vs}$. $\log \underline{v}$ defined a line whose slope agreed with the theoretically calculated slope of 19.7 mV/decade $\underline{v}$, at 25°C. within experimental uncertainty (Figure 19).

The determinations of k_d via all three methods give values of k_d which agree within experimental error and are summarized in Table VII. Of the three methods employed to determine the rate constant for the dimerization of $NA\dot{D}$, fast-scan cyclic voltammetry demonstrated the best reproducibility and therefore appears to be better suited for determinations of second-order rate constants on the order of 10^7 $\underline{M}^{-1}s^{-1}$. If special steps are taken to reduce background noise, i.e., the construction of a faradaic cage, it is possible that the double potential-step method might also show a precision in rate constant determinations which is comparable to the precision of the fast-scan cyclic voltammetric determinations.

The values determined for k_d show a reasonable agreement with that of 5.6×10^7 $\underline{M}^{-1}s^{-1}$ determined by Land and Swallow (44), using pulse radiolysis for 0.2 m$\underline{M}$ NAD^+ in 0.1 $\underline{M}$ sodium formate (pH 6.4). The larger rate constant determined at an ionic strength of 0.1 $\underline{M}$ may

Figure 19. Variation of cyclic voltammetric peak potential-concentration function with scan rate for initial one-electron reduction of NAD^+ in 0.4 M TeaCl and 0.1 M carbonate at pH 9.1 at 25°C. Circles: 0.30 mM NAD^+; triangles: 0.50 mM NAD^+. Error bars correspond to an uncertainty of ± 3 mV in the measurement of the peak potential.

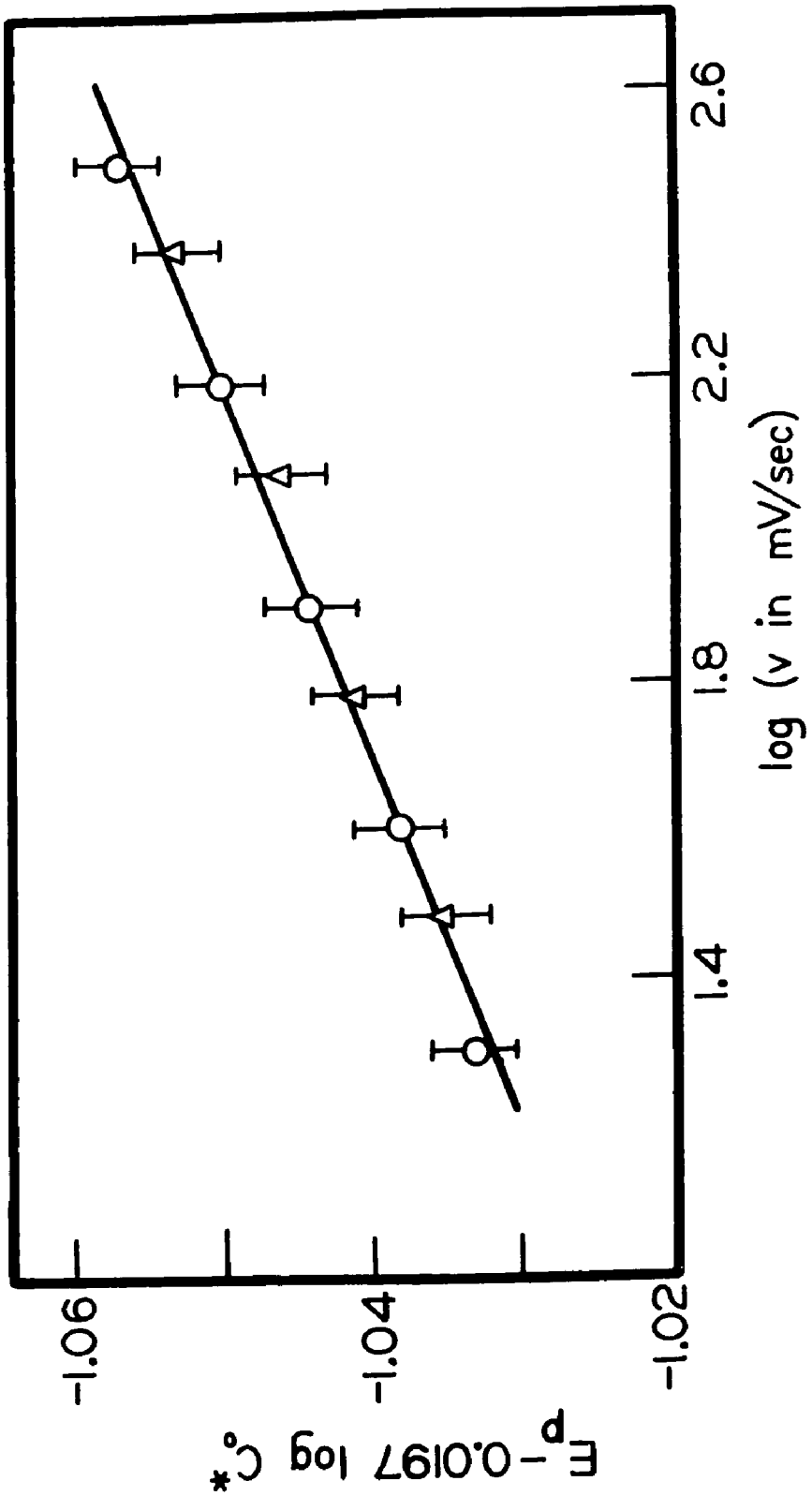


Figure 19.

Table VII. Summary of Determinations of the Rate Constant for the Dimerization of NAD in 0.4 M TeaCl and 0.1 M Carbonate at pH 9.1 at 1° and 25°C.

Method	Temp. C	Concentrations mM, NAD^+	$k_d \times 10^{-7}$ $M^{-1}\ s^{-1}$
DPSC[a]	25°	0.12, 0.18	4 ± 2.7[b]
FSCV[c]	25°	0.30, 0.50	2 ± 0.3[d]
	1°	0.40, 0.60	1 ± 0.2[d]
SSCV[e]	25°	0.30, 0.50	3 ± 1.7[f]
	1°	0.40, 0.60	1.5 ± 0.9[f]

[a] Double potential-step chronoamperometry.

[b] Uncertainty represents one standard deviation for six determinations.

[c] Fast-scan cyclic voltammetry.

[d] Uncertainty represents one standard deviation for six determinations at 25°C. and seven determinations at 1°C.

[e] Slow-scan cyclic voltammetry.

[f] Uncertainty represents the maximum and minimum values of k_d assuming a ±3 mV uncertainty in measuring the peak potential.

be attributable to a lower activity coefficient for NAD· at the ionic strength of 0.5 M, at which the cyclic voltammetry studies were done.

c. Activation Energy. From the values of k_d at 25° and 1°C., it was possible to calculate an activation energy, ΔH_a, and an effective frequency of successful collisions, s, for the dimerization of NAD·. The activation energy was calculated from

$$\ln\left(\frac{k_{n2}}{k_{n1}}\right) = \frac{\Delta H_a(T_2 - T_1)}{RT_1T_2} \tag{20}$$

which follows from the Arrhenius rate law,

$$k_n = s\, e^{\left(\frac{-\Delta H_a}{RT}\right)} \tag{21}$$

The activation energy and effective frequency calculated from the fast-scan voltammogram dimerization rates were ΔH_a = 6 kcal/mole and s = 7 x 10^{10} $M^{-1}s^{-1}$. Using the slow-scan voltammetric data, a ΔH_a of 5 kcal/mole and an s of 3 x 10^{11} $M^{-1}s^{-1}$ were computed.

The values determined for ΔH_a are in reasonable agreement with the activation energy calculated for other 1-substituted nicotinamide dimerizations, e.g., an activation energy of 4 kcal/mole has been reported for both 1-methylnicotinamide and nicotinamide mononucleotide (45).

5. Controlled Electrode-Potential Electrolysis

Electrolyses of NAD^+ were carried out at -1.27 V in both 0.4 M KCl and 0.4 M TeaCl with a 0.1 M carbonate buffer at pH 9.1. Values for the faradaic n ranged from 0.96 to 0.98 eq./mole. These n values are in agreement with those determined in previous electrolysis studies

of NAD^+ in the same potential region (4). As had been reported (4), the electrolysis solution took on a yellowish-green color, which was most intense ca. 80% into the electrolysis and which faded to a pale yellow as the electrolysis was carried to completion. Ultraviolet absorption (UV) spectra of the electrolysis product showed absorption bands at 260 (ε = 34,000) and 340 nm (ε = 6,600). Within instrumental error, there was no absorbance which could be observed in the wavelength region from 420 to 600 nm.

a. Determination of Dimeric Structure. The product of the 1e reduction product of NAD^+ has been previously isolated and was reported to have absorption maxima at 260 nm (ε = 33,100) and 340 nm (ε = 6,650) (46). The formation of a 2,2' dimer can be ruled out on the basis of the ultraviolet absorption spectra of the reduction product, since the 2,2' dimers of 1-substituted nicotinamides have an absorption maximum in the wavelength region of 400 nm (46). The 4,4' dimers of 1-substituted nicotinamides show a single absorption maximum in the region of 350 nm, while the 6,6' dimers show absorption maxima at both 270 and 350 nm (46). Since adenine absorption at 260 nm could obscure an absorption maximum due to a 6,6' dimer, the 4,4' and 6,6' forms can not be distinguished on the basis of the ultraviolet absorption spectra of the NAD^+ reduction product.

A comparison of the nuclear magnetic resonance spectra of the 1,4-NADH and the reduction product of NAD^+ shows spectra which are quite similar except that the resonance lines for the C(4) protons of 1,4-NADH are broadened and split in the nmr spectra of the dimer (14). This led to the conclusion that the product of the 1e NAD^+ reduction is probably the 4,4' dimer (14).

b. Decomposition of the Dimer. It has been reported in the literature (14) that, at a potential of -1.85 V, 4,4'-$(NAD)_2$ is gradually reduced to a 1,4-NADH with 10% conversion over a period of 10 hours and with no change in the ultraviolet absorption spectra. To ascertain whether the dimer itself or the decomposition products of the dimer are reduced to 1,4-NADH, electrolysis solutions containing the dimer in 0.4 M TeaCl and 0.1 M carbonate at pH 9.1 were allowed to stand for 24 to 72 hours under a N_2 atmosphere. The solutions were then examined polarographically to determine what polarographically active species were present and, in particular, to ascertain whether NAD^+ was one of the decomposition products of the dimer. Since NAD^+ is reduced to 1,4-NADH at a potential of -1.85 V, if NAD^+ were a dimer decomposition product, then what had been reported as a reduction of the dimer to 1,4-NADH would actually be a reduction of NAD^+.

In the period following the electrolysis, the dimer underwent partial decomposition in solution under N_2 atmosphere. One-half of the dimer which decomposed was converted to either nicotinamide or a 1-substituted nicotinamide (Table VIII). This decomposition pattern indicates that cleavage of the bond between the two nicotinamide moieties of the dimer occurs with the formation of one unreduced, polarographically active, nicotinamide moiety. The other half of the dimer is converted to a species, which does not show any electrochemical activity in the available potential range and which tends to broaden the absorption band observed at 260 nm. A summary of the decomposition study of $(NAD)_2$ appears in Table VIII.

Table VIII. Products of Decomposition of $(NAD)_2$ in a Nitrogen Atmosphere at 25°C. and pH 9.1[a].

Decompn. Time	Initial Concentrations		Final Concentrations[b]					$\frac{[NMN^+] + [Nico.]}{2\Delta [(NAD)_2]}$
	$(NAD)_2$	NAD^+	$(NAD)_2$	NMN^+	Nico.[c]	[Nico.] + [NMN^+]	$2\Delta [(NAD)_2]$[e]	
hr.	mM	mM	mM	mM	mM	mM[d]	mM	
24	0.194	0.01	0.126	0.04	0.05	0.08	0.08	0.57
72	0.380	0.12	0.10	0.185	0.20	0.265	0.56	0.47

[a] Background solution: 0.1 M carbonate buffer plus 0.4 M TeaCl. All concentrations were measured polarographically.

[b] No detectable amount of NAD^+ was present.

[c] Nicotinamide concentration was corrected for the small amount of nicotinamide present in the original solution.

[d] Summation of the final NMN^+ and nicotinamide concentrations, corrected for the original nicotinamide content (cf. footnote *c*) and for the NAD^+ initially present which had completely decomposed during the experiment to NMN^+ and nicotinamide.

[e] Difference in the initial and final dimer concentrations, multiplied by 2 to indicate the concentrations of nicotinamide moieties involved.

In weakly basic media, NAD^+ undergoes slow hydrolysis at both the nicotinamide-ribose linkage and the pyrophosphate linkage (47). In the case of the dimer, these linkages would also be expected to be susceptible to hydrolysis. If hydrolysis of the nicotinamide-ribose bond occurs during the course of dimer decomposition, then nicotinamide will be one of the end products of the decomposition. Similarly, if hydrolysis occurs at the pyrophosphate linkage, nicotinamide mononucleotide (NMN^+) would appear as one of the dimer decomposition products. Cleavage of the bond between the two nicotinamide moieties of $(NAD)_2$ prior to hydrolysis at either of the two sites mentioned would produce one molecule of NAD^+ for each molecule of $(NAD)_2$.

In the 24-hour decomposition study, the 1-substituted nicotinamide reached a concentration of 0.04 mM after 24 hours, assuming a polarographic I_d of 1.3. (I_d values for NMN^+ and NAD^+ both fall within 5-10% of 1.3 in 0.4 M TeaCl (48)) and had an $E_{1/2}$ of -1.12. At 0.04 mM concentration, $E_{1/2}$ values reported for NMN^+ and NAD^+ were -1.11 and -1.08 V, respectively. In the 72-hour decomposition study, the electrolysis was stopped prior to complete reduction of the NAD^+. In this way, the NAD^+ polarographic wave could provide a reference for comparison with polarographic waves produced by decomposition of the dimer. Immediately following the electrolysis, the NAD^+ wave had an $E_{1/2}$ of -1.06 V. After 72 hours, the only wave present in this potential region had an $E_{1/2}$ of -1.09 V and a wave height which corresponded to a concentration 0.185 mM for either NAD^+ or NMN^+. At 0.185 mM concentration, $E_{1/2}$ values reported for NMN^+ and NAD^+ were -1.09 and -1.04 V, respectively (48).

The polarographic $E_{\frac{1}{2}}$ values strongly suggest that the 1-substituted nicotinamide decomposition product is nicotinamide mononucleotide. This, however, does not prove that $(NAD)_2$ does not to some extent decompose by way of NAD^+. It simply means that the rate of hydrolysis at the pyrophosphate linkage of NAD^+ is more rapid than the decomposition of the C(4)-C(4) bond of the dimer.

The suggestion that $(NAD)_2$ is reduced very slowly at a potential of -1.85 V should now be examined in light of the fact that, in the course of dimer decomposition, cleavage of the bond between the two nicotinamide moieties of the dimer results in the regeneration of one species containing an unreduced nicotinamide moiety. The dimer absorption band at 340 nm has a molar absorptivity of 6650 $\underline{M}^{-1}cm^{-1}$. Since the dimer has two nicotinamide moieties, this is equivalent to an absorptivity of 3325 $\underline{M}^{-1}cm^{-1}$ for each nicotinamide moiety. 1,4-NADH has one nicotinamide moiety and an absorptivity of 6200 $\underline{M}^{-1}cm^{-1}$ at 340 nm. If 10% of the dimer is reduced directly to 1,4-NADH, then one should observe a 9% increase in absorptivity at 340 nm.

The polarographic evidence indicates that one molecule of a species containing an unreduced nicotinamide moiety is produced for each dimer molecule which is cleaved at the C(4)-C(4') bond between the two nicotinamide moieties. At the potential where dimer reduction was reported to occur, -1.85 V, any species containing an unreduced nicotinamide moiety would be reduced to the corresponding dihydronicotinamide. Since effectively one-half of each dimer molecule would be reduced to a species with a molar absorptivity of 6200 $\underline{M}^{-1}cm^{-1}$ at 340 nm, while the other half of the dimer molecule was broken down to a species which did not absorb at 340 nm, reduction of the dimer by

this pathway would result in a change in absorbance at 340 nm of less than 1%.

Inasmuch as the ultraviolet absorbance was reported to have been unchanged by the electrochemical reduction of the dimer at -1.85 V, an electrochemical reduction of a dimer decomposition product, instead of the dimer, must be considered as a possible source of 1, 4-NADH.

c. Nature of the Yellow-Green Color. The yellowish-green color which appears near the completion of the one-electron electrolysis of NAD^+ may be indicative of the formation of a charge transfer complex between NAD^+ and the reduction product $(NAD)_2$. The current-potential behavior, which was observed in dc polarographic (Figure 16) and slow-scan cyclic voltammetric studies of the $NAD^+/N\dot{A}D$ couple, indicate that some form of chemical interaction between NAD^+ and its reduction product is taking place.

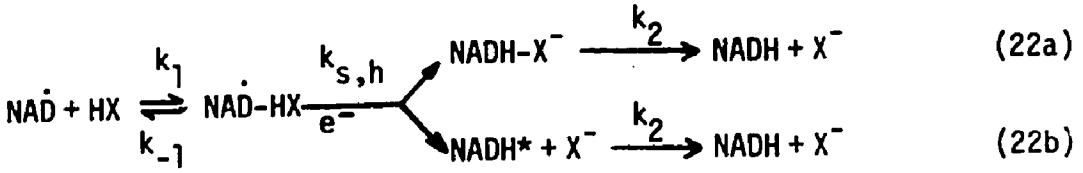
The formation of charge transfer complexes between the oxidized and reduced (dihydro) forms of several 1-substituted nicotinamides including NAD^+ has been reported (38, 39). One effect of the formation of these charge transfer complexes is the broadening of the ultraviolet absorption band of the 1-substituted dihydronicotinamide. Depending on the relative concentrations of oxidized and reduced species, this band, which usually has an absorption maximum at 340 to 350 nm, may show measurable absorbance at wavelengths of up to 550 nm. Since this absorptivity extends into the visible light wavelength region, the presence of the charge transfer complex in these solutions often results in a colored solution. Orange-colored solutions have been observed for mixtures of the oxidized and reduced forms of 1-propyl-

nicotinamide (38) and 1-methylnicotinamide (39). Mixtures of NAD^+ and 1,4-NADH also produce a broadened 340 nm absorption band. However, since the absorptivity in the visible region was quite small at concentrations of up to 0.15 M, no solution coloring was reported (38).

At the present time, there have been no reports of charge transfer complex formation between 1-substituted nicotinamides and their corresponding dimers. However, since each dimeric species contains two reduced nicotinamide moieties, the formation of this type of charge transfer complex is not unreasonable. The formation of a charge transfer complex between NAD^+ and its one-electron reduction product $(NAD)_2$ may account for the yellowish-green color which was observed during the electrolysis of NAD^+.

B. Reduction of the Free Radical $\dot{NAD}$

The second step in the reduction of NAD^+ to NADH involves a charge transfer to the uncharged free radical nicotinamide moiety, which occurs simultaneously with or shortly after the formation of a free radical-proton donor adduct, $\dot{NAD}$-HX (the evidence for the species $\dot{NAD}$-HX being involved is subsequently presented). (The reaction sequence for the charge transfer and the formation of the proton donor adduct is based on the observation that the free radical is not reduced in aprotic media in the absence of a proton donor (9).) Following the charge transfer, the reduced adduct undergoes a rearrangement to form a dihydronicotinamide-adenine dinucleotide. The reaction sequence can be summarized as follows:



$$\dot{NAD} + HX \underset{k_{-1}}{\overset{k_1}{\rightleftharpoons}} \dot{NAD}\text{-}HX \xrightarrow[e^-]{k_{s,h}} \begin{cases} NADH\text{-}X^- \xrightarrow{k_2} NADH + X^- & (22a) \\ NADH^* + X^- \xrightarrow{k_2} NADH + X^- & (22b) \end{cases}$$

where $NADH\text{-}X^-$ or NADH* represent the reduced species prior to its rearrangement. Controlled potential electrolyses of NAD^+ at potentials sufficiently negative to bring about a 2e reduction of NAD^+, produce better than 90% NADH with less than 10% of the starting material going to the dimer. Since the free radical dimerizes at a rate of 2×10^7 $M^{-1}s^{-1}$, the formation of NAD̈-HX must be quite rapid.

Since both of the redox participants of the NAD̈/NADH redox couple are involved in homogeneous reactions, suppositions concerning the causes of changes in electrochemical behavior must take into consideration the series of complex factors which determine the relative concentrations of oxidized and reduced species. These factors include the reactions which consume electroactive species, e.g., the dimerization of the free radical and the rearrangement following the reduction of the free radical, and the reactions which are required to produce an electroactive species, e.g., the formation of the free radical-proton donor adduct. These reactions restrict the determinations of rate constants for heterogeneous and homogeneous reactions involving redox participants to being qualitative or at best semiquantitative in nature.

1. Effect of Brønsted Acids

a. pH. Since the reduction of NAD̈ requires the net addition of a proton and an electron, the effect of pH on the ease of reducibility of the free radical was examined. Although the dc

polarographic wave for the reduction of $\dot{NAD}$ can be reasonably well resolved from the background discharge at pH greater than 9, polarographic techniques could not be used to study the effect of pH over a broad pH range. At pH greater than 10, the wave for the reduction of $\dot{NAD}$ is obscured by the reduction wave for nicotinamide (48), which is produced by the base-catalyzed hydrolysis of the nicotinamide-ribose linkage (47).

Effects of pH could be studied, however, using fast-scan cyclic voltammetry. Owing to the highly irreversible character of the background discharge, at scan rates of 100 to 300 V/s the discharge was shifted sufficiently negative that a voltammetric peak due to the reduction of the free radical could be resolved. Use of a scan rate of 100 V/s offered the broadest pH range in which the peak for reduction of the free radical could be at least partially resolved. The pH-dependence of the voltammetric peak potential for the reduction of $\dot{NAD}$ in 0.1 M Teap and 0.01 M Tris between pH 7.2 and 9.3 at a scan rate of 100 V/s (Figure 20) is given by

$$E_p = -1.59 - 0.021\ pH \tag{23}$$

In the case where an equilibrium protonation precedes the reduction, E_p would be expected to shift positively by 59 mV if the pH is decreased one unit. For an equilibrium involving protonation of the free radical

$$\dot{NAD} + H^+ \rightleftharpoons \dot{NADH}^+ \tag{24}$$

preceding the reversible charge transfer, the redox equilibrium between the protonated free radical, $\dot{NAD}\text{-}H^+$, and the reduced species,

Figure 20. Variation of voltammetric peak potential with pH for the reduction of NAD· to NADH. Solution conditions: 0.30 m$\underline{M}$ NAD^+ in 0.1 $\underline{M}$ Teap and 0.01 $\underline{M}$ Tris at 25°C. The pH was adjusted by the addition of $HClO_4$. Voltammetric scans at a dme were initiated manually 10 seconds after drop birth for a mercury drop with a natural drop-time of 13 seconds. Scan rate = 100 V/s. The error bars indicate a ± 10 mV uncertainty in the determination of the peak potential.

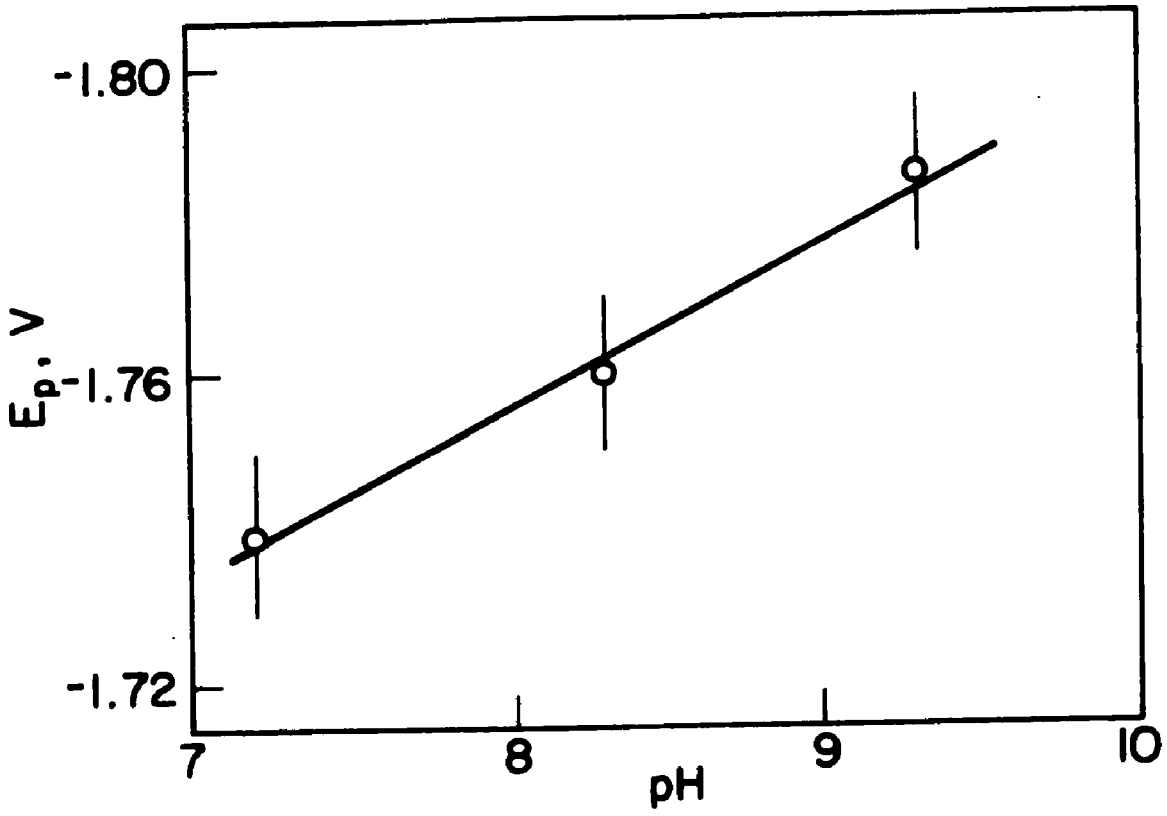


Figure 20.

$NADH^*$, would be described by

$$E = E^{o}_{NA\dot{D}\text{-}H^+/NADH^*} - 0.059 \log \frac{[NADH^*]}{[NA\dot{D}\text{-}H^+]} \quad (25)$$

where $[NAD\text{-}H^+]$ is described by

$$[NA\dot{D}\text{-}H^+] = \frac{[H^+]\,[NA\dot{D}]}{K_a} \quad (26)$$

Substitution of equation 26 into equation 25 produces

$$E = E^{o}_{NA\dot{D}\text{-}H^+/NADH^*} - 0.059 \log \frac{[NADH^*]}{\left[\frac{[H^*]\,[NA\dot{D}]}{K_a}\right]} \quad (27)$$

which can be rewritten as

$$E = E^{o}_{NA\dot{D}\text{-}H^+/NAD^*} - 0.059 \log \frac{[NADH^*]}{[NA\dot{D}]} - 0.059\ pH + 0.059\ pK_a \quad (28)$$

From equation 28, it follows that E^o for the $NA\dot{D}/NADH^*$ redox couple would be given by

$$E^{o}_{NA\dot{D}/NADH^*} = E^{o}_{NA\dot{D}\text{-}H^+/NADH^*} + 0.059\ pK_a - 0.059\ pH \quad (29)$$

From equation 29, it follows that $E^{o}_{NA\dot{D}/NADH^*}$ and hence E_p, should shift positively by 59 mV if the pH is decreased by one unit, providing that there is an equilibrium protonation of $NA\dot{D}$ prior to the charge transfer.

The slope of 21 mV/pH unit, which was observed for a plot of E_p vs. pH (Figure 20), indicates that the equilibrium formation of protonated free radical can not be the only kinetically significant pathway for the production of a reducible free radical. This is probably related to the minute proton concentration range of pH 7.2

to pH 9.3 and to the extremely weak base character of 1-substituted nicotinamide free radicals (Hayon (49) has reported a pK_a of 1.3 for the protonated free radical of 1-methylnicotinamide). Since free proton, H_3O^+, is evidently not the only kinetically significant contributor to the formation of reducible free radical, solvent water and/or buffer constituent, e.g., protonated Tris, must also serve as proton donors.

b. Ammonium Ion. In order to observe the effect of a proton donor other than H_2O or H_3O^+ on the electrochemical redox properties of $\dot{NAD}$, the ac, dc and differential pulse polarographic behavior of 0.42 mM NAD^+ was observed for a series of solutions, in which the ratio of NH_4Cl to KCl in the background electrolyte was varied but the pH was maintained at pH 9.0 with an ionic strength of 0.4 M. The pH in the solutions containing NH_4Cl was adjusted to pH 9.0 by the addition of NH_3.

The dc polarographic behavior of the reduction of $\dot{NAD}$ in the presence of the KCl/NH_4Cl mixtures is summarized in Table IX. The polarogram of 0.42 mM NAD^+ in 0.4 M KCl at pH 9.0 showed a wave corresponding to the reduction of $\dot{NAD}$ with an $E_{\frac{1}{2}}$ of -1.673 V and a slope of 86 mV. As KCl was replaced by NH_4Cl, this wave shifted towards more positive potential and became drawn out. When all of the KCl had been replaced with NH_4Cl, the wave had an $E_{\frac{1}{2}}$ of -1.53 and a slope of 110 mV. AC and differential pulse polarographic studies of the KCl/NH_4Cl mixtures showed shifts in the reduction potential of $\dot{NAD}$, which were comparable to those observed for the dc polarographic wave and are summarized in Table IX and Figure 21, respectively.

Table IX. Summary of Polarographic Behavior of the NAD/NADH Redox Couple as KCl is Replaced with NH_4Cl at Constant pH and Ionic Strength[a]

DC Polarography

KCl/NH_4Cl M/M	$-E_{1/2}$ V	$E_{1/4} - E_{3/4}$ mV	I_d[b] μA
0.40/0.00	1.673	90	1.1
0.36/0.04	1.630	110	1.3
0.32/0.08	1.593	110	1.1
0.24/0.16	1.575	110	1.4
0.08/0.32	1.545	110	1.3
0.00/0.40	1.530	110	1.3

AC Polarography[c]

KCl/NH_4Cl M/M	$-E_s$ V	$E^d_{+s/2} - E_s$ mV	$E_s - E^d_{-s/2}$ mV	ΔE_s mV	i_s[e] nA
0.040/0.0	1.745	71	52	123	30
0.36/0.04	1.642	60	90	150	30
0.32/0.08	1.622	59	74	133	25
0.24/0.16	1.610	46	42	88	25
0.08/0.32	1.600	47	39	86	30

[a] All solutions are 0.42 mM in NAD^+ with μ = 0.4 M. The solutions were maintained at pH 9 by the addition of NH_3.

[b] Polarographic diffusion current constant, calculated from the average diffusion current.

[c] AC modulation voltage = 5 mV peak; frequency = 40 Hz.

[d] Defined in Table IV.

[e] In-phase summit current.

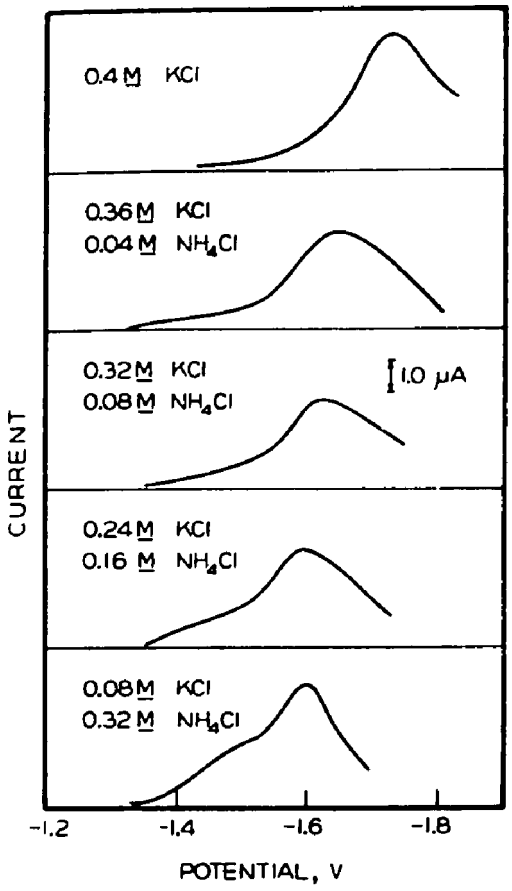


Figure 21. Differential pulse polarograms of 0.42 mM NAD^+ for the solution conditions specified in the figure. The mixtures were maintained at pH 9.0 by the addition of NH_3. Controlled drop-time = 2.0 s; scan rate = 2 mV/s; modulation amplitude = 10 mV.

The increase in the ease of reducibility of $\dot{NAD}$, brought about by the addition of NH_4^+, can probably be attributed to two factors. First, since the adduct has a net charge of +1 in the area of the nicotinamide moiety, when NH_4^+ is the proton donor but not when H_2O is the proton donor, the $\dot{NAD}$-NH_4^+ adduct itself may be more easily reduced than the $\dot{NAD}$-H_2O adduct. Second, since NH_4^+ (pK_a = 9.25) is a stronger acid than H_2O (pK_w = 14), the equilibrium for the rearrangement of NADH-X^- to NADH and X^- (equation 22a) would lie more in favor of the products, with a corresponding decrease in the concentration of NADH-X^-, when NH_4^+ is the proton donor. This decrease in the concentration of the electroactive reduced species, NADH-X^-, would tend to facilitate the reduction of $\dot{NAD}$-HX.

An increase in the rate of the following reaction, k_2, in the presence of NH_4^+ could not be demonstrated experimentally, using fast-scan cyclic voltammetry. The adsorption of NAD^+ in the potential range which extends from the potential for mercury oxidation (E = 0.0 V) to the potential where NAD^+ is reduced to the free radical, meant that any cyclic voltammetric studies of the second electron transfer would be complicated by the adsorption of NAD^+. This adsorption sufficiently alters the electrochemical redox behavior that theoretical predictions for electrochemical behavior of diffusion controlled or kinetically controlled charge transfers with intervening homogeneous chemical reactions involving redox participants, cannot be even semiquantitatively applied.

2. Effect of Lewis Acids: Ca(II)

a. DC and AC Polarography. The effect of $Ca(ClO_4)_2$ addition on

the reduction of NAD· to NADH was examined. To a 0.42 mM NAD^+ solution (0.1 M Teap and 0.01 M Tris solution at pH 9.3), Ca (II) was added in a concentration range of 0.25 mM to 100 mM; the behavior of the NAD·/NADH redox couple was then studied using ac and dc polarography.

Although the dc polarographic $E_{\frac{1}{2}}$ was relatively insensitive to Ca(II) (Table X), the slope of the polarographic wave became markedly steeper with increasing Ca(II). In the absence of Ca(II), the polarographic wave had a slope of 90 mV. However, when Ca(II) was added at the 100 mM level, the slope was 55 mV. The addition of 100 mM Ca(II) also produced a 20% decrease in the polarographic diffusion current constant.

The ac polarographic response of the NAD·/NADH redox couple was relatively sensitive to the addition of Ca(II) (Table XI). In the case where sufficient Ca(II) was added to produce a ratio of Ca(II): NAD^+ of 1.2:1, the in-phase summit current, i_s, for the reduction of NAD· had increased 35%. The increase in summit current in the presence of 100 mM Ca(II) was slightly over 100%. The increase in i_s was accompanied by a slight positive shift in the summit potential, E_s, and a substantial decrease in the peak width, $\Delta E_{s/2}$.

Cyclic voltammetry could not be used to study the effects of Ca(II) addition on the NAD·/NADH redox couple since, in 0.1 M Teap and 0.01 M Tris at pH 9.3, Ca(II) shows an adsorption peak in the same potential region as the NAD· reduction peak.

The most viable explanation for the changes in the dc and ac polarograms, brought about by the addition of Ca(II), is that the presence of Ca(II) increases the rate of charge transfer for the

Table X. DC Polarographic Behavior of the NAD/NADH Redox Couple in the Presence of Ca(II)[a]

Ca(II)	$-E_{1/2}$	$E_{1/4} - E_{3/4}$	I_d[b]
mM	V	mV	
0.00	1.670	90	1.30
0.25	1.670	85	
0.50	1.665	75	1.25
1.00	1.665	85	
10.0	1.665	60	1.15
50.0	1.665	65	1.15
100	1.660	55	1.10

[a] All solutions contain 0.42 mM NAD^+ in 0.1 M Teap and 0.01 M Tris at pH 9.3 and 25°C.

[b] Polarographic diffusion current constant, calculated from average diffusion current.

Table XI. AC Polarographic[a] Behavior of the NAD̈/NADH Redox Couple in Presence of Ca(II)[b]

Ca(II) mM	E_s V	$E_{+s/2} - E_s$ mV	$E_s - E_{-s/2}$ mV	$\Delta E_{s/2}$ mV	i_s nA
		40 Hz			
0.00	1.690	68	60	128	56
0.25	1.685	65	67	132	59
0.49	1.682	57	58	115	75
1.00	1.690	62	57	119	78
50	1.680	57	43	100	122
100	1.674	50	38	88	110
100	1.671	51	40	91	132
		100 Hz			
0.00	1.696	76	72	148	57
0.25	1.690	67	66	133	63
0.49	1.692	64	62	126	78
1.00	1.694	67	61	128	80
10.0	1.696	61	55	116	103
50	1.687	57	48	105	118
100	1.680				117
100	1.677				122

[a] AC modulation voltage = 5 mV peak.

[b] All solutions were 0.42 mM in NAD^+, 0.10 M Teap and 0.010 M in Tris at pH 9.3.

reduction of $\dot{NAD}$. The following type of behavior is predicted (50) for an ac polarographic peak for an increase in the heterogeneous rate constant when the charge transfer is preceded by a reversible chemical reaction, e.g., the formation of $\dot{NAD}$-HX:

(1) The in-phase ac current should increase.

(2) The summit potential should shift slightly positive.

(3) The negative half-summit potential $E_{-s/2}$ should shift substantially positive.

(4) The positive half-summit potential $E_{+s/2}$ should shift very little.

Examination of Table XI shows that the addition of Ca(II) brought about the type of behavior just described. The increase in the steepness of the dc polarographic wave (Table X) with the addition of Ca(II) is also indicative of an increase in $k_{s,h}$.

b. Titration of Ca(II) with NAD^+. Since the presence of Ca(II) did produce some modifications in the electrochemical behavior of NAD^+, Ca(II) was titrated with NAD^+ at pH 7.2 in a 0.01 M Tris buffer to determine to what degree NAD^+ would complex with Ca(II). The titration was monitored potentiometrically with a liquid-membrane calcium electrode (Teap had to be excluded from the titration since the tetraethylammonium ion showed a significant interference with the Ca(II) ion-selective electrode).

Since the formation constant of the Ca(II)-NAD^+ complex, K_f, was not sufficiently large for the titration to show a clear cut end-point, it was necessary to calculate K_f from the potentiometrically determined free Ca(II) concentration (Table XII). A formation constant of $K_f = 38 \pm 4\ M^{-1}$ (mean and standard deviation for 11 measurements) was determined

Table XII. Formation Constants of NAD^+: Ca(II) Complex in 0.01 M Tris at pH 7.2

Total [Ca(II)] mM	Total [NAD^+] mM	Uncomplexed [Ca(II)][a] mM	[NAD^+: Ca(II)] mM	K_f[b,c] M^{-1}
1.028	.580	0.994	0.034	63 ± 19
0.941	1.194	0.900	0.041	40 ± 10
0.881	1.615	0.823	0.058	45 ± 8
0.804	2.155	0.744	0.060	38 ± 6
0.740	2.609	0.667	0.073	43 ± 5
0.669	3.112	0.598	0.071	39 ± 4
0.624	3.430	0.552	0.072	39 ± 4
0.561	3.874	0.504	0.057	30 ± 3
0.514	4.203	0.447	0.067	36 ± 3
0.474	4.482	0.405	0.069	39 ± 3
0.437	4.746	0.370	0.067	39 ± 3

[a] The free Ca(II) concentration was determined potentiometrically.

[b] The uncertainty in K_f reflects an uncertainty of ± 0.2 mV in the potentiometric determination of the free Ca(II) concentration.

[c] Weighted mean based on the uncertainty in each K_f determination = 38 M^{-1} ; standard deviation = ± 4.

for a 1:1 Ca(II):NAD^+ complex.

Inasmuch as the formation constant for a Ca(II):NAD^+ complex is quite small, it seems unlikely that the complexation of NAD^+ with Ca(II) is entirely responsible for changes in the electrochemical behavior of the $NA\dot{D}$/NADH redox couple, unless the free radical $NA\dot{D}$ complexes Ca(II) exceedingly rapidly and this Ca(II):$NA\dot{D}$ complex has a K_f which is very large.

c. Effect of Ca(II) Adsorption on $k_{s,h}$. Since the changes in polarographic behavior are substantial even at low Ca(II) concentrations, e.g., 0.50 mM, it is unlikely that these changes are solely due to an increase in ionic strength. However, it is possible that the adsorption of Ca(II), which shows an ac polarographic peak at a potential only slightly negative of the reduction potential of the $NA\dot{D}$/NADH redox couple, could be responsible for the increase in the heterogeneous rate constant for the reduction of $NA\dot{D}$.

Since the size of the ac polarographic peak for the adsorption of Ca(II) was dependent on the concentration of Ca(II), the peak was sufficiently large at the 50 and 100 mM Ca(II) levels that it began to overlap the ac peak for the reduction of the free radical. Moreover, in cyclic voltammetric studies of 0.42 mM NAD^+ in 0.1 M Teap with a 0.01 M Tris buffer at 9.3 and 50 mM Ca(II), the adsorption peak due to the presence of Ca(II) completely obscured the $NA\dot{D}$ reduction peak. The potential regions of the polarographic and voltammetric Ca(II) adsorption peaks indicate that some Ca(II) is adsorbed at the electrode-solution interphase in the potential region where reduction of $NA\dot{D}$ occurs.

The adsorption of a positively charged species such as Ca(II) at the electrode-solution interphase of an electrode which is at a potential negative to the potential of zero-charge, i.e., the electrode has a net negative charge, will have the effect of reducing the apparent negative charge on the electrode. As a result, there will be less electrostatic repulsion between the electrode surface and ions of the same charge, e.g., NAḊ-HX which has a net charge of -2 due to the presence of 2 singly ionized phosphate groups, and the population of negative ions at the outer Helmoltz plane will increase. With a decrease in electrostatic repulsion between NAḊ-HX and the electrode surface, an increase in the rate of charge transfer is quite reasonable,

3. Determinations of the Rate Constant for the Rearrangement

The effects of ionic strength and of available proton donor, HX, on the rate constant of the follow-up reaction involving NADH-X^- (k_2 of equation 22a) were examined via dc polarography and cyclic voltammetry.

a. Effect of Available Proton Donor. Both the separation of the cyclic voltammetric cathodic and anodic peaks, ΔE_p, and the ratio of their current, i_{pa}/i_{pc}, are dependent on the rate constant k_2 for the reaction shown in equation 22a. However, because of the unknown effects of the dimerization of NAḊ on the observed voltammetric behavior of the NAḊ/NADH couple, the rate constant determined for k_2 will have a large uncertainty and should be considered to be only semiquantitative.

In 0.4 M TeaCl and 0.1 M carbonate at pH 9.1, the rate constant for the follow-up reaction was determined at three temperatures, (2°, 25° and 40°C). These rate constants were compared with those determined for the same reaction in 0.5 M TeaCl and 0.01 M Tris at pH

9.3 at the same temperatures. A summary of the determinations of k_2 appears in Table XIII.

The difference in the rate constants for the follow-up reaction in the two backgrounds used varies with temperature. This variation indicates that the activation energy for the follow-up reaction in the two media differ. At 2°, both solutions gave a first-order rate constant of 2.5×10^3 s^{-1}. When the temperature was increased to 40°C. the reaction in carbonate was too rapid to measure, exceeding 3×10^4 s^{-1}, whereas in Tris the reaction rate constant was 1.6×10^4 s^{-1}. Activation energies for the rearrangement were calculated for each buffer system from plots of ln k_2 vs. T^{-1} (Figure 22). In 0.4 M TeaCl and 0.1 M carbonate at pH 9.1, the rearrangement had an activation energy of 10 kcal/mol with an effective frequency factor of 1×10^{11} s^{-1}. In 0.5 M TeaCl and 0.01 M Tris at pH 9.3, the activation energy was 8 kcal/mol with an effective frequency factor of 2×10^9 s^{-1}.

The principal difference between the two background and buffer systems, aside from a slight difference in pH, lies in the fact that the 0.1 M carbonate buffer at pH 9.1 has a much greater capacity to absorb an increase in the hydroxyl ion concentration ($[HCO_3^-]$ = 0.093 M) than does the Tris buffer at pH 9.3 ([protonated-Tris] = 5×10^{-4} M). This capacity to buffer OH^- generated when H_2O serves as the proton donor, may be the factor which influences the rate of the rearrangement following the reduction of NAD$\dot{}$-H_2O.

The apparent increase in the rate of the follow-up reaction in the presence of HCO_3^- suggests two possibilities:

Table XIII. Summary of the Variation with Temperature and Ionic Strength of the Rate Constant for the Rearrangement of NADH-X^-

Buffer[a]	pH	μ	T	k_2[b] x 10^{-3}
		M	C°	s^{-1}
2	9.3	0.1	25	3
5	9.1	0.5	2	2.5
5	9.1	0.5	25	10
5	9.1	0.5	40	>30
6	9.3	0.5	2	2.5
6	9.3	0.5	25	7
6	9.3	0.5	40	16

[a] Buffers are described in Table I.

[b] First-order rate constant for the rearrangement of NADH-X^-. The uncertainties in the determinations of k_2 may be as high as 100% due to the unknown effects of the dimerization of NAD· on the voltammetric peak current ratio of i_{pa}/i_{pa}, which was used to calculate k_2.

Figure 22. Variation of the first-order rate constant for the rearrangement of NADH-X^- with temperature. Solution conditions: circles, 0.30 m$\underline{M}$ NAD^+ in 0.4 $\underline{M}$ TeaCl and 0.1 $\underline{M}$ carbonate at pH 9.1; squares, 0.45 m$\underline{M}$ NAD^+ in 0.5 $\underline{M}$ TeaCl and 0.01 $\underline{M}$ Tris at pH 9.3.

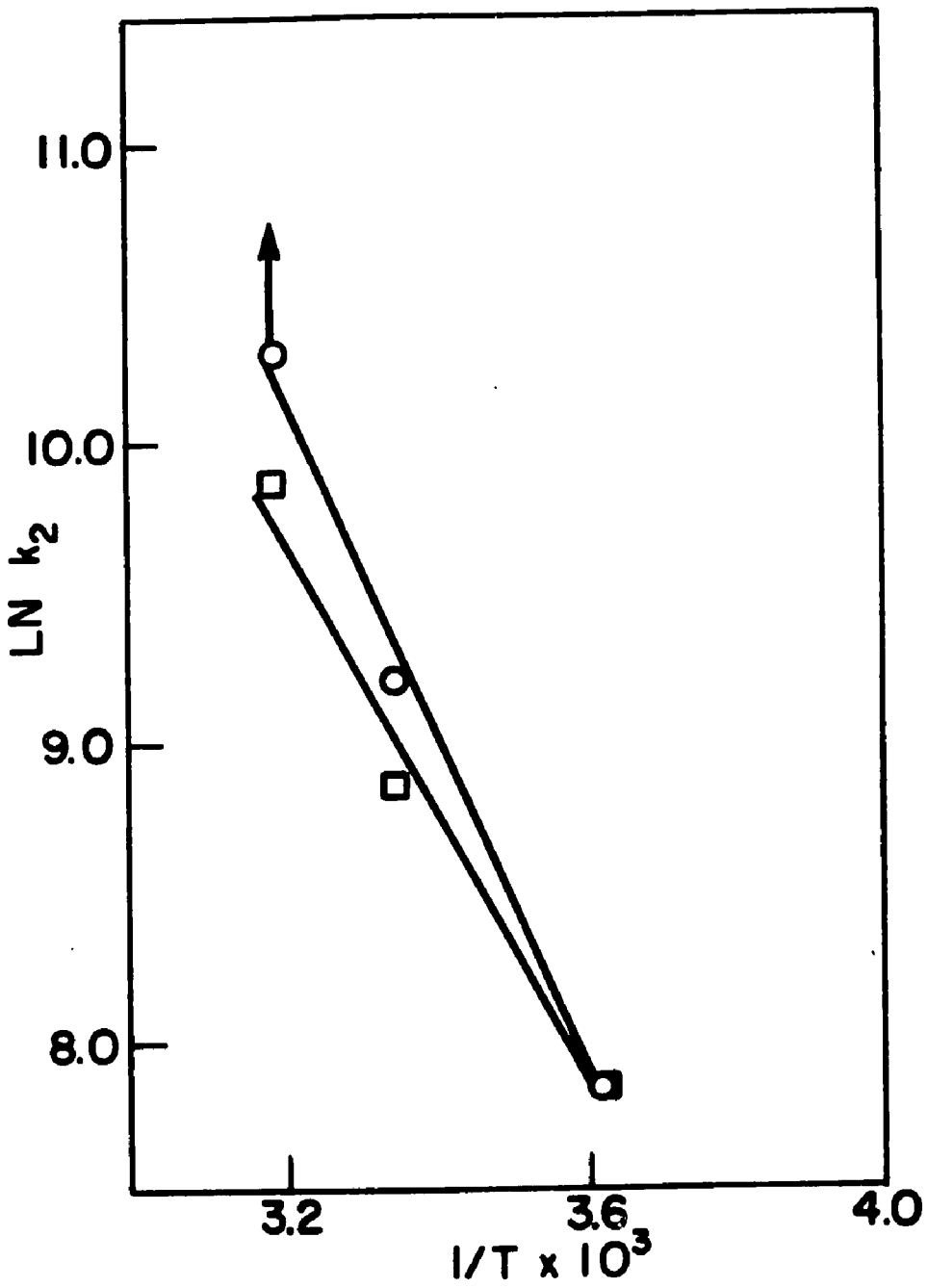


Figure 22.

(1) The capability to neutralize OH^- shifts the equilibrium in favor of NADH by consuming one of the products, i.e.,

$$NADH\text{-}OH^- \rightleftharpoons NADH + OH^- \xrightleftharpoons{HCO_3^-} NADH + H_2O + CO_3^= \qquad (30)$$

(2) HCO_3^- facilitates the loss of OH^- in the rearrangement in a second-order reaction, i.e.,

$$NADH\text{-}OH^- + HCO_3^- \longrightarrow NADH + H_2O + CO_3^= \qquad (31)$$

where the contribution of this reaction to the rate of disappearance of $NADH\text{-}OH^-$ is highly temperature dependent. Considering the time scale on which these proton transfers occur, it is rather difficult to distinguish between them.

The possibility of the formation of a proton donor adduct between $NA\dot{D}$ and the bicarbonate anion cannot be excluded. However, since the anion has a net charge of -1, it seems likely that an $NA\dot{D}\text{-}HCO_3^-$ adduct would be more difficult to reduce than a $NA\dot{D}\text{-}H_2O$ adduct, because of the negative charge in the area of the nicotinamide free radical, and, consequently, would not contribute to the production of NADH.

DC polarographic studies of NAD^+ in the two buffer systems being discussed demonstrated that the polarographic wave for the reduction of $NA\dot{D}$ was relatively insensitive to the type of buffer used, i.e., $E_{\frac{1}{2}}$ for the reduction of $NA\dot{D}$ was -1.64 V in the presence of either the 0.1 M carbonate buffer or the 0.01 M Tris buffer. Since the rate constants for the rearrangement at 25° are relatively close (Table XIII), the polarographic behavior of the $NA\dot{D}$ reduction wave at 25° would be expected to be the same regardless of which buffer system was used.

b. Effect of Background Electrolyte Concentration on k_2 and $k_{s,h}$.

The reduction of NAD· in 0.01 M Tris at pH 9.3 was also examined by cyclic voltammetry in order to ascertain what effects a 5-fold decrease in ionic strength would have on the rates of the charge transfer and of the follow-rearrangement. At 25°, a $k_{s,h}$ of 0.04 cm/s and a k_2 of 3×10^3 s^{-1} were determined for the NAD·/NADH redox couple.

Since the charge transfer was not reversible, these values of $k_{s,h}$ and k_2 were determined from cyclic voltammograms using a digital simulation program (51) based on the procedures developed by Feldberg (52). In these procedures, the partial differential equations, which describe the factors controlling the concentrations of redox participants at a given time and distance from the electrode surface, e.g., diffusion, rate of charge transfer and rates of reactions involving redox participants, are solved using finite difference methods. The finite difference descriptions of these factors are used to simulate, through an iterative process, profiles (concentration vs. distance from the electrode surfact) of the concentrations of the redox participants at a given point in time. From the surface concentrations of electroactive species, obtained by the simulation, it is possible to generate the current-time relationship for the conditions specified. If the electrode potential is changing with time, the relationship which is simulated is one of current vs. potential.

The effect of ionic strength and concentration of Tea^+ on the rate of charge transfer is summarized in Table XIV. The decrease in the rate of charge transfer to NAD· for a 5-fold decrease in ionic strength was similar to the decrease in charge transfer rate observed for the reduction of NAD^+ under the same conditions.

Table XIV. Effect of Tea^+ Concentration on the Heterogeneous Charge-Transfer Rate Constants for the Reductions of NAD^+ and of NAD̈-HX at 25°C.

A. $NAD^+ + e \xrightarrow{k_{s,h}} NA\dot{D}$

Buffer	$[Tea^+]$ M	μ M	$k_{s,h}$ cm/s
2	0.1	0.1	0.16
5	0.4	0.5	$> 1^a$

B. $N\dot{A}D\text{-}HX + e \xrightarrow{k_{s,h}} [NADH\text{-}X]^-$

Buffer	$[Tea^+]$ M	μ M	$k_{s,h}$ cm/s
2	0.1	0.1	0.04
5	0.4	0.5	$> 1^a$
6	0.5	0.5	$> 1^a$

[a] 1 cm/s is the smallest rate constant, which would show a ΔE_p of 60 mV within an experimental uncertainty of ± 5 mV in measuring the peak potentials, for the maximum scan rate used to study the reduction, 500 V/s.

The dependence of $k_{s,h}$ on either ionic strength or concentration of Tea^+ may be a consequence of the fact that, in the reduction of both NAD^+ and $NA\dot{D}$, the species undergoing reduction have a net negative charge (NAD^+ has a net charge of -1, where the plus sign denotes only the charge on the nicotinamide moiety, and $NA\dot{D}$ a net charge of -2). Since the electrode is similarly charged, there will be a repulsion of the electroactive species. As the ionic strength is increased, the activity of the charged electroactive species decreases, resulting in less repulsion between it and the electrode. In addition, since the increase in ionic strength is brought about by an increase in the concentration of the Tea^+ salt, which is adsorbed over the potential regions where NAD^+ and $NA\dot{D}$ are reduced, the increase in ionic strength will be accompanied by an increased adsorption of Tea^+. This increased adsorption of a positively charged ion on an electrode with a net negative charge will decrease the apparent negative charge on the electrode and will also result in less electrostatic repulsion of negatively charged ions, which serves to increase the amount of negatively charged ions at the outer Helmholtz plane.

Clearly, both the increase in ionic strength and the increase in adsorbed cation will have the effect of decreasing the electrostatic repulsion between either NAD^+ or $NA\dot{D}$ and the electrode surface. In the case of NAD^+, where the molecule has a net charge of -1 at pH 9.1, a decrease in ionic strength from 0.5 to 0.1 M results in a reversible charge transfer decreasing to one of 0.16 cm/s. In the case of $NA\dot{D}$, where the molecule has a net charge of -2 at pH 9.3, a similar decrease in ionic strength results in a reversible charge transfer decreasing

to one of 0.04 cm/s. Since the repulsion between the electroactive species and the interface would be expected to be greater for a molecule with a greater net negative charge, the larger decrease in $k_{s,h}$ in the second case is not surprising. The fact that the electrode has a greater negative potential during the reduction of $\dot{NAD}$ than in the initial reduction of NAD^+, -1.7 V and -1.1 V, respectively, would also contribute to a greater electrostatic repulsion of the electroactive species in the case of $\dot{NAD}$ and may also be a contributing factor in the greater decrease in $k_{s,h}$ with ionic strength.

The reasons for the decrease in the rate of the follow-up reaction, k_2, as the ionic strength decreases is less clear. The initial expectation would be that a decrease in ionic strength should result in an increase in activity coefficients and hence an increase in the apparent reaction rate. Since the rate of the follow-up reaction is more rapid at higher ionic strengths, it is possible that at higher ionic strength $\dot{NAD}$ may undergo some type of conformational change or ion-pair formation, which facilitates the rearrangement.

4. Controlled Electrode-Potential Electrolysis

Two-electron reductions of NAD^+ were carried out to ascertain the effects of Lewis and Brønsted acids on the nature of the reduction products. The potential required was dependent on the background electrolyte. In all of the electrolyses, the potential applied was quite near the potential where background discharge occurs. Because some background discharge occurred concurrent with the reduction of NAD^+, faradaic $\underline{n}$ values for the NAD^+ reduction were on the average slightly greater than 2.0 (Table XV).

Table XV. Summary of Data for the Two-Electron Electrolysis of NAD^+

Buffer	E_{CPE} V	NAD^+ mM	$(NAD)_2^a$ %	1,6-NADH[b] %	1,4-NADH[c] %	$\frac{\text{1,4-NADH}}{\text{1,6-NADH}}$	n eq/m
3	-1.65	0.41	7	23	63	2.7	
3	-1.68	0.44	3	26	65	2.5	2.2
3	-1.68	0.92	4	21	66	3.1	1.8
4	-1.80	0.44	11	30	60	2.0	2.3
5	-1.80	0.44	3	38	66	1.7	2.2
5	-1.80	0.88	4	38	72	1.9	1.9
6[e]	-1.78	0.44	2	38	60	1.6	2.2
6[e]	-1.78	0.84	2	39	58	1.5	2.0

[a] $(NAD)_2$ was determined polarographically.

[b] 1,6-NADH was determined from the ultraviolet absorption maximum at 345 nm.

[c] 1,4-NADH was determined by enzymatic assay.

[d] Percentages are given in terms of % NAD^+, which has gone into forming the product.

[e] Buffer 6 was made 0.05 M in $Ca(ClO_4)_2$.

a. Determination of Reduction Products. The determination of the electrolysis products was carried out using the following procedures:

(1) The concentration of the $(NAD)_2$ dimer was determined from a dc polarogram of the electrolyzed solution, in which the dimer produced an anodic wave at about -0.3 V.

(2) One ml of the electrolyzed solution was removed and diluted with 0.1 M phosphate buffer at pH 7.5 (Solution I).

(3) One ml of the electrolyzed solution was removed and mixed with one ml of 0.2% alcohol dehydrogenase (ADH). This mixture was diluted to 10 ml with 0.2 M acetaldehyde in 0.1 M phosphate buffer at pH 7.5 (Solution II). When Ca(II) was present in the electrolyzed solution, the 0.1 M phosphate buffer was replaced with 0.04 M Tris at pH 7.2, since Ca(II) would precipitate PO_4^{-3} and thus increase the solution pH. When phosphate buffer was replaced with 0.04 M Tris, it was also necessary to reduce the acetaldehyde concentration to 0.02 M, since higher concentrations of acetaldehyde appeared to bring about the denaturization of the ADH in the presence of 0.04 M Tris and 0.05 M $Ca(ClO_4)_2$ at pH 7.2 (Solution II').

(4) In solutions II and II', the 1,4-NADH was oxidized enzymatically to NAD^+. However, the ultraviolet absorption spectra of these solutions still showed an absorption maximum at 340-345 nm, which resulted from the presence of the dimer $(NAD)_2$ with an ε_{340} = 6,650 (14) and, most likely, of 1,6-NADH with an ε_{345} = 6,200 (46). The portion of the absorbance attributable to the dimer was calculated from the polarographically determined dimer concentration and the molar absorptivity given; the concentration of the 1,6-NADH was then calcu-

lated, assuming that the remainder of the absorbance was due to 1,6-NADH.

Since 1,4-NADH was not oxidized to NAD^+ in solution I, the absorptivity of solution I at 340 nm was due to 1,4-NADH, 1,6-NADH and $(NAD)_2$. Since only 1,4-NADH had been oxidized to NAD^+ in solutions II and II' the concentration of 1,4-NADH in solution I was calculated from the absorbance difference between solution I and either solution II or II' at 340 nm, using a molar absorptivity of 6,200 for 1,4-NADH.

A material balance of the product concentrations with the initial NAD^+ concentration, assuming the absorbance at 340 nm to be due solely to 1,4-NADH, 1,6-NADH and $(NAD)_2$, gave an agreement of within 10% in most cases (Table XV). However, since no attempt was made to isolate 1,6-NADH, its identity as one of the products of the electrochemical reduction of NAD^+ is not confirmed.

The modified assay procedure, which was used in the presence of Ca(II), was evaluated by applying it to commercially obtained 1,4-NADH. The modified procedure gave 1,4-NADH purity levels for the latter commercial sample which were within 2 to 4% of the levels determined using the assay discussed in Section II-A.

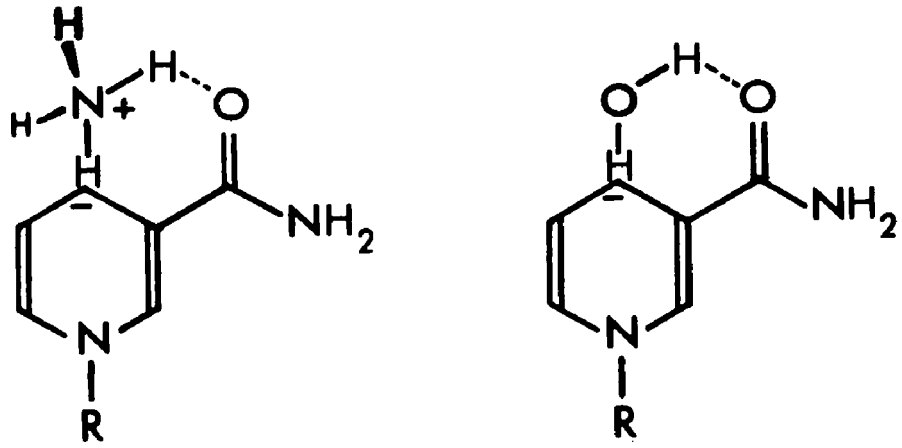
b. Relationship of k_2 to 1,4-NADH:1,6-NADH Ratio. The principal difference in the products of the reduction of NAD^+ lay in the calculated ratio of 1,4-NADH:1,6-NADH as a function of Brønsted acid concentration and strength in a given buffer (Table XV). In 0.1 M Teap and 0.05 M $Ca(ClO_4)_2$ in 0.01 M Tris at pH 9.3, where the concentration of protonated Tris was ca. 0.5 mM (protonated Tris pK_a = 8), the ratios of 1,4:1,6-NADH were 1.5 and 1.6 for a two-fold change in NAD^+

concentration. In 0.4 M KCl or 0.4 M TeaCl in 0.1 M carbonate at pH 9.1, where the concentration of bicarbonate is ca. 93 mM (HCO_3^- pK_a = 10.25), the average ratio of 1,4:1,6-NADH was 1.9. For the background, which was 0.32 M in NH_4Cl and 0.08 M in KCl at pH 9.05, the concentration of NH_4^+ was 0.32 M (NH_4^+ pK_a = 9.25) and the average ratio of 1,4:1,6-NADH was 2.8. This increase in the ratio 1,4:1,6-NADH with an increase in the capacity of the background to buffer OH^- is interesting in light of the fact that the rate constant for the rearrangement following the reduction of NAD·-HX shows a similar dependence.

The rate of the rearrangement was slowest in 0.1 M Teap and 0.01 M Tris at pH 9.3, increasing more than three-fold when the background was changed to 0.4 M TeaCl and 0.1 M carbonate at 25°C (Table XIII). Since NH_4^+ is a stronger acid than either H_2O or HCO_3^-, it is reasonable to assume that in the presence of NH_4Cl, where NH_4^+ is the proton donor, the rearrangement will occur faster than in the presence of bicarbonate where either HCO_3^- or H_2O is the proton donor.

Since the overall reduction of NAD· to NADH involves the addition of a proton and an electron, it is not surprising that the reduction of NAD· and the rearrangement, which involves the addition of a proton at the C(4) or C(6) carbon, are affected by the concentration and acidity of available proton donors. The fact that the rearrangement is slowest in 0.1 M Teap and 0.01 M Tris at pH 9.3 indicates that, although protonated Tris is a stronger acid than H_2O, HCO_3^- and NH_4^+, its concentration at pH 9.3, i.e., ca. 5×10^{-4} M, is too small for protonated Tris to be a kinetically significant proton donor.

It is not apparent why the increased capacity to buffer OH^- should result in an increase in the relative fraction of NAD^+ which is electrochemically reduced to 1,4-NADH, as is the case for the electrolyses done in the presence of 0.32 M NH_4^+. One explanation for this behavior lies in the possible structure of NADH-X^-. The following two structures can be drawn for the reduced proton donor adduct, when either NH_4^+ or H_2O is the proton donor:



For these two structures, hydrogen bonding of the proton donor with the amide oxygen could orient the proton donor such that a hydrogen was near the C(4) carbon. This orientation would facilitate protonation at the 4 position. When NH_4^+ is the proton donor, the positively charged nitrogen near the C(4) carbon may result in the C(4) carbon having more carbanion character than the C(6) carbon; with the end result that a larger fraction of NAD^+ is reduced to 1,4-NADH in the presence of NH_4^+.

Since some 1,6-NADH is produced in the reduction, regardless of whether NH_4^+ is present or not, it seems probable that the C(6)

carbon of NADH-X^- still retains some carbanion character. The 1,6-NADH is probably produced when a carbanion at the 6 position is protonated through the abstraction of a proton from the solvent water or buffer.

IV. OXIDATION OF 1,4-NADH

The oxidation of 1,4-NADH to NAD^+ occurs by way of the loss of two electrons and a proton,

$$NADH \xrightarrow{k_{s,h}} NAD^+ + 2e + H^+ \qquad (32)$$

A. Pretreatment of Glassy Carbon Electrode

The electrochemical characteristics of the oxidation of NADH on a glassy carbon electrode, gce, are strongly dependent on the method used to prepare the electrode. In cyclic voltammetric studies of the oxidation of NADH, use of the following procedure to prepare the electrode surface prior to the running of each voltammetric sweep, resulted in a reproducible electrochemical response:

(1) The electrode is sanded vigorously with 600-grade silicon carbide paper.

(2) The electrode is then sprayed with distilled water under pressure to remove any loose particulate carbon.

(3) The excess water is daubed off the electrode surface with lens paper.

(4) The electrode surface is allowed to air dry.

It was necessary to repeat the above procedure before each scan because prolonged exposure of the electrode to NADH had the effect of passivating the electrode surface. Within 2 to 3 minutes of being immersed in a solution of 2.6 mM NADH in 0.1 M Teap and 0.01 M Tris, the voltammetric peak for the oxidation of NADH showed a noticeable attenuation in the peak current accompanied by a positive shift in the oxidation potential. Exposure of the gce to 0.1 M Teap and 0.01 M Tris alone produced no observable changes in electrode behavior. Since rinsing the electrode surface with distilled water, after exposing the electrode to NADH, did not regenerate the original characteristics of the electrode, a very strong adsorption of NADH on the glassy carbon surface is indicated.

Polishing the electrode surface with lens paper prior to the running of each voltammetric sweep did not result in a reproducible electrochemical response for the oxidation of NADH. It was found that polishing had the effect of passivating the electrode surface. Figure 23 shows a comparison between the oxidation of NADH at a gce which was sanded, rinsed, and allowed to air dry. (A), and the oxidation at a gce which was sanded, rinsed, and polished with lens paper, (B). Voltammogram (B) shows an electrochemical response which is significantly more irreversible than that of (A); the peak potential was ca. 320 mV positive and the peak current was ca. 30% less. In general the magnitude of the positive peak potential shift and the attenuation of

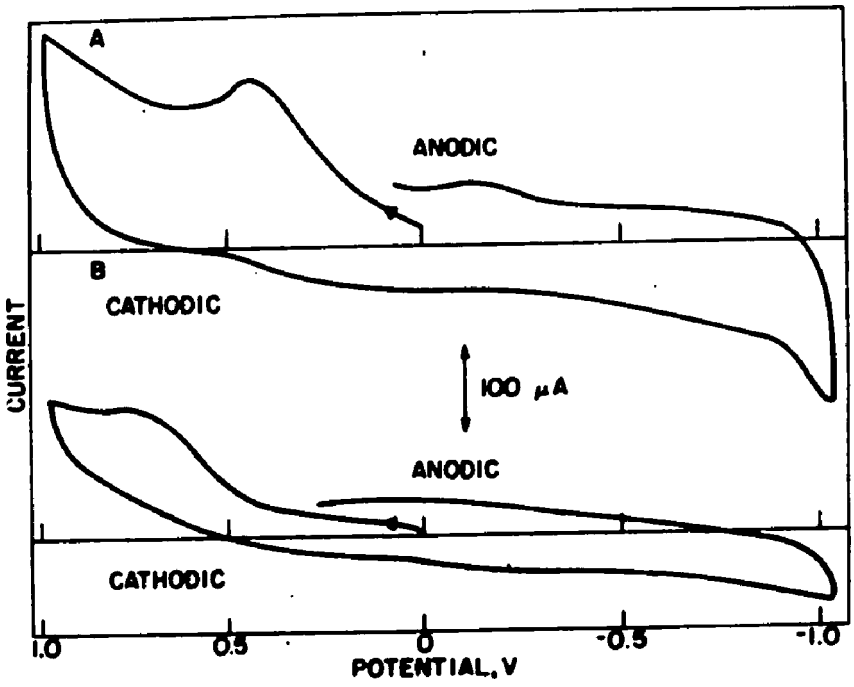


Figure 23. Cyclic voltammograms of 2.6 mM NADH in 0.1 M Teap and 0.01 M Tris showing the effects of electrode pretreatment. Pretreatment procedure: (A) sand with 600-grade silicon carbide paper, rinse with distilled water, and air dry; (B) sand with 600-grade silicon carbide paper, rinse with distilled water, and polish with lens paper. Scan rate = 40 mV/s. Arrowhead indicates the direction of the scan.

the current are dependent on the duration and vigor of the surface polishing.

B. Effect of pH on the Oxidation of NADH

The effect of pH on the electrochemical oxidation of NADH at a gce was examined over the range of pH 7.2 to pH 9.6 in 0.1 M Teap and 0.01 M Tris (the pH was adjusted by the addition of $HClO_4$).

In the range of pH 7.2 to 9.6, the oxidation of NADH on a gce was highly irreversible. Within the range of applied scan rates, 0.04 to 20 V/s, no complementary cathodic peak was observed. At scan rates in excess of 20 V/s, the anodic peak for the oxidation of NADH was quite broad and extended into the potential region where the oxidation of water to evolve oxygen occurred. Hence, meaningful determinations of peak potentials and currents could not be made at scan rates of greater than 20 V/s.

The effect of pH on the voltammetric peak potential for the oxidation of NADH was found to be dependent on the sweep rate of the cyclic voltammogram (cyclic voltammetric data for the oxidation of NADH is summarized in Table XVI). The relationship of peak potential to pH for a scan rate of 0.2 V/s is given by

$$E_p = 0.53 - 0.012\ pH \qquad (33)$$

At a rotating glassy carbon electrode (214 rpm), Blaedel and Jenkins (10) reported that the oxidation potential-pH relationship for 10 μM NADH in 0.1 M NaCl and 0.005 M phosphate buffer is given by

$$E_{1/2} = 0.512 - 0.017\ pH \qquad (34)$$

Table XVI. Cyclic Voltammetric Data for the Oxidation of 2.6 mM 1,4-NADH on a Glassy Carbon Electrode

pH[a]	v mV/s	E_p V	$E_p - E_{p/2}$ mV	i_p μA	$(1 - \alpha)n_a$[b]
Background: 0.1 M Teap and 0.01 M Tris					
7.2	40	0.40	175	95	0.27
7.2	90	0.425	165	155	0.29
7.2	200	0.45	165	270	0.29
8.3	40	0.40	175	105	0.27
8.3	90	0.41	165	155	0.29
8.3	200	0.43	155	230	0.31
9.6	40	0.39	185	95	0.26
9.6	90	0.41	180	160	0.26
9.6	200	0.42	155	245	0.31
Background; 0.1 M Teap, 0.01 Tris and 50 mM Ca(II)					
7.2	40	0.41	145	115	0.33
7.2	90	0.425	155	210	0.31
7.2	200	0.46	135	370	0.35
9.6	40	0.41	145	135	0.33
9.6	90	0.425	135	210	0.35
9.6	200	0.455	130	375	0.37
Background; 0.1 M Teap, 0.01 M Tris and 21 mM Zn(II)					
7.2	40	0.425	120	130	0.40
7.2	90	0.455	115	220	0.42
7.2	200	0.485	130	355	0.37

[a] The solution pH was adjusted by the addition of $HClO_4$.

[b] The product $(1 - \alpha)n_a$ was calculated from the slope of the voltammogram and is equivalent to 1.857 RT [F $(E_p - E_{p/2})$] (54).

The agreement in oxidation potentials and pH dependence is reasonable considering the difference in electroanalytical techniques. The slight differences may be attributable to the fact that the adsorption of NADH, which is more predominant at the 2.6 mM level than at the 10 μM level, tends to inhibit the oxidation of NADH and, in general, makes the electrode less responsive.

If the oxidation of NADH proceded reversibly with the loss of two electrons and a proton, the peak potential would be predicted to shift 30 mV positive for a decrease in pH of one unit at 25°C. The relationship of E_p to pH and the irreversible character of the cyclic voltammograms indicate that the oxidation of NADH does not occur reversibly.

The slopes of 155 to 185 mV for the cyclic voltammetric peaks, $E_p - E_{p/2}$, for the oxidation of NADH (Table XVI) indicate that the rate-controlling step in the oxidation of 1,4-NADH is the rate of the charge transfer (31). In order to determine a charge transfer rate constant, $k_{s,h}$, it would be necessary either for the rate to be sufficiently rapid that a cathodic peak could be observed or for a thermodynamic E^o to be previously known. Since neither of these conditions could be met, a value of $k_{s,h}$ for the oxidation of NADH could not be determined. However, the product, $(1 - \alpha)n_a$, could be calculated from the slopes of the voltammetric peaks; α is the transfer coefficient for the charge transfer process (53) and n_a is the number of electrons involved in the process, which is generally taken to be one. The term $(1 - \alpha)$ represents the fraction of the applied overpotential which promotes the oxidation step. The relationship of

the slope to $(1 - \alpha)n_a$ is given by equation 35 (54).

$$E_p - E_{p/2} = \frac{1.857\ RT}{F(1 - \alpha)n_a} \qquad (35)$$

Determinations of $(1 - \alpha)n_a$ based on nine cyclic voltammograms run at scan rates of 0.04, 0.09 and 0.20 V/s were independent of solution pH with an average value of 0.28 and a standard deviation of 0.02. For 10 μM NADH in 0.1 M NaCl and 0.005 M phosphate buffer, Blaedel and Jenkins (10) reported a slope for a plot of E vs. log $[(i_d - i)/i]$, which corresponds to a $(1 - \alpha)n_a$ of 0.17, at a rotating glassy carbon electrode (214 rpm).

In the limiting case, where all of the electroactive species undergoing a charge transfer is adsorbed at the solution-electrode interphase, the peak current, i_p, will be proportional to the scan rate, v, and, hence, a plot of ln i_p vs. ln v will have a slope of 1.0 (55). In the case where a non-adsorbed electroactive species undergoes charge transfer either reversibly or irreversibly, a slope for ln i_p vs. ln v of 0.50 is predicted (31). A slope in excess of 0.50 indicates that some of the species undergoing charge transfer are adsorbed at the solution-electrode interphase. Since a plot of ln i_p vs. ln v for 2.6 mM NADH in 0.1 M Teap and 0.01 M Tris over the range of pH 7.2 to 9.6 had a slope of 0.58 (Figure 24), it is apparent that some reduction of adsorbed NADH is taking place. In view of the passivation of the gce brought about by its exposure to NADH, it is not surprising that the relationship of the peak current to the scan rate indicates the occurrence of adsorption.

The NADH adsorbed at the electrode-solution interphase is more difficult to oxidize than the NADH, which is in solution. Since

Figure 24. Variation of cyclic voltammetric peak current with scan rate for the oxidation of 2.6 mM NADH on a glassy carbon electrode. Solution conditions: (A) 0.1 M Teap and 0.01 M Tris (ln i_p values were calculated from the average of i_p at pH 7.2, 8.3 and 9.6); (B) 0.1 M Teap, 50 mM Ca(II) and 0.01 M Tris (ln i_p values were calculated from the average of i_p at pH 7.2 and 9.6); (C) 0.1 M Teap, 21 mM Zn(II) and 0.01 M Tris at pH 7.2. pH adjustments were made by addition of $HClO_4$.

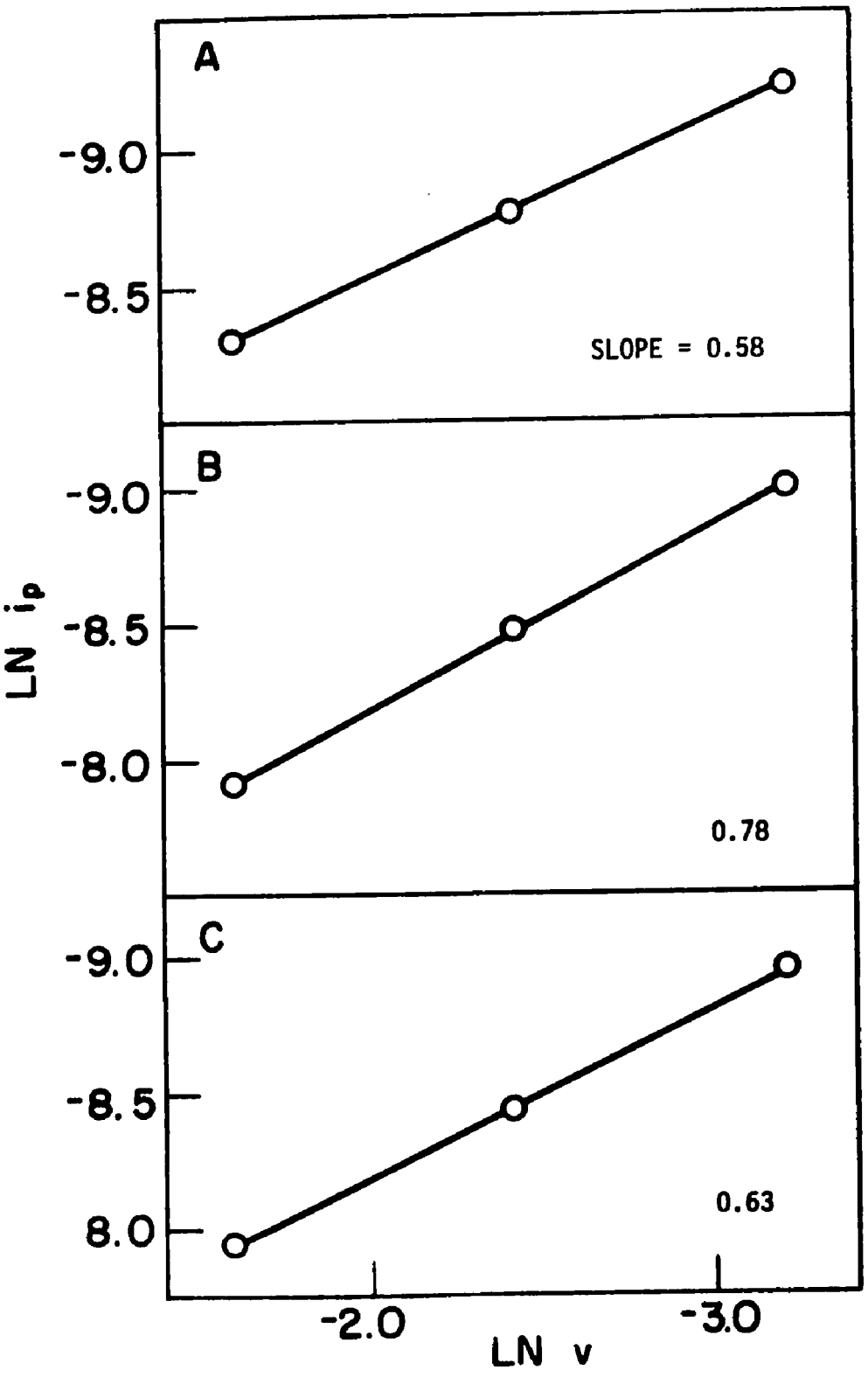


Figure 24.

adsorbed NADH occupies a lower free energy state, in order to oxidize the adsorbed NADH, the electrode potential must increase to overcome the energy of adsorption. Hence, the oxidation of adsorbed NADH requires a more positive potential. Since the peak current-scan rate relationship indicates that some NADH is adsorbed, the true peak potentials for the oxidation of non-adsorbed NADH may be expected to fall at somewhat less positive potentials than were experimentally observed. However, since the oxidation only shows one voltammetric peak, the oxidation potentials for adsorbed and non-adsorbed NADH must be sufficiently close that the experimentally observed voltammetric peak is a composite of the oxidation peaks for adsorbed and non-adsorbed NADH.

C. Effect of Lewis Acids: Ca(II)

The electrochemical oxidation of NADH at a gce in the presence of 50 mM Ca(II) in 0.1 M Teap and 0.01 M Tris was studied at pH 7.2 and 9.6, using cyclic voltammetry to ascertain whether the addition of a Lewis acid would modify the oxidation of NADH.

In the presence of 50 mM Ca(II), the oxidation of NADH was relatively insensitive to a change in pH. Cyclic voltammograms at pH 7.2 and pH 9.6 were quite similar (Table XVI). The addition of Ca(II) produced a slight positive shift in E_p (0-10 mV at pH 7.2 and 20-35 mV at pH 9.6) and an increase in i_p which ranged from 25% at 0.04 V/s to 40% at 0.20 V/s. The slope of ln i_p vs. ln v was 0.73 (Figure 24) as compared to a slope of 0.58 in the absence of Ca(II). This increase in slope indicates that the addition of Ca(II) resulted

in increased adsorption of NADH, since the slope in the presence of Ca(II) more closely approximates the slope predicted for the oxidation of an adsorbed species.

Since increased adsorption of NADH has the effect of producing a greater surface concentration of NADH, the increase in i_p brought about by the addition of Ca(II) is probably a consequence of the increased NADH adsorption. The slight positive shift in E_p may also be the result of an increase in the amount of adsorbed NADH, since a larger fraction of the species undergoing charge transfer will be in a lower energy adsorbed state and will be more difficult to oxidize.

In the potential region where NADH oxidation occurs, the electrode-solution interphase and NADH are of opposite charge. Since the addition of 50 m$\underline{M}$ Ca(II) increases the ionic strength from 0.1 $\underline{M}$ to 0.25 $\underline{M}$, a decrease in the activity coefficient of NADH and a corresponding decrease in adsorption would be expected. However, since adsorption of NADH was increased in the presence of Ca(II), it is likely that Ca(II) serves to further stabilize the NADH adsorbed at the interphase.

Studies of the complexation of Ca(II) by adenine nucleotides have shown that Ca(II) is bound at the phosphate groups of the nucleotide (56,57). If Ca(II) forms a 1:1 complex with NADH, the Ca(II) would probably bind at the pyrophosphate linkage (Figure 1). The resulting complex would be electrically neutral. Although the lack of a negative charge on the complexed NADH would result in a decreased electrostatic attraction towards the positively charged electrode-solution interphase, the electrostatic repulsion between molecules of adsorbed complexed NADH

would be less than the electrostatic repulsion between molecules of adsorbed uncomplexed NADH which have a charge of -2. With less electrostatic repulsion between adsorbed species, a greater surface excess at the interphase will occur. In the presence of 50 mM Ca(II), it is probably the diminished repulsion between adsorbed molecules of complexed NADH which is responsible for the increased NADH adsorption.

D. Effect of Lewis Acids: Zn(II)

The oxidation of 2.6 mM NADH in the presence of 21 mM Zn(II) with a background electrolyte of 0.1 M Teap and 0.01 M Tris buffer at pH 7.2 was studied by cyclic voltammetry. On the addition of Zn(II), E_p for the oxidation of NADH was shifted 20-35 mV positive of the E_p observed in the absence of Zn(II). This shift in E_p was accompanied by a 35% increase in i_p. A plot of ln i_p vs. ln v gave a slope of 0.63 (Figure 24) indicating that the adsorption of NADH was increased slightly by the addition of 21 mM Zn(II) at 7.2. However, this increase in adsorbed NADH was not as large as the increase brought about by the addition of 50 mM Ca(II) at pH 7.2 as evidenced by the steeper slope for the ln i_p vs. ln v plot for the Ca(II) solution.

Although much of the increase in i_p can be attributed to the increase in adsorbed NADH, the shift in E_p can not. Adsorption of NADH occurs to a lesser extent in the solution which was 21 mM in Zn(II) than in the solution which was 50 mM in Ca(II). However, E_p in the presence of Zn(II) was 10-25 mV positive of E_p in the presence of Ca(II) at the same pH. Since the positive shift is not the result of

increased NADH adsorption, it may be indicative of some type of interaction between Zn(II) and NADH.

If NADH complexes with Zn(II), the Lewis acid character of the Zn(II) ion could serve to lower the electron density in the dihydronicotinamide moiety, which would make NADH more difficult to oxidize. Nuclear magnetic resonance (58) and infrared (59) spectroscopic studies have indicated that, in adenosine-5'-triphosphate, Zn(II) binds at both the adenine and phosphate moieties. It is highly probably that Zn(II) will bind these sites in NADH as well. It is not clear whether there is any significant interaction between Zn(II) and the dihydronicotinamide moiety. However, in view of the rather small shift in E_p at a Zn(II):NADH ratio of 8:1, any interaction of this type would have to be quite weak.

V. ADSORPTION OF ADENINE AND NAD^+

AC polarographic studies of both NAD^+ and NMN^+ have indicated that NAD^+ is adsorbed to a substantially larger degree at the mercury-solution interphase. In 0.4 M KCl and 0.1 M carbonate buffer at pH 9.6, the presence of NAD^+ produced a large depression in the differential double layer capacitance in a potential region which extended from the mercury oxidation at -0.05 V to about -1.4 V. NMN^+ under the same solution conditions gave only a slight decrease in the differential double layer capacitance prior to the first reduction peak (48). Since similar sugar and phosphate moieties are present in both NMN^+ and NAD^+, the adenine moiety of NAD^+ is suspected of being responsible for the greater surface activity of NAD^+.

In order to elucidate the role of adenine in the electrochemical reduction of NAD^+, studies of the potential-dependent adsorption of adenine and NAD^+ were carried out using the pulse polarographic technique described in Section II. The timing sequence for the application of the potential pulse and for the current sampling is described in Figure 6.

The pulse polarographic studies of adenine and NAD^+ were conducted in 0.5 M McIlvaine buffer at pH 4.8 (Table I), using a controlled drop time of 5 seconds. An average current and standard deviation was calculated for each initial polarization potential, E_{ip}, from the sampled current of 5 to 10 drops.

The pulse polarographic currents for adenine were obtained by stepping the potential at the dme from E_{ip} to a final polarization potential, E_{fp}, of -1.48 V and then sampling the current 2.9 ms after the application of the pulse. At a concentration of 10 μM adenine showed maximum adsorption in the potential range from -0.25 to -0.45 V (Figure 25). The pulse polarographic current due to the reduction of adenine was relatively constant within this potential region. Using the same pulse polarographic technique but with current sampling delayed until 6.2 ms after pulse application, Flemming (21) reported maximum adsorption at a potential of -0.43 V for 6.25 μM adenine in 0.5 M McIlvaine buffer at pH 5.

The pulse polarographic current for NAD^+ was obtained by stepping from E_{ip} to -1.3 V, which lies on the plateau of the initial diffusion-controlled reduction wave for NAD^+. At a concentration of 10 μM, NAD^+ showed maximum adsorption in the potential region from -0.15 to -0.55 V (Figure 25).

The substantially lower currents which were observed for the reduction of NAD^+, compared to the currents observed for the reduction of adenine, result from the fact that, at an E_{ip} of -1.3 V, NAD^+ undergoes a one-electron transfer whereas in the case of adenine, calculations of a diffusion current constant based on the average dc

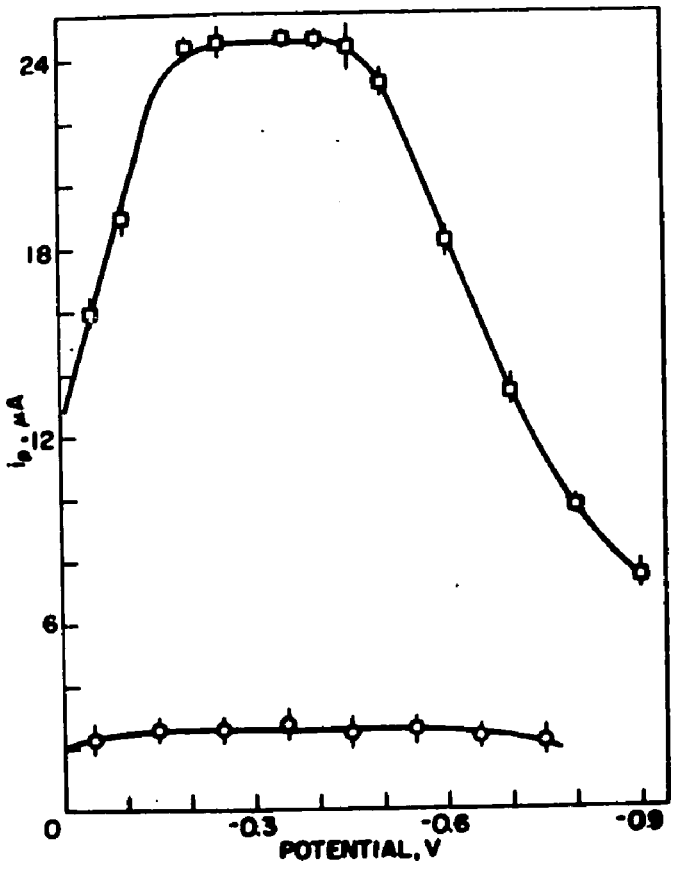


Figure 25. Currents obtained for 10 μM adenine (squares) and 10 μM NAD^+ (circles) in pH 4.8 McIlvaine buffer on modified pulse polarography (Section II) on stepping the potential from the initial polarization potential shown in the figure to the final polarization potential, E_{fp}. For adenine, E_{fp} = -1.48 V; for NAD^+, E_{fp} = -1.30 V. The discharge period was 3 ms; the current measurement period was 25 μs; controlled drop-time was 5.0 s.

polarographic current at -1.48 V gave an I_d which was indicative of a six or seven-electron transfer (22). Hence, the pulse polarographic current for the reduction of adenine was far greater than the current for the reduction of NAD^+.

The I_d for the reduction of adenine is larger than one would expect. Electrochemical studies of adenine indicate that, in all likelihood, the polarographic reduction of adenine involves only four electrons, with deamination and an additional two-electron reduction occurring relatively slowly on the time scale of dme polarography. A catalytic reduction of hydrogen superimposed on the reduction wave for adenine is probably responsible for the large I_d value. Since the adenine reduction wave occurs on the shoulder of the background discharge due in part to the fact that the discharge is shifted to a more positive potential by the presence of adenine, some catalytic reduction of hydrogen by adenine or its reduction products is considered to be likely (60,61). In spite of the catalytic discharge, a plot of the dc polarographic, i_d *vs.* $h^{\frac{1}{2}}$, where h is the height of the mercury above the capillary tip, was linear, indicating that the polarographic wave is diffusion controlled; consequently, the rate of hydrogen discharge must be dependent upon the diffusion of adenine to the electrode-solution interface.

Solutions of NAD^+ also showed a combined reduction and catalytic discharge wave at the shoulder of the background discharge. Since this wave was of the same magnitude and in the same potential region as the adenine wave, the wave in the presence of NAD^+ probably results from the reduction of the adenine moiety of NAD^+ and from the catalytic discharge of hydrogen by this adenine moiety and its reduction products.

A. Comparison of the Relative Adsorption of Adenine and NAD^+

In order to determine the relative increase in the pulse polarographic current, i_p, brought about by the preconcentration of electroactive species through adsorption at the solution-electrode interface, compared to that current, i_t, which would be predicted for a simple diffusion controlled electron transfer, i_p was divided by the current predicted by

$$i_t = C_o nFAD_o^{\frac{1}{2}}/(\pi t)^{\frac{1}{2}} \qquad (36)$$

where A is the area of the mercury drop at 5 seconds, t is the period time between the application of the pulse and the cessation of current sampling and i_t is the current which would be predicted for a diffusion controlled charge transfer at time t. The calculations of i_t were based on values for $nD_o^{\frac{1}{2}}$ of 0.022 for adenine and 0.0020 for NAD^+. These values were calculated from I_d values reported for adenine (22) and NAD^+ (4) where $I_d = 607\ nD_o^{\frac{1}{2}}$. Plots of i_p/i_t vs. E_{ip} were made for both adenine and NAD^+ (Figure 26).

For 10 μM NAD^+, the ratio of i_p/i_t reached a value of 6 in the potential region of maximum adsorption. Adenine at the 10 μM level reached a maximum i_p/i_t ratio of 5.1. However, the error bars, which describe an uncertainty of one standard deviation for the i_p/i_t values of NAD^+ and adenine, do overlap in the potential region from -0.25 to -0.45 V. The similarity in the i_p/i_t ratios indicate that the number of molecules adsorbed per unit area of the interface is nearly the same for adenine and NAD^+.

The uncertainty (one standard deviation) in the measurements of i_p for adenine and NAD^+ was about 1 μA. However, since pulse

Figure 26. Variation of normalized pulse polarographic current with initial polarization potential, E_{ip}, for 10 μM adenine (squares) and 10 μM NAD^+ (circles) in pH 4.8 McIlvaine buffer. The modified pulse polarographic current, i_p, is obtained on stepping the potential from E_{ip} to the final polarization potential, E_{fp} (-1.48 for adenine; -1.30 for NAD^+). The discharge period was 3 ms; the current measurement period was 25 μs; controlled drop-time was 5.0 s. The predicted diffusion controlled current, i_t, was calculated from equation 36.

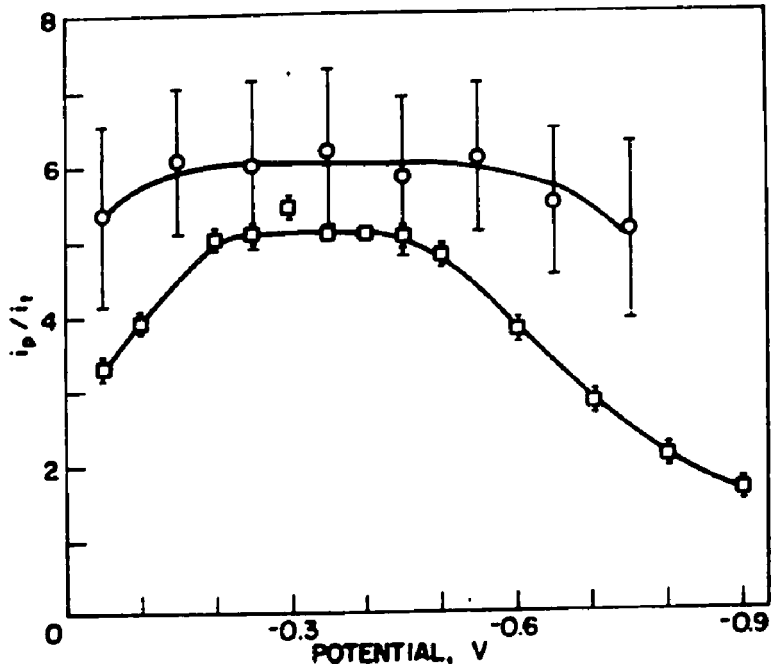


Figure 26.

polarographic currents for NAD^+ were smaller than those determined for adenine, the relative uncertainty in determining i_p is much larger for NAD^+ and the error bars for the i_p/i_t values for NAD^+ are substantially greater.

B. Adsorption Site of NAD^+

Polarographic studies of NMN^+ have shown that the presence of nicotinamide, ribose and phosphate moieties do not by themselves result in a high degree of surface activity (4). NAD^+, which contains one additional sugar and phosphate along with an adenine moiety, shows a much greater surface activity. Since the addition of such hydrophilic groups as the sugar and phosphate could hardly be expected to produce a substantial increase in adsorption, the adenine moiety must be the most likely site for the adsorption of NAD^+.

Inasmuch as NAD^+ contains more hydrophilic groups than adenine, i.e., two phosphates and two sugars, it may seem somewhat surprising that NAD^+ is adsorbed strongly over a broader potential region and that the surface concentration of NAD^+ is slightly greater than the surface concentration of adenine. Adsorption studies of adenine nucleosides and nucleotides (60,62-64) have shown that when ribose and phosphate functionalities are added to adenine, forming adenosine monophosphate, the species formed is adsorbed over a broader potential region than adenine itself, with the extension of the potential region of adsorption occurring in the region which is positive of the potential of zero charge. Since the electrode-solution interface has a net positive charge in this potential region, the increased adsorption

may result from an electrostatic attraction between the negatively charged phosphate group and the interface.

In view of the effect of the ribose-phosphate functionality on the potential-dependent adsorption of adenine nucleotides, it may be the presence of the ribose-phosphate groups in NAD^+ which is responsible for the facts that NAD^+ adsorption occurs over a broader potential region than adenine adsorption and that in the potential region of maximum adsorption the number of molecules per unit area is slightly larger for NAD^+.

Inasmuch as the potential-dependent adsorption of NAD^+ and adenine are quite similar, with only minor differences which can be attributed to the presence of the phosphate groups in NAD^+, it is considered extremely likely that the site of NAD^+ adsorption at the solution-electrode interface is the adenine moiety.

VI. RELATION OF BIOLOGICAL AND ELECTROCHEMICAL REDOX PROCESSES

A. Summary of Electrochemical and Biological Redox Behavior

The initial one-electron reduction of NAD^+ involves a reversible charge transfer to form the free radical, $\dot{NAD}$ (equation 11). Assuming comparable diffusion coefficients for NAD^+ and $\dot{NAD}$, the thermodynamic E^o for this reduction is -1.156 V in 0.4 M TeaCl and 0.1 M carbonate buffer at pH 9.1 at 25°C.

Before being reduced, the free radical, $\dot{NAD}$, first forms a free radical-proton donor adduct, $\dot{NAD}$-HX. The reduction potential of this adduct is dependent on the concentration and acid strength of HX. In the presence of 0.4 M NH_4^+ at pH 9, the polarographic $E_{\frac{1}{2}}$ is -1.53 V. When 0.1 M carbonate at pH 9.1 is used as buffer, the $E_{\frac{1}{2}}$ is -1.665 V (for a detailed discussion of the effect of HX on the reduction potential, see Section IV). Following the charge transfer, the reduced adduct undergoes a rearrangement to form the final reduction product, NADH (equation 22). The rate constant for this rearrangement, assuming the reaction to be first order, is 1×10^4 s^{-1} in 0.4 M TeaCl

and 0.1 M carbonate at pH 9.1 at 25°C.

The reduction product, 1,4-NADH, is irreversibly oxidized to NAD^+ at a potential of +0.4 V in 0.1 M Teap and 0.01 M Tris with the loss of a proton and two electrons (equation 32). Although a proton is one of the oxidation products, the oxidation potential of NADH shows only a marginal dependence on the solution pH (equation 33). This behavior suggests that the loss of an electron is the rate controlling step in the oxidation of NADH.

The electrochemical NAD^+/NADH redox cycle, as related to potential, is summarized in Figure 27.

In biological systems, the NAD^+/NADH redox couple behaves macroscopically reversibly in the presence of the appropriate enzyme and substrate. Formal redox potentials for this couple have been calculated from thermodynamic measurements on several NAD^+-substrate systems and have also been determined potentiometrically from measurements on systems containing NAD^+, a mediator and an appropriate enzyme. Both methods of determining E_C^o yield a formal redox potential of -0.56 ± 0.01 V vs. sce at pH 7 (2,3,6,65-68).

B. NAD^+/NADH Redox Mechanism

The electrochemical redox processes for the NAD^+/NADH couple have been shown to be markedly different from those for the biological redox couple. It is possible to rationalize these differences, however, in terms of the chemical species formed following each charge transfer and of the subsequent rearrangements and chemical reactions which take place during the electrochemical redox process.

Figure 27. Composite representation of the voltammetric waves for the NAD^+/NADH system. Solution conditions: (A) 0.4 M KCl in 0.1 M carbonate buffer at pH 9.1 (solid lines) and 0.5 M NH_4Cl at pH 9.05 (broken line); (B) 0.4 M TeaCl in 0.1 M carbonate buffer at pH 9.1 (solid lines) and 0.1 M Teap in 0.01 M Tris at pH 9.6 (broken line). The calculated formal potential, E_C^o, is -0.557 V vs. sce for the half-reaction, $NAD^+ + 2e + H^+ \rightleftharpoons$ 1,4-NADH at pH 7 at 25°C (65).

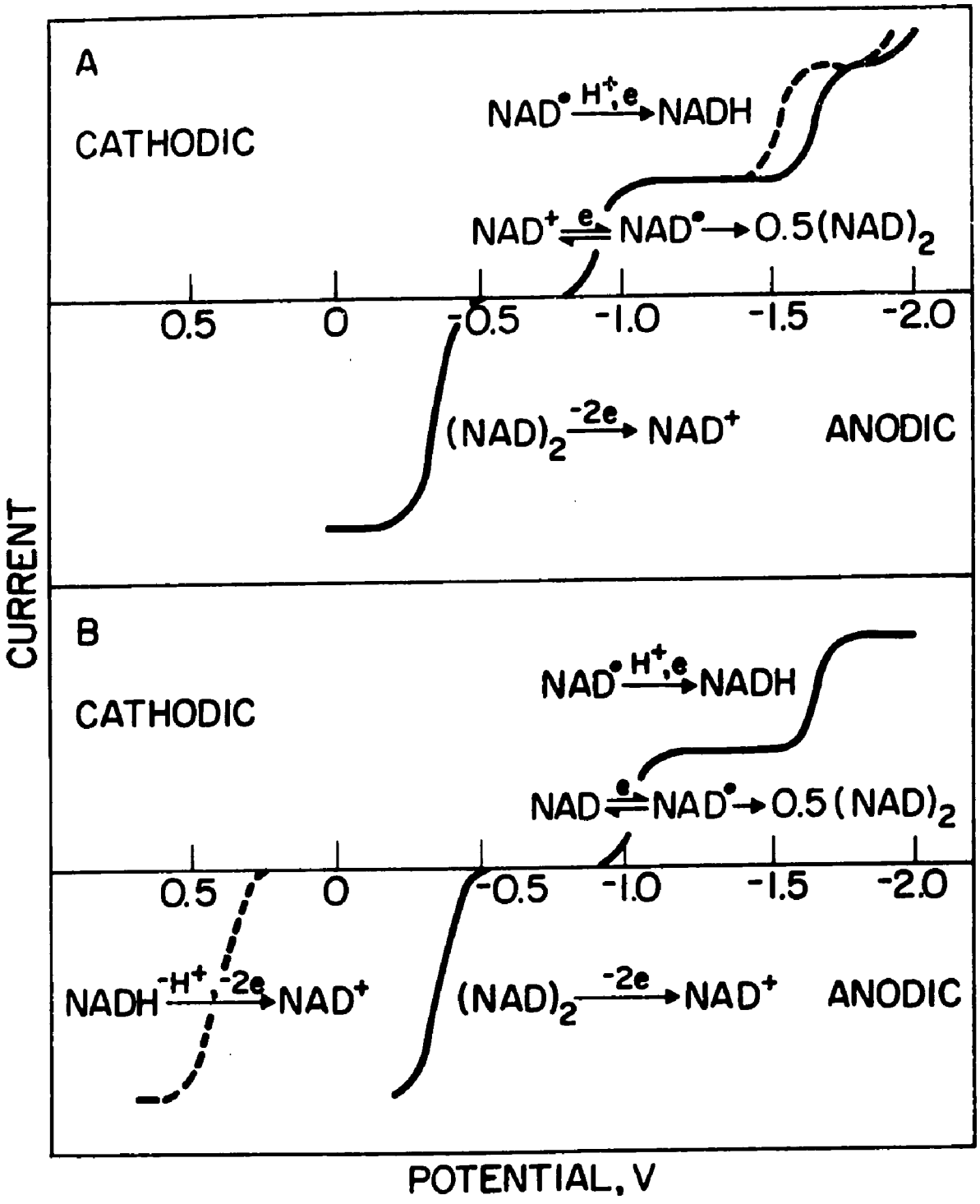

A
CATHODIC
NAD• H+,e NADH
NAD+ e NAD• 0.5(NAD)2
0.5
0
-0.5
-1.0
-1.5
-2.0
(NAD)2 -2e NAD+
ANODIC
B
CATHODIC
NAD• H+,e NADH
NAD e NAD• 0.5 (NAD)2
0.5
0
-0.5
-1.0
-1.5
-2.0
NADH -H+,-2e NAD+
(NAD)2 -2e NAD+
ANODIC
CURRENT
POTENTIAL, V

Figure 27.

In the initial reduction of NAD^+, which involves the addition of an electron to the nicotinamide moiety to form the free radical species, it is possible to draw at least six resonance structures for the free radical which is formed (Figure 28). The first series of resonance structures involve just the pyridine ring with the free radical at the 2,4 or 6 position, while the amide functionality remains unaltered. A series of resonance structures can also be drawn, where the amide oxygen has a negative charge, while the pyridine nitrogen retains its positive charge, as in the case of NAD^+. In this series as well, it is possible to form resonance structures with the free radical at the 2,4 or 6 position.

Prior to the second reductive step, $\dot{NAD}$ forms an adduct with a proton donor, HX. This adduct, O_1, ($\dot{NAD}$-HX shown in Figure 29) would be formed with HX bonding to $\dot{NAD}$ through a hydrogen bridge. The formation of this hydrogen bridge can occur at either the pyridine nitrogen, for those resonance structures where the nitrogen has a significant amine character, or at the amide oxygen, for those structures where the oxygen has a negative charge. The adduct formed by the addition of HX to $\dot{NAD}$ would be in equilibrium with a second structure, O_2, which may be formed from O_1 through the loss of X^- and the addition of hydrogen at the 4 position with the subsequent realignment of the pi bonding system.

At a potential of -1.6 V, O_1 is reduced to R_1 (the bonds from X---H and H---O are drawn as broken lines for both O_1 and R_1 since it is difficult to evaluate to what degree these bonds are dissociated at each step of the reduction sequence), After the reduction, R_1

Figure 28. Schematic diagram of the resonance structures for the free radical NAD· and the reaction sequence showing the coupling of the formation of the free radical proton-donor adduct, O_1 (shown in Figure 29), to the initial charge transfer. R represents adenosine diphosphoribose.

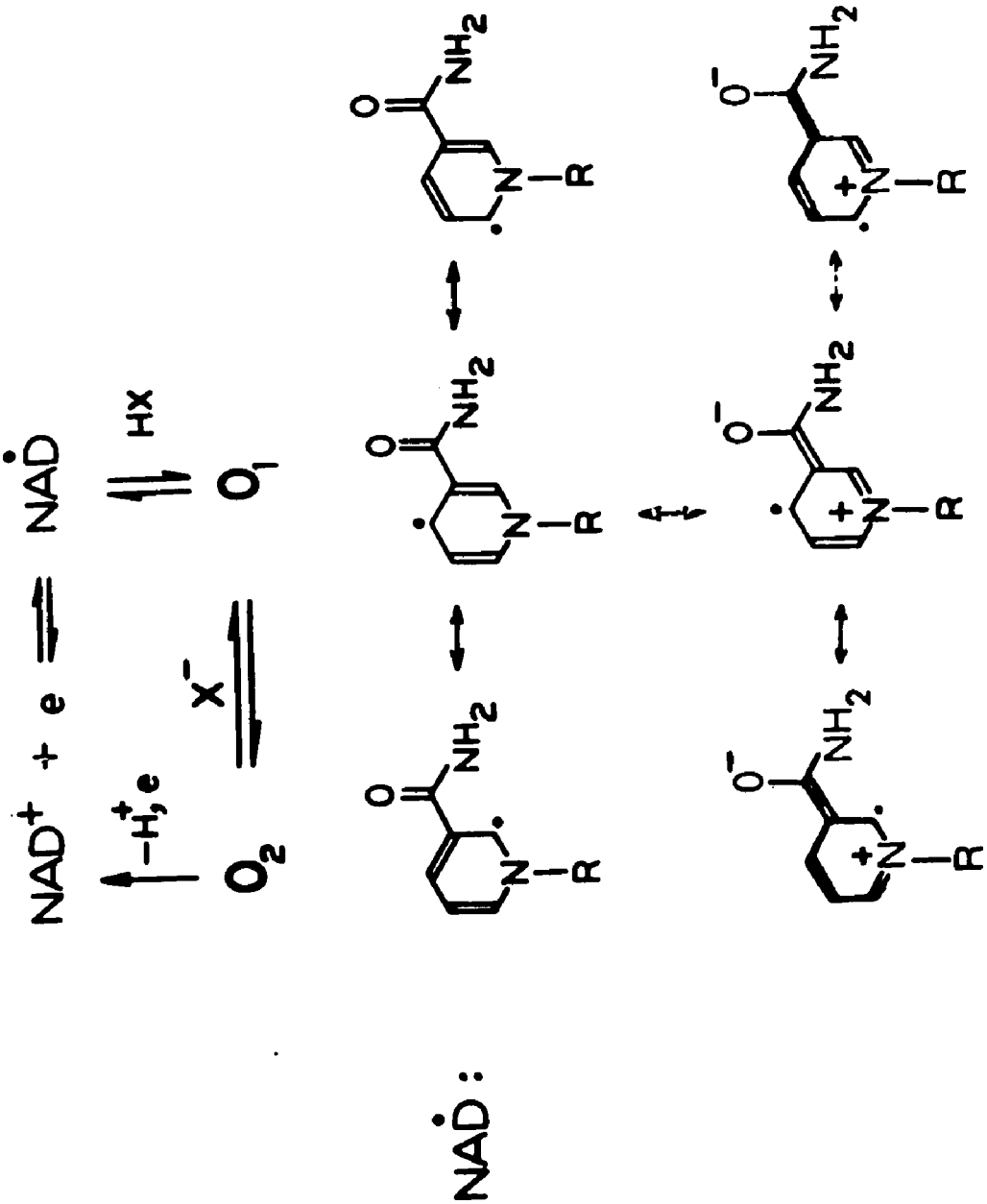


Figure 28.

Figure 29. Schematic diagram of the redox participants in the NAD̈/NADH redox couple and the equilibria of the chemical reactions coupled to the charge transfer processes. E_1^o and E_2^o represent estimations of the formal redox potentials of NAD̈-HX (O_1) and 1,4-NADH (R_2). R represents adenosine diphosphoribose.

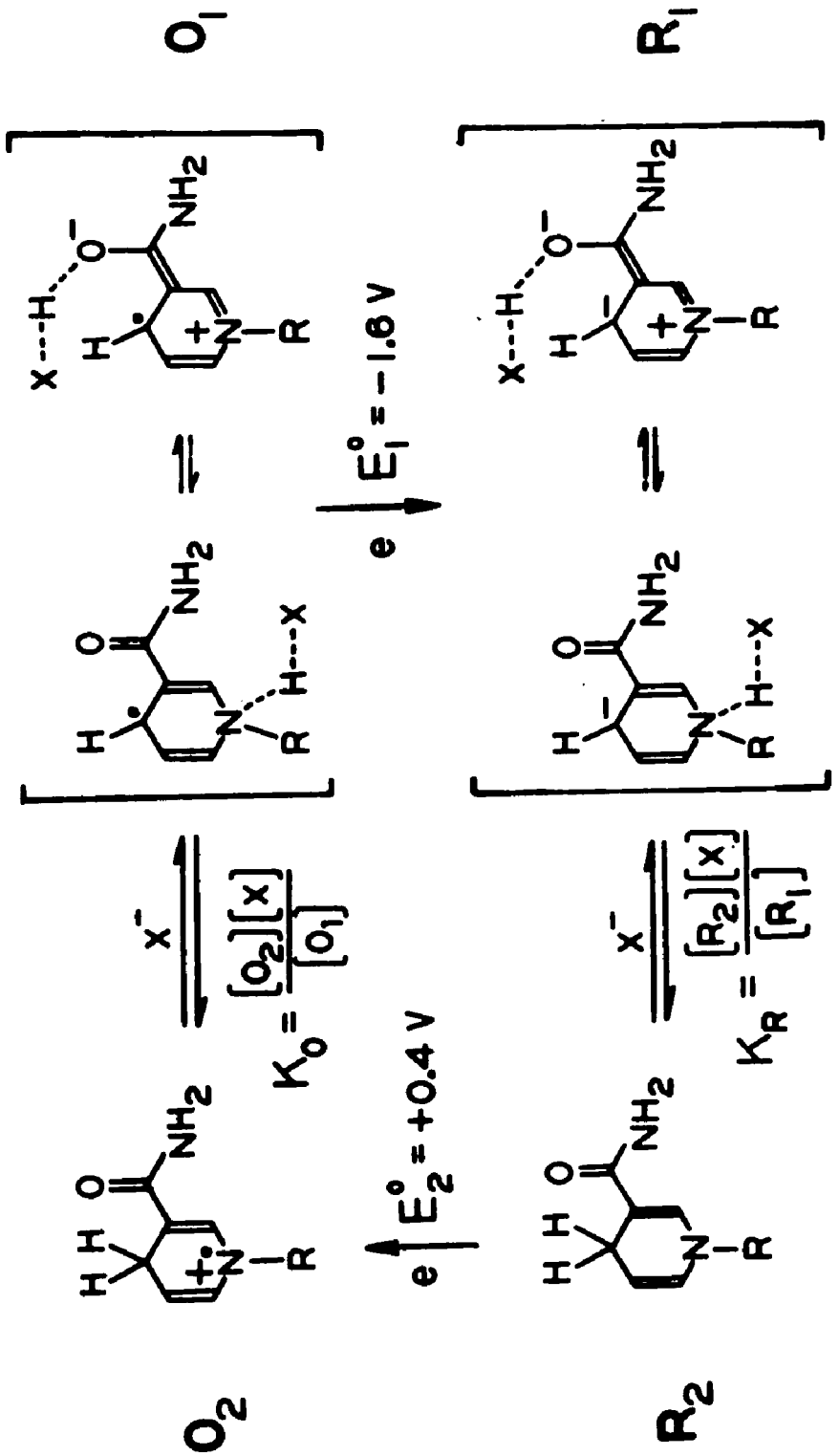


Figure 29.

undergoes a rearrangement forming R_2 (1,4-NADH). This rearrangement could occur either through the transfer of a proton to the C(4) carbon, in the case of the zwitterion ion resonance structure or through the abstraction of a proton from a second proton donor in solution by the carbanion in the case of the other resonance structure. In either circumstance, the total reaction involves the net loss of the conjugate base X^-.

A potential of 0.4 V is required to oxidize R_2 to O_2. This oxidation probably proceeds by the removal of an electron from the dihydropyridine nitrogen. The species which is formed immediately undergoes further oxidation with the loss of a proton and an electron to form NAD^+. Since the oxidation occurs by way of a direct 2e transfer, the species formed by the 1e oxidation of R_2, i.e., O_2, must be more easily oxidized than R_2 itself.

The potentials, which are observed for the reduction of $NA\dot{D}$ and the oxidation of NADH, may be related to the equilibria involved in the reaction sequence shown in Figure 29. Assuming an equilibrium condition, the following equation can be written relating O_1, O_2 R_1 and R_2:

$$E = E_1^o + \frac{RT}{F} \ln \frac{[O_1]}{[R_1]} = E_2^o + \frac{RT}{F} \ln \frac{[O_2]}{[R_2]} \qquad (37)$$

where E_1^o is the formal potential for the O_1/R_1 redox couple and E_2^o is the formal potential for the O_2/R_2 redox couple. Equation 37 may be rewritten to describe E_1^o and E_2^o in terms of the oxidized and reduced species:

$$E_1^o - E_2^o = \frac{RT}{F} \ln \frac{[O_1]\,[R_2]}{[R_1]\,[O_2]} \qquad (38)$$

By substituting K_O and K_R, where K_O and K_R are the equilibrium constants, for the rearrangements involving O_1 and R_1 respectively, shown in Figure 29, for the concentrations of the oxidized and reduced species, the following expression is obtained:

$$E_2^o - E_1^o = \frac{RT}{F} \ln \frac{K_R}{K_O} \qquad (39)$$

Equation 39 describes the potential difference between E_1^o and E_2^o in terms of the two equilibrium constants K_O and K_R. Experimentally, the difference between the potential for the oxidation of NADH and the potential for the reduction of NAḊ is 2.0 V. For this 2.0-V potential difference, the ratio of K_R/K_O calculated from equation 39 would be 10^{34}.

This ratio has been calculated on the assumptions that the dc polarographic $E_{\frac{1}{2}}$ for the reduction of NAḊ is reasonably close to E_1^o ($E^o_{\text{NAḊ-HX/NADH-X}^-}$), and that the voltammetric peak potential for the oxidation of NADH is a good approximation of E_2^o.

$E_{\frac{1}{2}}$, as determined experimentally, is affected by three intervening chemical reactions: (1) the dimerization of the free radical, (2) the formation of the free radical-proton donor adduct, O_1 (NAḊ-HX), and (3) the rearrangement which follows the reduction of the adduct. The first reaction, the dimerization of the free radical, will shift $E_{\frac{1}{2}}$ to more negative potentials since it is consuming the oxidized species in the redox couple. Since the free radical is a weak base, the product of reaction 2, NAḊ-HX, will have a small formation constant and,

the polarographic $E_{1/2}$ will be shifted negative of the formal reduction potential, E_1^0. In the third reaction, the rearrangement of the reduced adduct consumes the reduced species in the couple. This will tend to shift the observed $E_{1/2}$ to more positive potentials.

Because the above three reactions are interrelated and because they each involve redox participants of the NAD̈/NADH-X^- couple, it is extremely difficult to predict the true relationship of $E_{1/2}$ and E_1^0. However, inasmuch as the potential shifts induced by reactions (1) and (2) will be opposed by the potential shift brought about by reaction (3), E_1^0 should lie in the same potential region as $E_{1/2}$.

Since the oxidation of NADH occurs by way of a kinetically controlled charge transfer, as evidenced by a voltammetric slope, $E_p - E_{p/2}$, of 155 to 185 mV, E_2^0 for this oxidation must lie at a more negative potential than the observed voltammetric E_p of 0.4 V. Because of the rate constant for the charge transfer could not be calculated, the potential difference between E_p and E_2^0 could not be accurately evaluated.

For a 59 mV error in estimating either E_1^0 or E_2^0, the calculated ratio of K_R/K_0 will change by a factor of ten.

1. Estimations of K_0 and K_R

A value for K_0 is rather difficult to predict. However, since the reduction of NAD̈ takes place through a reversible charge transfer to form a chemical species which rearranges to NADH rather than through a charge transfer to produce NADH directly, the equilibrium between O_2 and O_1 probably favors O_1, i.e., $K_0 < 1$.

K_R, on the other hand, would be expected to be extremely large.

The product of the rearrangement, R_2(1,4-NADH) is a stable uncharged moiety, while either of the structures attributed to R_1 would be quite unstable. In the R_1 structure, where the proton donor associates at the pyridine nitrogen, the adduct has formed a proton bridge at a site which is a weak base. There is also present on the same moiety a carbanion, which will act as a strong base. For this particular structure, the equilibrium clearly favors protonation of the carbanion which yields R_2. Essentially the same argument can be made concerning the other structure shown for R_1. The zwitterion character of the nicotinamide moiety can be removed by shifting electrons through the conjugated double bonds toward the pyridine nitrogen. This would result in an uncharged pyridine nitrogen, the original amide functionality, where the uncharged amide oxygen is associated with the proton donor, HX, and a carbanion in the 4 position of the pyridine ring. Clearly, the carbanion is a much stronger base than the carbonyl group and one would expect the equilibrium again to be very strongly in favor of R_2.

It is also possible to make semiquantitative calculations of K_R and K_0 based on the formal electrochemical reduction potentials, $E^o_{NAD^+/NAD\cdot}$, $E^o_{NAD\cdot/NADH\text{-}X^-}$ and E^o_2, and the formal redox potential for the biological redox couple, NAD^+/NADH, assuming that the formal potentials $E^o_{NAD\cdot/NADH\text{-}X^-}$ and E^o_2 are comparable to the standard state potentials for these couples.

The net change in standard state free energy which occurs when NAD^+ is reduced to 1,4-NADH at pH 7 can be calculated from the formal E^o for the couple:

$$\Delta G^{o}_{NAD^+/NADH} = -nFE^{o}_{NAD^+/NADH} \quad (40)$$

Using an $E^{o}_{NAD^+/NADH}$ of -0.32 V vs. a normal hydrogen electrode (nhe) and an n of 2, a ΔG^{o} of 15 kcal/mole is calculated.

Similarly, the standard state free energy change for the reduction of NAD^+ to $NADH\text{-}X^-$ can be calculated from the standard state free energy change for the reduction of NAD^+ to $NA\dot{D}$

$$\Delta G^{o}_{NAD^+/N\dot{A}D} = -nFE^{o}_{NAD^+/N\dot{A}D} \quad (41)$$

plus the standard state free energy change for the reduction of $NA\dot{D}$ to $NADH\text{-}X^-$

$$\Delta G^{o}_{N\dot{A}D/NADH\text{-}X^-} = -nFE^{o}_{N\dot{A}D/NADH\text{-}X^-} \quad (42)$$

The E^{o} for the reduction of NAD^+ to $NA\dot{D}$ has been previously determined (Section III) and is equal to -0.91 V vs. nhe. The $\Delta G^{o}_{NAD^+/N\dot{A}D}$ calculated for this reduction is 21 kcal/mole.

The E^{o} for the reduction of $NA\dot{D}$ to $NADH\text{-}X^-$ could not be determined. In order to calculate the $\Delta G^{o}_{N\dot{A}D/NADH\text{-}X^-}$, the assumption is made that $E^{o}_{N\dot{A}D/NADH\text{-}X^-}$ is -1.4 V vs. nhe, i.e., the polarographic $E_{\frac{1}{2}}$. The $\Delta G^{o}_{N\dot{A}D/NADH\text{-}X^-}$ calculated using this assumption is 32 kcal/mole.

The change in standard state free energy in going from $NADH\text{-}X^-$ to NADH is given by

$$\Delta G^{o}_{NADH\text{-}X^-/NADH} = \Delta G^{o}_{NAD^+/NADH} - (\Delta G^{o}_{NAD^+/N\dot{A}D} + \Delta G^{o}_{N\dot{A}D/NADH\text{-}X^-}) \quad (43)$$

The standard state free energy change for the rearrangement of $NADH\text{-}X^-$ to NADH calculated from equation 43 is -38 kcal/mole. The equilibrium constant for the rearrangement, K_R, is determined by the relationship

$$\Delta G = -RT \ln K_R \qquad (44)$$

A K_R of approximately 10^{27} is calculated from equation 44. From the previously suggested ratio for K_R/K_0 of 10^{34}, the equilibrium constant, K_0, for the rearrangement between O_1 and O_2 would then be 10^{-7}. This value agrees with the initial supposition that K_0 should be less than 1.

For a 59-mV error in estimating $E^{o}_{\dot{NAD}/NADH\text{-}X^-}$ and E_1^o ($E^{o}_{\dot{NAD}\text{-}HX/NADH\text{-}X^-}$), K_R will change by an order of magnitude and K_0 will be unaffected. For example, if $E^{o}_{\dot{NAD}/NADH\text{-}X^-}$ and E_1^o lie 59 mV more positive, K_R will decrease by a factor of ten. However, since the ratio of K_R/K_0 will also decrease by a factor of ten (equation 39), K_0 will be unchanged. K_0 will change by an order of magnitude for a 59-mV error in estimating E_2^o. In this case, K_R is calculated from equations 40 through 44 will be unaffected.

In order to calculate values for K_0 and K_R, it was necessary to make estimations of formal redox potentials in those cases where the potentials could not be determined experimentally. Because of these estimations, there is an uncertainty of several orders of magnitude in the values calculated for K_R and K_0. In spite of this uncertainty, the determinations of K_R and K_0 still provide strong support for the mechanism shown in Figure 29.

The relationships between the redox participants, O_1, O_2, R_1 and R_2, predicted by K_R and K_0 are quite reasonable in view of the structures which were proposed for these participants. An examination of the chemical species involved in the equilibrium described by K_R has shown that K_R would be expected to be extremely large. Similarly,

the voltammetric response of the $\dot{NAD}$/NADH couple has shown that the equilibrium between O_1, and O_2 would be expected to favor O_1. Inasmuch as the calculated values of K_R and K_O describe the anticipated relationships between the redox participants, these calculations provide corroboration of the mechanism shown in Figure 29.

C. Correlation of Electrochemical and Biological Redox Potentials

The potentials for the reduction of NAD^+ and $\dot{NAD}$ are both negative of the formal potential for the NAD^+/NADH redox couple (Figure 27). This deviation of electrochemical reduction potentials from the formal E^O of the couple is ordinarily attributed to the fact that an overpotential or additional energy is needed to overcome the activation energy for the electrochemical reactions. The magnitude of the overpotential is a measure of the overall irreversibility of the electrochemical reaction. However, in the cases of the reductions of NAD^+ and $\dot{NAD}$, cyclic voltammetric cathodic and anodic peak separations for both charge transfers are indicative of reversible charge transfers. Hence, the potential difference between the formal E^O and the electrochemical reduction potentials can not be attributed to overpotentials that are required for these electrochemical charge transfers.

Since the biological redox couple has an E^O of -0.56 V while the $NAD^+/\dot{NAD}$ redox couple has an E^O of -1.15 V, it appears as if the free radical should be more easily reduced than NAD^+ and that the reduction of NAD^+ should therefore proceed directly to 1,4-NADH by way of a two-electron transfer. However, the product of the electrochemical reduction of NAD^+ is not reduced directly to 1,4-NADH but rather to an

intermediate species, $NADH\text{-}X^-$ or R_1. Since two discrete reversible electron transfers are observed for the overall reduction of NAD^+ to R_1, the overall reduction of $NAD\dot{}$ to R_1 obviously does not proceed more easily than the reduction of NAD^+ to $NAD\dot{}$.

Since the two charge transfers involved in the electrochemical reduction of NAD^+ proceed reversibly, it follows that the activation energy for these charge transfers is virtually zero. Moreover, if the enzymatic reduction of NAD^+ were to proceed along the same pathway as the electrochemical reduction, with the electron density in the nicotinamide moiety unaltered, the enzymatic reduction of NAD^+ would have a rather large activation energy. This can be seen by comparing the standard state free energy change for the enzymatic reduction of NAD^+ to 1,4-NADH with the free energy change for the electrochemical reduction of NAD^+ to $NADH\text{-}X^-$ (cf. discussion of NAD^+/NADH redox mechanism). Since the enzymatic reduction is macroscopically reversible, it is very unlikely that a large activation energy is required for the reduction. Hence, one function of the enzyme must be to chemically modify the nicotinamide moiety of NAD^+ such that the addition of electrons to the moiety is facilitated.

In the enzyme liver alcohol dehydrogenase, X-ray crystallographic studies have indicated that the nicotinamide moiety is bound to close to a zinc atom in the enzyme (69). The NAD^+, which is bound, is more easily reduced than the free coenzyme in the solution, with the reduction potential for the NAD^+-enzyme complex being 60 to 80 mV positive of that for free NAD^+. This behavior suggests that the binding of NAD^+ on the enzyme surface brings about a change in the reactivity of the

nicotinamide moiety (70).

In addition to changing the reactivity of NAD^+, the enzyme also serves to orient the substrate near the nicotinamide moiety. In the mechanism proposed by Bränden and coworkers (69,71) for the catalytic oxidation of alcohol, based on crystallographic studies, kinetic studies and primary structure work, it is suggested that the alcohol is bound directly to the zinc atom as an alcoholate ion. This binding must occur in such a fashion that a hydrogen on the α-carbon atom of the alcohol is near the C(4) carbon of the nicotinamide moiety. The oxidation of the alcohol then occurs with the net transfer of a hydride ion from the alcohol to NAD^+.

The intermediate steps in the hydride transfer have not yet been elucidated. It is not clear whether this reaction procedes via the formation of a free radical or through the direct transfer of a hydride ion. Electron spin resonance studies of the enzymatic oxidation of alcohols by NAD^+ have not detected the presence of a free radical species (72). Although this does not disprove the existence of a free radical intermediate, it does indicate that the life time of such an intermediate must be sufficiently short that the free radical can not be detected. If the enzymatic oxidation does occur in two steps where the transfer of an electron to NAD^+ is immediately followed by the transfer of a hydrogen atom, the two-step mechanism would be indistinguishable from a hydride transfer.

VII. ANALYTICAL APPLICATION

The oxidation of NADH at solid electrodes has generally resulted in poorly defined current-potential curves (73,8). The recent development of conditions in which reproducible current-potential curves could be obtained (74,10) has made possible the use of NAD^+ as a cofactor in enzyme-substrate electrodes (75). With this type of electrode, it is possible to determine chemical species which undergo enzymatically catalyzed redox reactions with NAD^+ from coulometric measurements of the NADH produced in the oxidation.

In the enzyme-substrate electrode, NAD^+ and an appropriate enzyme are immobilized in a semipermeable membrane, sealed onto a glassy carbon electrode (NAD^+ and the enzyme can also be provided to the electrode via a flow-through system). When the electrode is immersed in a solution containing the appropriate substrate, the substrate which penetrates the membrane is enzymatically oxidized, converting NAD^+ to NADH in the process. With the glassy carbon electrode fixed at a potential where NADH is oxidized back to NAD^+, the current

which results from the electrochemical oxidation of NADH can be related to the substrate concentration (75).

Although this type of electrode is still in the developmental stages and has not proved capable of providing a linear current-substrate concentration response, subsequent refinements may make possible its use for the determination of chemical species which undergo enzymatically catalyzed redox reactions with NAD^+.

REFERENCES

1. L. A. Lehninger, "Bioenergetics," W. A. Benjamin, New York, 1965.

2. K. Burton, Biochem. J., 143, 365 (1974).

3. E. S. G. Barron and A. B. Hastings, J. Biol. Chem., 107, 567 (1973).

4. C. O. Schmakel, K. S. V. Santhanam, and P. J. Elving, J. Amer. Chem. Soc., 97, 5083, (1975).

5. B. Ke, Biochim. Biophys. Acta, 20, 547 (1956).

6. P. Leduc, D. Thevenot, and R. Buvet, Comm. IIIrd Symp. Bioelectrochem., Julich, GFR (1975).

7. A. J. Cunningham and A. L. Underwood, Biochemistry, 6, 266 (1967).

8. J. N. Burnett and A. L. Underwood, Biochemistry, 4, 2060 (1965).

9. K. S. V. Santhanam and P. J. Elving, J. Amer. Chem. Soc., 95, 5482 (1973).

10. W. J. Blaedel and R. A. Jenkins, Anal. Chem., 47, 1337 (1975).

11. R. D. Braun, K. S. V. Santhanam, and P. J. Elving, J. Amer. Chem. Soc., 97, 2591 (1975).

12. P. Leduc and D. Thevenot, Bioelectrochem. Bioenergetics, 1, 96 (1974).

13. M. Aizawa, R. W. Coughlin, and M. Charles, Biochim. Biophys. Acta, 385, 362 (1975).

14. R. W. Burnett and A. L. Underwood, Biochemistry, 7, 3328 (1968).

15. S. P. Colowick and N. O. Kaplan, "Methods in Enzymology," Vol. III, Academic Press, New York, 1957.

16. H. M. Siegel, G. A. Montgomery, and R. M. Bock, Arch. Biochem. Biophys., 82, 288 (1959).

17. B. L. Horecker and A. J. Kornberg, J. Biol. Chem., 175, 385 (1948).

18. J. Heyrovsky and J. Kuta, "Principles of Polarography," Academic Press, New York, 1966.

19. L. Meites, "Polarographic Techniques," John Wiley and Sons, New York, 1965.

20. D. E. Smith, "Electroanalytical Chemistry," Vol. 1, A. J. Bard, Ed., Marcel Dekker, New York, 1966.

21. J. Flemming, J. Electroanal. Chem., 75, 421 (1977).

22. M. A. Jensen, T. E. Cummings, and P. J. Elving, Bioelectrochem. Bioenergetics, accepted for publication.

23. T. E. Cummings, M. A. Jensen, and P. J. Elving, submitted for publication.

24. D. E. Smith, Crit. Rev. Anal. Chem., 2, 247 (1971).

25. J. J. Lingane, Chem. Rev., 29, 1 (1941).

26. M. v. Stackelberg and H. Freyhold, Z. Elektrochem., 46, 120 (1940).

27. J. E. B. Randles and K. W. Somerton, Trans. Faraday Soc., 48, 937 (1952).

28. R. de Leeuwe, M. Sluyters-Rehbach, and J. H. Sluyters, Electrochim. Acta, 14, 1183 (1969).

29. J. J. Lingane, J. Amer. Chem. Soc., 68, 2448 (1946).

30. L. Meites, Anal. Chem., 20, 895 (1948).

31. R. S. Nicholson and I. Shain, Anal. Chem., 36, 706 (1964).

32. T. E. Cummings and J. A. Cox, J. Electroanal, Chem, 60, 245 (1975).

33. G. S. Alberts and I. Shain, Anal. Chem., 35, 1859 (1963).

34. W. M. Schwarz and I. Shain, J. Phys. Chem., 69, 30 (1965).

35. M. L. Olmstead and R. S. Nicholson, Anal. Chem., 41, 851 (1969).

36. R. Brdicka, Collec. Czech. Chem. Communs., 12, 522 (1947).

37. R. Bonnaterre and G. Cauquis, J. Electroanal. Chem., 32, 199 (1971).

38. J. Ludowieg and A. Levy, Biochemistry, 3, 373 (1964).

39. G. Blankenhorn, Eur. J. Biochem., 67, 67 (1976).

40. R. S. Nicholson, Anal. Chem., 37, 667 (1965).

41. J. W. Hayes, I. Ruzic, D. E. Smith, G. L. Booman, and J. R. Delmastro, J. Electroanal. Chem., 51, 269 (1974).

42. R. S. Nicholson, Anal. Chem., 37, 1351 (1965).

43. M. L. Olmstead, F. G. Hamilton, and R. S. Nicholson, Anal. Chem., 41, 260 (1969).

44. E. J. Land and A. J. Swallow, Biochim. Biophys. Acta, 162, 327 (1968).

45. C. O. Schmakel, K. S. V. Santhanam, and P. J. Elving, J. Electrochem. Soc., 121, 1033 (1974).

46. K. Wallenfels and M. Gellrich, Ber., 92, 1406 (1959).

47. N. O. Kaplan, "The Enzymes," Vol. 3, P. D. Boyer, H. Lardy, and K. Myrback, Eds., Academic Press, New York, 1960.

48. C. O. Schmakel, Ph.D. Thesis, University of Michigan, Ann Arbor, Michigan, 1971.

49. U. Bruhlmann and E. Hayon, J. Amer. Chem. Soc., 96, 6169 (1974).

50. T. G. McCord and D. E. Smith, Anal. Chem., 41, 116 (1969).

51. T. E. Cummings, Ph.D. Thesis, Southern Illinois University, Carbondale, Illinois, 1975.

52. S. W. Feldberg, "Electroanalytical Chemistry," Vol. 3, A. J. Bard, Ed., Marcel Dekker, New York, 1969, p. 199.

53. H. H. Bauer, J. Electroanal. Chem., 16, 419 (1968).

54. E. R. Brown, and R. F. Large, "Physical Methods of Chemistry," Vol. I, Part IIA, A. Weissberger, and B. W. Rossiter, Eds., Wiley-Interscience, New York, 1971, p. 423.

55. R. H. Wopschall and I. Shain, Anal. Chem., 39, 1514 (1967).

56. M. M. Taqui Khan and A. E. Martell, J. Amer. Chem. Soc., 84, 3037 (1962).

57. R. M. Smith and F. A. Alberty, J. Amer. Chem. Soc., 78, 2376 (1956).

58. J. A. Happe and M. Morales, J. Amer. Chem. Soc., 88, 2077 (1966).

59. H. Brintzinger, J. Amer. Chem. Soc., 87, 1805 (1965).

60. B. Janik and P. J. Elving, J. Amer. Chem. Soc., 92, 235 (1970).

61. D. L. Smith and P. J. Elving, J. Amer. Chem. Soc. 84, 1412 (1962).

62. V. Vetterl, Biophysik, 5, 255 (1968).

63. D. Krznaric, P. Valenta, and H. W. Nurnberg, J. Electroanal. Chem., 65, 863 (1975).

64. P. Valenta, H. W. Nurnberg, and D. Krznaric, Bioelectrochem. Bioenergetics, 3, 418 (1976).

65. W. M. Clark, "Oxidation-Reduction Potentials of Organic Systems," Williams and Wilkins, Baltimore, 1960.

66. K. Burton and T. H. Wilson, Biochem. J., 54, 86 (1953).

67. F. L. Rodkey, J. Biol, Chem., 213, 777 (1955).

68. F. L. Rodkey, J. Biol. Chem., 234, 188 (1959).

69. C-I. Branden, H. Jornvall, H. Eklund, and B. Furugren, "The Enzymes," Vol. II, P. D. Boyer, Ed., Academic Press, New York, 1975.

70. H. Sund, "Biological Oxidations," T. P. Singer, Ed., Interscience, New York, 1967, p. 603.

71. H. Eklund, B. Nordstrom, E. Zeppezauer, G. Soderlind, I. Ohlsson, T. Boiwe, and C-I. Branden, F.E.B.S. Lett., 44, 200 (1974).

72. H. R. Mahler, and L. Brand, in "Free Radicals in Biological Systems," M. S. Blois Jr., J. W. Brown, R. W. Lemmon, R. O. Lindblom, and M. Weissbluth, Eds., Academic Press, New York, 1961.

73. R. G. Hass, Ph.D. Thesis, University of Wisconsin, Madison, Wisconsin, 1970.

74. L. C. Thomas, and G. D. Christian, Anal. Chim. Acta, 78, 281 (1975).

75. W. J. Blaedel and R. A. Jenkins, Anal. Chem., 48, 1240 (1976).